Colorimetric and Fluorescent Chemosensors for Selective Detection of Biologically and Environmentally Important Metal Ions at PPM Level

A Thesis

Submitted in Partial Fulfillment of the Requirements

for the Degree of

DOCTOR OF PHILOSOPHY

By

VIPIN KUMAR JAIN

to the

Department of Chemistry

Indian Institute of Technology Kanpur

Kanpur, India

January, 2020

Declaration

This is to certify that the thesis titled **"Colorimetric and Fluorescent Chemosensors for Selective Detection of Biologically and Environmentally Important Metal Ions at PPM Level"** is authored by me. It presents the research conducted by me under the supervision of **Prof. Pratik Sen** at IIT Kanpur. To the best of my knowledge, it is an original work, both in terms of research content and narrative, and has not been submitted elsewhere, in part or in full, for a degree. Due credit has been attributed with appropriate citations and acknowledgements, in line with established norms and practices.

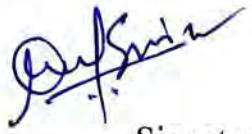

Signature

Vipin Kumar Jain
Programme: PhD
Department of Chemistry
Indian Institute of Technology Kanpur
Kanpur 208016
India

CERTIFICATE

It is certified that the work reported in the thesis entitled **"Colorimetric and Fluorescent Chemosensors for Selective Detection of Biologically and Environmentally Important Metal Ions at PPM Level"** has been carried out by **Mr. Vipin Kumar Jain** under my supervision and has not been submitted elsewhere for a degree.

(Dr. Pratik Sen)

December, 2019

IIT Kanpur

Thesis Supervisor

Department of Chemistry

Indian Institute of Technology Kanpur

Kanpur-208016, India

Department of Chemistry
Indian Institute of Technology Kanpur

Certificate of course work

This is to certify that Ms. Vipin Kumar Jain has satisfactorily completed all the courses required for PhD degree. The courses include:

AE698	Introduction to Virtual Instrumentation
CHM636	Physical Photochemistry
CHM684	Computer Programming in Chemistry
CHM629	Principal of Physical Chemistry
CHM685	Molecular Radiation Interaction
CHM695	Molecular Modelling in Chemistry
CHM799	Research
CHM800	General Seminar
CHM801	Graduate Seminar

Mr. Vipin Kumar Jain was admitted to the candidacy of the Ph.D. degree in April 2014 after he successfully completed the written and oral qualifying examinations.

Head
Department of Chemistry
Indian Institute of Technology Kanpur
Kanpur-208016, India

Amalendu Chandra
Professor & Head
Department Of Chemistry
I.I.T. Kanpur

Convener, DPGC
Department of Chemistry
Indian Institute of Technology Kanpur
Kanpur-208016, India

Dedicated to my all Teachers
And Tax payers of India

Acknowledgement

First and foremost, with the sense of deep gratitude and humble submission, I bow down to the almighty GOD for giving me strength and energy to complete this research work successfully.

It's my great privilege to convey my unpretentious and overwhelming gratitude and heartfelt thanks to my thesis supervisor, Prof. Pratik Sen for his excellent guidance, continuous motivation, and support during all stages of my Ph.D. He ignored all my negative points and always stood by my side. His unstinting encouragement and inspiration helped me during the journey of my research work and in the completion of the dissertation. I am highly indebted to him for his patience in provoking me to develop independent research skills. I am highly inspired by his excellent teaching capabilities, his ardent devotion towards research that ignites the love of learning the new dimensions of chemistry.

I offer my sincere thanks to Prof. S. Manogaran, Prof. A. Chandra, Prof. P. Sen, Prof. K. Poddar, and Prof. K. Srihari for teaching highly informative and interesting courses as a part of my course work. My thanks are also due for Prof. K. Srihari, allowing me to attend his lectures, which were very inspiring and motivating. I will always miss the versatile teaching approach of Prof. K. Srihari.

I extend my warm gratitude towards the Department of Chemistry, IIT Kanpur for making me an important part of it, and it's student community. Thanks to former (Prof. P. K. Bharadwaj, Prof. S. Verma) and present (Prof. A. Chandra) Heads of the Department and office staffs especially Sudha madam and Geeta madam honestly deserves a whelming acknowledgment for being very cooperative and helpful whenever needed.

This work would not be possible without the help and support from spectrometer operators - Mr. Raja Babu, Mr. Bhanu Tiwari, Mr. Pramod Kumar, Mrs. Sunita Sharma for 500 and 400 NMR experiments, Dr. Veena

Singh for IR and Mr. P. Kadigachalam for ESI-MS.

A sincere gratitude is due to the Department of Chemistry, Jamia Millia Islamia University, New Delhi from where I have earned my postgraduate degree. I would like to thank Dr. Anwar Ali, Dr. Sharif Ahmad, Dr. S. K. Jain, Dr. Tokeer Ahmad and Dr. Rabia Ahmad for being excellent aspiration faculties who have always inspired me to pursue research as my career. I sincerely acknowledge all my teachers in school and college specially thanks to B. P. Goyal sir, Manish Jain sir who have enriched me with knowledge besides imbibing me with a good moral character.

My life inside and outside the lab has been never-to-be-forgotten experience alongside my colleagues, who have been all great companion. I thank all of them from the core of my heart. I am grateful to my lab seniors Dr. Rajeev Yadav, Dr. Shradhey Gupta, Dr. Shahnawaz R. Rather, Dr. Bhaswati who helped me in various ways during my Ph.D. It was an absolute pleasure working with Dr. Puspal and Dr. Vaisakh, Navin, Aritra, Nilimesh, Sovon, Faizida, Vijaykantda, Gulabda, Sandeep, and Tanmoy who have helped me achieve the desired scrutiny and disquisition for my dissertation. Their caring and love have made my long stay an unforgettable one. I also want to acknowledge M.Sc. project students Barun, Shubrangshu, Ashish, Ankur, Sunil, Santosh, and Pratyush for their cooperation, help whenever I needed.

My time at IIT Kanpur was made enjoyable and blessed with the presence of many caring and affectionate friends and groups that became a part of my life. I am grateful to Bhupesh, Rajesh, Jitendra, Sumit, Pankaj, Abhishek, Kuldeep, Srikanth, Kalpana, Sakthi, Hilal, Akhilesh, Indresh, Chandan, Mayank, Keerti, Poonam, Sarvesh, Gurmeet, Ravi, Sayeed, Vijay, and all my IITK friends for making my stay very pleasant. My friends Pawan, Vivek, Fauda had always been a source of joy for me during my stay in Delhi. My B.Sc. friends Chander Pratap, Anil, and Jitendra deserve a very warm acknowledgment. A Special mention to my dear friends from my home town

who always wishes and made me feel special, Yogesh, Arvind, Sonu and Gangaram for their cooperation and support when needed.

I am very grateful to University Grant Commission (UGC), India for providing fellowship and to Research and Development section IIT Kanpur for their best cooperation.

Words fail to express my gratitude to my beloved parents whose teaching since childhood, everlasting love and affection, motivation, constant inspiration, and sacrifice have made me to complete my dissertation successfully. My father have always been a torchbearer for me and taught me the lesson of morality to be a good human being. I also want to acknowledge my grandparents with my full heart for their love and affection. My heartfelt thanks to my brother, Abhishek, my sister, Priyanka and brother in-law Rahul for their love and constant support. I would like to express my greetings to all my relatives and other family members.

Vipin Kumar Jain

SYNOPSIS

Name of the student:	Vipin Kumar Jain
Roll No.:	12207081
Degree for which the thesis is submitted:	Ph.D.
Department:	Chemistry
Thesis supervisor:	Prof. Pratik Sen
Thesis title:	Colorimetric and Fluorescent Chemo-sensors for Selective Detection of Biologically and Environmentally Important Metal Ions at PPM Level
Month and Year of submission:	January, 2020

The work reported in this thesis outlines a substantial development and application of the 'Schiff-base' based chemosensors. Schiff-base generally functions as linker/spacer within the molecule, which imparts magnificent photophysical properties to the chromophore/fluorophore. As a result, chemosensors based on Schiff-base become a prime focus for chemists. Due to various types of health hazards caused by excess metal ions (e.g. noxious ions like Fe^{3+}, Cu^{2+}, and Hg^{2+}) there is a need for rapid, sensitive and selective detection of them consumable products on a regular basis. Such an effort demands an easier and cheaper way to detect these metal ions selectively and my thesis work aimed the same using varieties of Schiff bases.

Summary of the Work Done

(a) Selective visual detection of Fe^{3+} at PPM level through 4-pyridin-2-ylmethyleneaminophenol (PYAP)

This chapter describes the design and synthesis of a new pyridine based Schiff-base, 4-((pyridine-2-ylmethylene)amino)phenol (PYAP) prepared by

the condensation of 4-aminophenol with pyridine-2-carbaldehyde in methanol. The chemosensor portrays a selective turn-on fluorescence at 612 nm in presence of only Fe^{3+} ion among other metal ions examined in methanol at room temperature. I observed a 200-fold increase in fluorescence intensity in the presence of 2 equivalents of Fe^{3+} with a limit of detection of 0.12 PPM. The signal transduction is proposed to occurred via a reversible chelation-enhanced fluorescence (CHEF) mechanism. The stoichiometry and binding constant of the PYAP–Fe^{3+} complex was estimated to be 1:2 and 5.12 ± 0.6 mM^{-2}, respectively. The short response time scale (in min) of detection makes this sensor suitable for real-life application.

(b) 4-((quinolin-2-ylmethylene)amino)phenol (QMAP) as a potential chemosensor for selective colorimetric detection of Cu^{2+} at PPM level

This chapter highlights the selective detection and estimation of copper through a quinolin based chemosensor, 4-((quinolin-2-ylmethylene)amino)phenol (QMAP). QMAP was synthesized through a one-step condensation process of quinoline-2-carbaldehyde and 4-aminophenol. Addition of Cu^{2+} renders a change in color of the QMAP solution from colorless to red with the formation of a new band around 555 nm. From Jobs plot and titration experiment, the stoichiometry and binding constant of the Cu^{2+}–QMAP complex are estimated to be 1:2 and 3.2×10^{10} M^{-2}, respectively. The limit of detection in methanolic solution was determined to be 15.3 PPB. Based on the results obtained a plausible mechanism for the sensing has been proposed with the help of HRMS, ^{1}H and ^{13}C NMR and FT-IR data. Density functional theory (DFT) approach has also been employed to understand the geometric and electronic property of the chemosensor (QMAP) and its metal complex (QMAP-Cu^{2+}). Based on our calculation, I proposed a ligand to metal charge transfer (LMCT) mechanism for the excellent capability of QMAP to detect copper.

(c) Synthesis and application of N^1,N^1-diethyl-N^4-(quinolin-2-ylmethyl)benzene-1,4-diamine (RQMBD) for selective and sensitive visual detection of Cu^{2+} at PPB level

In this chapter, I synthesized a novel chemosensor N^1,N^1-diethyl-N^4-(quinolin-2-ylmethyl)benzene-1,4-diamine (RQMBD) through the reduction of a Schiff base N^1,N^1-diethyl-N^4-(quinolin-2-ylmethylene)benzene-1,4-diamine (QMBD) with sodium borohydride ($NaBH_4$). QMBD was also synthesized by condensation reaction. RQMBD showed high selectivity towards Cu^{2+} ions and a concomitant change in the color from pale yellow to red is observed. This vivid colorimetric change with fast response time can be observed visually. Moreover, RQMBD exhibits great sensitivity towards Cu^{2+} ions as there was no interference observed with other metal ions. The prospective binding mechanism between RQMBD and Cu^{2+} ions was studied using the Job's method. An excellent limit of detection of 18 PPB and a high binding constant ($10.8 \times 10^9\ M^{-2}$) makes RQMBD a potential detector of copper, which can be used onsite.

(d) A fluorescence turn-off based selective detection of Cu^{2+} at PPB level through 2,4-di-*tert*-butyl-6-(((4-(phenylamino)phenyl)imino)methyl)-phenol (BPIMP)

A new Schiff-base, 2,4-di-*tert*-butyl-6-(((4-(phenylamino)phenyl)-imino)methyl)phenol (BPIMP), was designed and synthesized, which shows a strong selectivity towards Cu^{2+}. The fluorescence of BPIMP was found to quenched only in the presence of copper without any effect of the counter anions. A stoichiometry ratio of 1:2 between Cu^{2+} and BPIMP was estimated through Job's plot analysis and the binding constant of the Cu^{2+}-BPIMP complex was found to be $1.5 \times 10^{11}\ M^{-2}$. The limit of detection for Cu^{2+} by BPIMP is found to be 32 PPB. It is interesting to note that filter paper based test kit of the chemosensor was capable to detect copper. This makes BPIMP an important copper sensor for commercialization.

(e) Highly sensitive and selective visual detection of Hg^{2+} by *N*-(quinolin-2-ylmethylene)-[1,1′-biphenyl]-4-amine (QMBA) with PPB level sensitivity

N-(quinolin-2-ylmethylene)-[1,1′-biphenyl]-4-amine (QMBA) was synthesized by the condensation of quinoline-2-carboxaldehyde and [1 1'-biphenyl]-4-amine through a nucleophilic substitution reaction. QMBA displayed an excellent selectivity and sensitivity for Hg^{2+} ion with a vivid color change from colorless to pink as a result of dramatic change in absorption maxima from 410 nm to 530 nm. This makes QMBA a suitable candidate for naked eyes detection of Hg^{2+}. The Job's plots indicate a 1:1 ratiometric complex formation between Hg^{2+} and QMBA. The binding constant for the complex was found 1.1×10^5 M^{-1} and the detection limit of QMBA for Hg^{2+} was estimated nearly 10 PPB.

Contents

THESIS OUTLINE

The thesis is divided in to following chapters:

Chapter 1. This chapter describes in detail the fundamental mechanistic pathways of operating protocol of chemosensors upon interaction with target ion, which should be kept in mind while designing a chemosensor.

Chapter 2. This chapter discussed various experimental techniques that have been used to characterize the chemosensor and its complex formed with target ion and also used to understand the nature of the interaction between chemosensor and analyte.

Chapter 3. This chapter reports the development of a novel pyridine based Schiff base chemosensor PYAP which can selectively detect Fe^{3+} ion with high sensitivity on PPM level with fluorescence turn-on mechanism.

Chapter 4. This chapter describes our work on the synthesis of a chemosensor QMAP and unfolds its capability of colorimetric selective detection of Cu^{2+} ion at PPM level. Theoretical study of this system which shows a LMCT type mechanism pathways of binding between QMAP and Cu^{2+} also discussed in detail.

Chapter 5. In this chapter, we have described the spectroscopic evidence of sensing behavior of a chemosensor RQMBD in presence of Cu^{2+} ion with a color change which makes it suitable for naked eye detection.

Chapter 6. This chapter deals with the design and synthesis of a new chemosensor BPIMP which shows a selective sensing behavior towards Cu^{2+} at PPB level with fluorescence turn-off pathway.

Chapter 7. This chapter enunciate the role of QMBA molecules as a potential chemosensor for the Hg^{2+} ion detection selectively and sensitively with a vivid color change which is visible with naked eyes.

Chapter 8 This chapter discussed the overall conclusion of the thesis and the future outlook of research work.

Chapter 1

Introduction

1.1 Introduction

Since the last few decades and until today, the development of chemosensors that can selectively and sensitively recognize the transition metal ions has become a key research area in chemistry.[1,2] This field has gained significant attention because of the vital function of transition metal ions in medicine, living systems, and environment. Metal ions like iron and copper are indispensable for human life.[3,4] Though a minute quantity of transition metals are crucial for living organisms, aberrations in normal levels of these metal ions in human body leads to chronic disorder in many organs like liver, bones, kidney, and central nervous system.[3–5]

Iron is most abundant transition metal present in human body. Its ability to readily take part in redox reactions makes it is an important component of catalytic site of many enzymes and proteins like hemoglobin and myoglobin.[3,6] The Fe^{3+} ion plays an essential roles in wide range of cellular metabolisms, most importantly the oxygen-carrying capacity of heme in hemoglobin.[7] Even though Fe^{3+} is essential, it can also oxidize proteins, lipids and other cellular components thereby making slightly toxic. Higher than normal levels of Fe^{3+} ions within the body has been linked with the occurrence of some form of cancers and abnormality of vital organs such as liver, pancreas and heart.[8–10] The deficiency or overload of iron can cause anemia, anthropathy, heart failure, diabetes, and damage to kidney and liver.[11,12]

Following iron, copper occupies the third place of transition metals in the human body,[13] and acts as a cofactor for a variety of metalloenzymes and transcriptional events.[14] Several proteins, namely zinc-copper superoxide dismutase, cytochrome *c* oxidase, lysyl oxidase, ascorbate oxidase and several transcription factors, need copper for their activities.[15–17] However, Cu^{2+} overload leads to the generation of reactive oxygen species and thus shows toxicity linked with Menkes disease, Alzheimer’s disease, prion disease, and Wilson’s diseases, and Parkinson's disease and.[18,19] In recent years, Cu^{2+}

overload has also been suspected of cause infant liver damage.[20] Further, higher levels of Cu^{2+} have been detected in tumors with a possible role in promoting angiogenesis.[21] Mercury is another toxic metal ions and mercury pollution is a global problem which caused many diseases prenatal brain damage, tubular necrosis, motion and cognitive disorders, hearing and vision loss, and proteinuria and death.[22] Hence, selective detection and quantitative analysis of these metals ions in biological samples have attained much importance in recent years.

There are several traditional techniques like atomic absorption spectroscopy (AAS),[23–25] inductively coupled plasma atomic emission spectrometry (ICP-AES),[26,27] inductively coupled plasma mass spectrometry (ICP-MS),[28,29] voltammetry,[30,31] quantum-dot-based assays,[32] X-ray fluorescence microscopy (XRFM)[33,34] and spatially resolved mass spectrometry techniques combined with electron energy loss spectroscopy (EELS),[35,36] have been developed that provide direct and quantitative information about such metal ions. Colorimetric and fluorescence probes has received wide spread application over these methods because of the experimental simplicity and less demanding sophisticated instrumentation. Hence, development of colorimetric and fluorescent chemosensors for the identification of metal ions has become an emerging area of current research interest.

The main requirement for a molecule to be a colorimetric and fluorescent chemosensor is its ability to show distinctly different photophysical properties before and after the interaction with target metal ion. Generally, such chemosensors comprise a chromophore/fluorophore (signaling moiety), which is responsible for the changes in the color/fluorescence and an ionophore (recognition moiety) for binding the metal ion. The recognition moiety is accountable for the selectivity and binding efficiency towards a particular metal ion. These characteristics mainly depend on the properties of metal ion (charge,

ionic radius, hardness, and coordination number), ligand topology, and the environmental conditions such as nature of the solvent, pH, and ionic strength. Generally, the signaling moiety can be linked to the recognition moiety directly or via a spacer. In the former case, some of the atoms of the signaling moiety may participate in the coordination of the metal ion, and the binding selectivity depend on the overall structure involving both recognition and signaling moieties.

1.2 Design of synthetic receptors

Chemosensors are molecules which are synthetically fabricated in labs, that produces a real-time response (usually within a few seconds) when interact with an analyte.[37–39] There are two well-known approaches that describe the working of chemosensors.

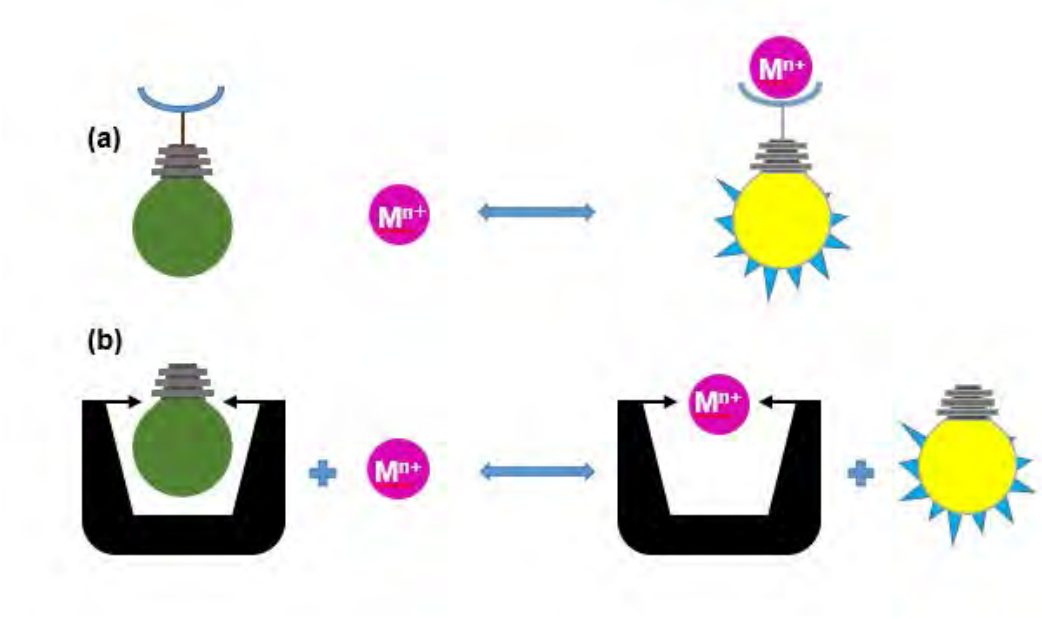

Figure 1.1 Pictorial presentation of binding approaches of chemosensor with metal ion.

The first one involves the signaling subunit/binding site approach as illustrated in Figure 1.1(a), where two units are linked through a covalent bond. An concomitant change in optical response usually observed as a result of coordination of selective analyte with binding site of chemosensor caused by the change in electronic properties of signal reporter subunits.[40–45] The other

working mechanism of chemosensor as shown in Figure 1.1(b) follows the displacement approach, which involves the use of molecular assemblies formed by the binding site and a signaling subunits.[46–50] The coordination of specific analyte with the binding site results in subsequent release of the signaling subunit in solution. This enormous literature data available today shows how the cation recognition chemistry has been matured. This literature data can be used to study the correlation between the structure of the receptors and specificity in binding to a particular cationic species. The concurrent advancement in molecular modeling software[51] and the computational facility[52] also helps scientists in efficiently designing of tailored-made chemosensor for targeted cation(s) for practical applications, e.g., for in-vivo or in-vitro detection of a metal ion in live organisms or environmental samples.

1.2.1 Characteristics of an ideal chemosensor

1. The chemosensor should selectively detects the target metal ion interference from the other metal ions in the detection process.
2. The sensitivity of the chemosensor should be high enough to measure trace levels of metal ions.
3. The measured signal from the chemosensor should be proportional with the amount of metal ion present for quantitative detection.

1.3 Mechanistic pathways of metal ion recognition

For the design of new colorimetric and fluorescent chemosensor, it was always a keen interest of chemists to explore new mechanistic pathways of interaction between the analyte and signaling unit. Many basic and important photophysical methods adopted by chemists for designing and fabrication of new chemosensors.[53,54] In fact, until now, there are several mechanisms that have been developed and commonly used for the optical recognition of different species. A concise description of each of them is discussed below.

1.3.1 Paramagnetic fluorescence quenching

There are broad range of metal complexes having a paramagnetic metal ion in the vicinity of the fluorophore (which may act like a ligand) that enhance the intersystem crossing (ISC) as shown in the schematic representation of Figure 1.2. This is known as paramagnetic effect.

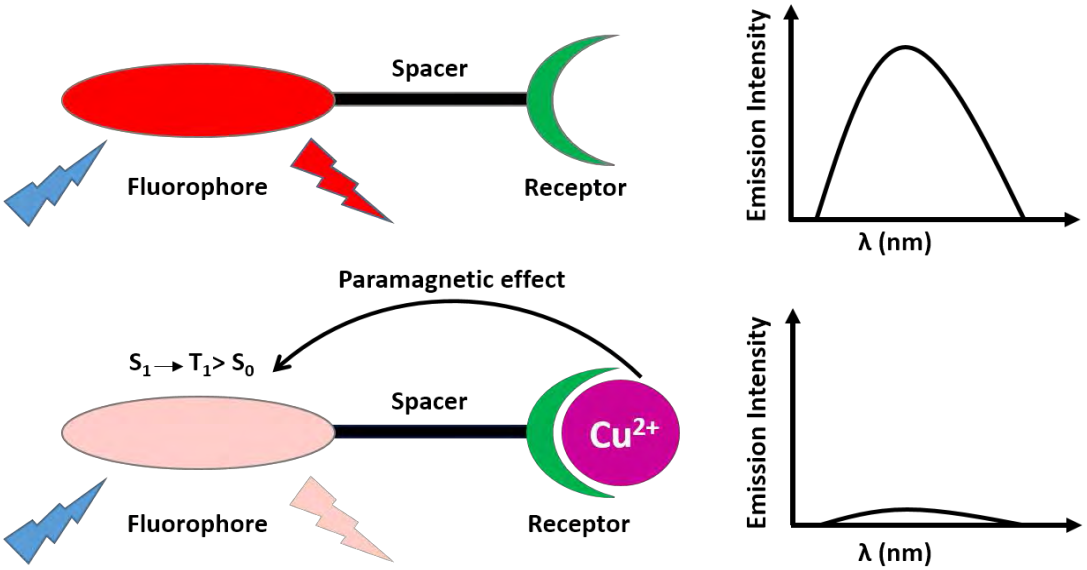

Figure 1.2 Pictorial representation of paramagnetic fluorescence quenching.

The paramagnetic metal ions, like Cu(II), Co(II), Cr(III) and Fe(III), when coordinated with fluorophore usually quench its fluorescence. The mechanism behind this process can be explained as the metal induced change in the photophysics of the fluorophore, usually involving the opening up the ISC pathway to the T_1 state. Thereafter, the complex relaxes back to S_0 state via non-radiation process.[53] Because of this alternative relaxation pathway, classical probes made for any paramagnetic metal ion are primarily based on fluorescence quenching.

1.3.2 Photoinduced electron transfer (PET)

The photoinduced electron transfer (PET) is a well-recognized photophysical mechanism for the effective recognition of a metal ions. The designing principle of the PET based chemosensors consists of three fundamental parts: fluorophore, spacer and receptor. Receptors are generally

electron rich whereas fluorophores are electron deficient. A significant difference in the electronic properties of ground state and excited state species is considered as a good characterization for this process.[55–57] A picture of transition between highest occupied molecular orbital (HOMO) and lowest unoccupied molecular orbital (LUMO) is crucial to understand the mechanism of PET. For unbound probe, the electron in the HOMO of the fluorophore can be excited to the LUMO upon irradiation with photon of appropriate energy. If the energy of the HOMO of the receptor is just higher than that of the fluorophore, the electron in the HOMO of receptor can move to the HOMO of the fluorophore through spacer after its excitation as shown in Figure 1.3.

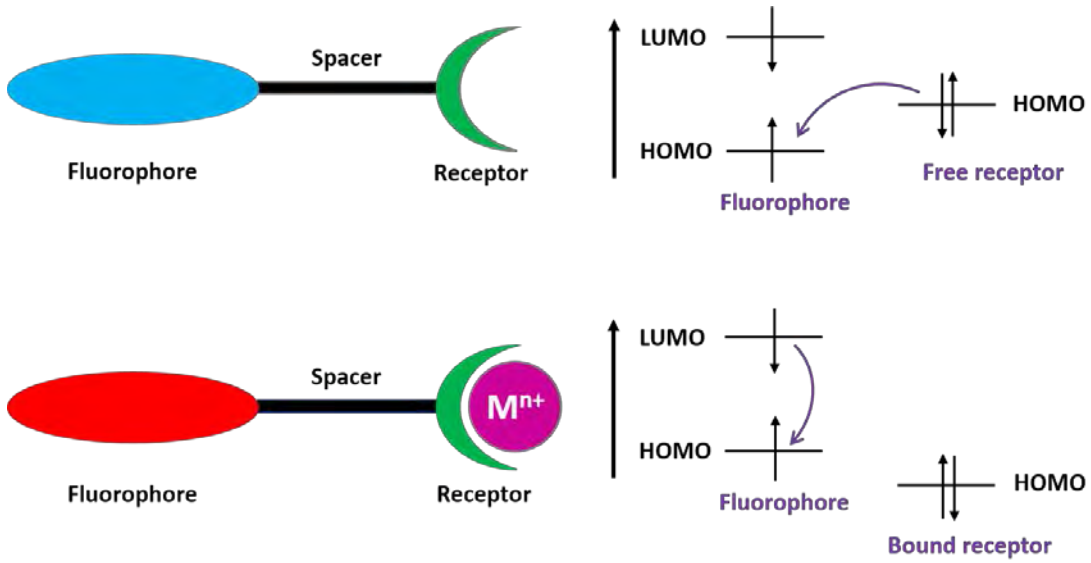

Figure 1.3 Diagrammatic representation of PET based fluorescent metal ion probes and their fluorescent enhancement mechanism.

This prevents the transition (relaxation) of excited electron from the HOMO of the fluorophore to LUMO through emission process. Since PET based sensors rely on electron transfer, electroactivity becomes an important factor, and thus molecular components of known redox potential would be helpful to choose the appropriate receptors, so that electron transfer between receptor and the fluorophore is energetically feasible due to low oxidation potential.[58,59] When a metal cation binds to the receptor unit of the sensor, the energy of the lone pair blocking the PET process is lowered after coordination,

and thus, resulting in the switch-ON of the fluorescence.

The oxidation potential of the receptor unit is affected by the solvent polarity, which in turn affect the PET. The electron transfer becomes easier in higher polarity solvent. Therefore, fluorescence quenching mediated by PET takes place immediately in high-polar environments.[60,61] We do not observe any spectroscopic shifts of the fluorescent response resulting from PET upon complexation with metal ions.

1.3.3 Photoinduced charge transfer (PCT)/ Internal charge transfer (ICT)

Chemosensor; whose working protocol is based on internal charge transfer (ICT), consist of a conjugated π-system of electron-donor/electron-acceptor (D/A) groups. Generally these type of sensors (molecular assemblies) exhibit large Stokes shift. The coordination of metal ion induces shift in emission and absorption spectra of chemosensor.

1.3.3.1 For fluorimetric detection

The mechanism behind this process involves electron transfer between donor and acceptor functional group to promoting fluorescence. The alteration of photoinduced internal charge transfer excited state achieved via changing the functionality of acceptor or donor as a ionophore results in blue or red shift of emission spectrum induced by the complexation of metal ion, which is an effective blueprint to develop novel probes for ratiometric metal ion detection. From Figure 1.4, we can see the binding of metal ion to the acceptor of a PCT fluorophore will decrease the LUMO energy and induce the bathochromic shift in emission maxima. An opposite change will be observed if complexation of metal ion occur with donor unit of the probe. The self-calibration effect of the two emission bands of these probes can eradicate the interference of local probe concentration, deviated microenvironments and experimental parameters, and photobleaching; which allow quantitative analysis of metal ion. Therefore, the

idea of formation of such PCT based ratiometric probes for metal ion will always make sense.[62]

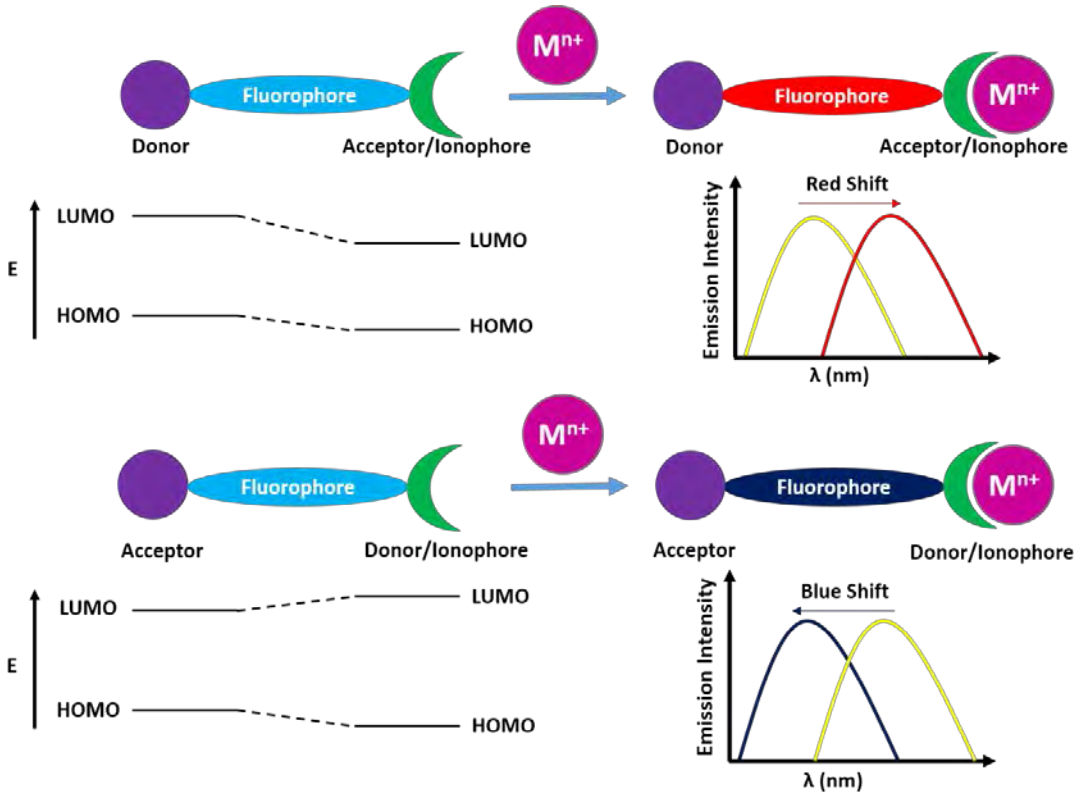

Figure 1.4 Diagrammatic representation of PCT/ICT based fluorescent probes metal ions and their ratiometric sensing mechanisms.

1.3.3.2 For colorimetric detection

The color changes appear after the binding of metal ion to the receptor is attributed to electronic properties of the sensor molecule accompanied with ICT. A chemosensor which is typically a D-π-A system, when combined with metal ion, exhibits excellent colorimetric detection of metal ions.

A good D-π-A coordination can be obtained by introducing the electron donating (ED) groups coupled with the electron acceptor (EW) groups in the chemosensor molecule at appropriate sites. The concept of HSAB helps us to evaluate the softness and hardness of the interacting sites and analyte and which further helps us in deciding whether a targeted metal ion will connect the ED or EW group.

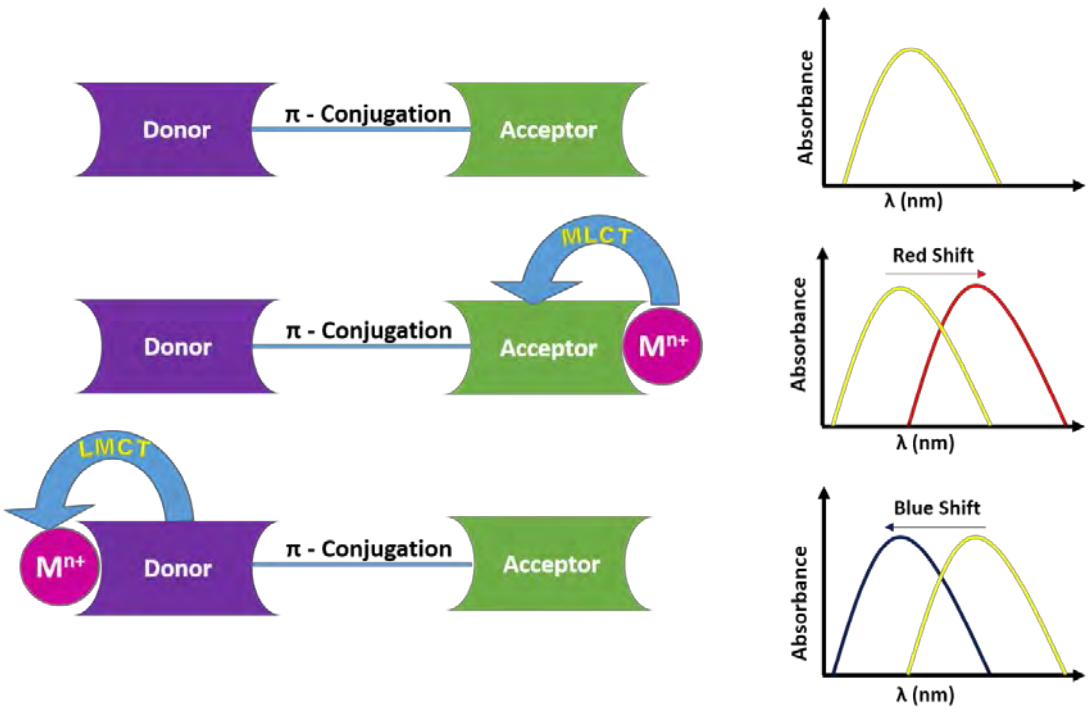

Figure 1.5 Schematic representation of PCT colorimetric probe and effect of cationic interactions on D-π-A system and on absorption spectrum.

Generally, the electron donating ability of the ED group decrease after metal ion binding, which in turn reduces the electron conjugation in D-π-A system and results in a hypsochromic or blue shift of the absorption spectrum that helps to promote possibility of MLCT transitions.[63–65] Whereas conjugation in the D-π-A system strengthens with amplified push-pull ICT ability after cationic binding to the EW group. This phenomenon results in a bathochromic or red shift along with high possibilities of LMCT transitions as shown in Figure 1.5.[66]

1.3.4 Fluorescence resonance energy transfer (FRET)

FRET is a well-known distance mediated interaction between the electronically excited fluorophore and an additional fluorophore. In FRET, radiation emitted from a donor fluorophore is transferred to an acceptor fluorophore without appearance of a photon.[67,68] There are three essential conditions for FRET:

1. The fluorescence spectrum of the donor molecule must effectively overlap with the acceptor's absorbance band.
2. FRET only occur over very short distances between donor and accepter, typically within 10 nm range.[69] The FRET efficiency is determined by the reciprocal of sixth power of the intermolecular distance.
3. The orientation of transition dipoles both donor and acceptor must be more or less parallel.

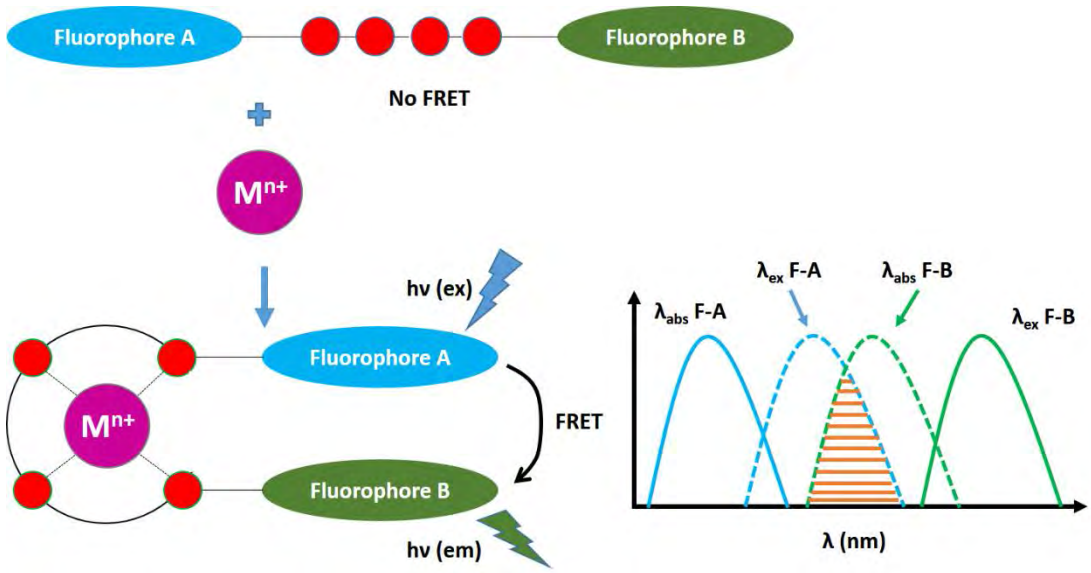

Figure 1.6 Schematic representation of FRET process where F-A and F-B stand for fluorophore A and fluorophore B respectively.

Herein, the presence of a metal ion does two things, either it pushes both the participating fluorophores come towards or move away from each other as illustrated in Figure 1.6. Photo-excitation of donor helps us in monitoring the occurrence and efficiency of the FRET event by examining the relative ratio of donor and acceptor emissions either sequentially or simultaneously.[70]

1.4 Synthetic receptors for Fe^{3+}, Cu^{2+}, and Hg^{2+} ion

As mentioned earlier, analytical techniques can provide away for the quantitative estimation of the Fe^{3+}, Cu^{2+}, and Hg^{2+} ions present in any samples.

However, these techniques usually require rigorous sample preparation and are not suitable for quick detection of Fe^{3+}, Cu^{2+}, and Hg^{2+} ions in real-time analysis. Further, these techniques are not suitable for in-vivo detection of Fe^{3+}, Cu^{2+}, and Hg^{2+} ions in the biological samples. These limitations have contributed to the recent advancement of small molecule chemosensors for different metal ions. Latest developments in Fe^{3+} Cu^{2+}, and Hg^{2+} chemosensor are presented below.

1.4.1 Fluorescent sensors for Fe^{3+} ion

Fe^{3+} is one of the most important metal ions in many living systems. There are several biological processes such as enzymatic reactions, cellular metabolism, transportation of oxygen by hemoglobin, where ferric ion plays a vital role. Therefore, a quantitative detection of Fe^{3+} ions is important. Due to its paramagnetic nature, Fe^{3+} ion has an ability to quench the fluorescence of the sensors and as a consequence makes the detection of Fe^{3+} in solution a difficult task using fluorescence technique. Nevertheless, several research groups have successfully developed Schiff-base chemosensors, which can efficiently detect Fe^{3+} ions by fluorescence enhancement through chelation. Few different types of Schiff-base Fe^{3+} chemosensors are described below.

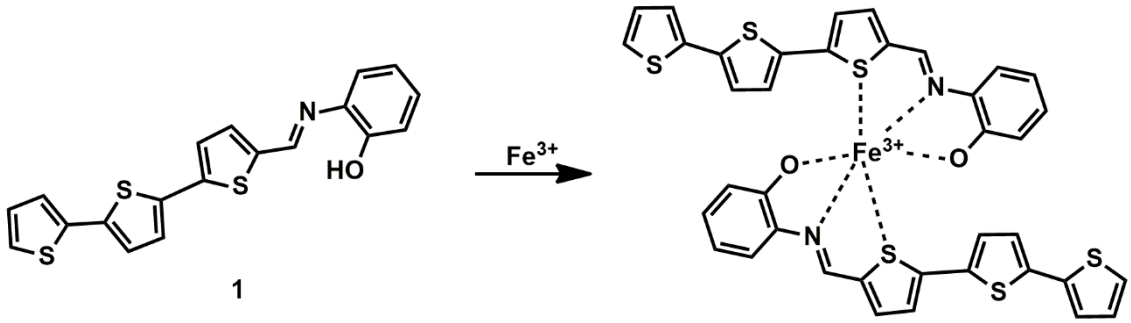

1

Li *et al.* have synthesized a novel oligothiophene Schiff-base (sensor 1) which acts as a 'turn-on' fluorescence chemosensor for Fe^{3+} and Hg^{2+}. Upon coordination with Fe^{3+} and Hg^{2+} in DMSO/H_2O (1/1, v/v) solution, the probe displayed a fluorescent enhancement, with a detection limit of 13.6 nM and

61.7 nM, respectively. The recognizing behavior toward Fe^{3+} was further confirm by IR and NMR spectrum. The observed binding constants of the probe with Fe^{3+} and Hg^{2+} were 1.34×10^6 $M^{-1}$and 8.99×10^4 M^{-1}, respectively.[71]

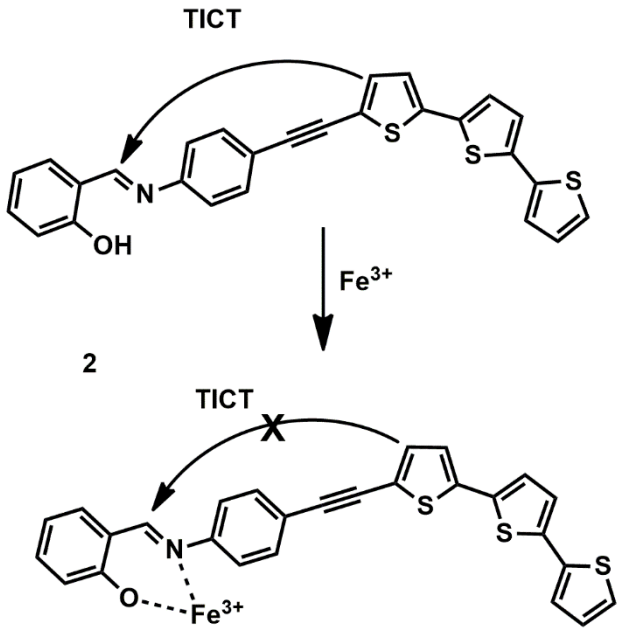

A novel dual-mode fluorescent "turn-on" chemosensor (sensor 2) based on oligothiophene-phenylamine Schiff-base has been designed and synthesized by Niu *et al*.[72] This chemosensor simultaneously discriminate both Fe^{3+} and Al^{3+} ions over other metal ions with great selectivity. Both the ESI-MS and Job plot showed that the sensor 2 coordinated with Fe^{3+} and Al^{3+} in a 1:1 stoichiometry with binding constant 1.04×10^4 M^{-1} and 8.66×10^5 M^{-1}, respectively. This sensor exhibited a good detection limit of 0.177 μM for Fe^{3+} ions and 0.177 μM for Al^{3+}. Importantly, sensor 2 worked efficiently over wide pH range (4.0-12.0) and has been successfully used to detect traces of Al^{3+} and Fe^{3+} ions in real samples such as water and food samples.

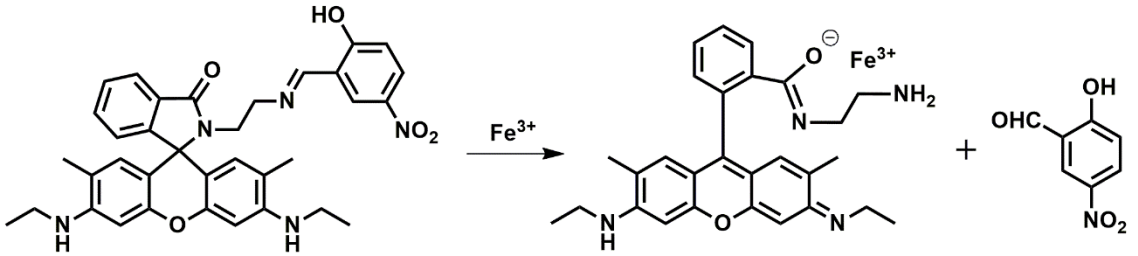

3

Lee *et al.* have synthesized a new fluorescence 'turn on' rhodamine based Schiff-base (sensor 3) suitable for detecting intracellular Fe^{3+} ions.[73] Unlike the other Schiff-bases, hydrolysis followed by spirolactam ring opening of sensor 3 occurred only when Fe^{3+} ions were added. The probe was stable over a broad range of pH. Moreover, the chemodosimetric reaction of sensor 3 was selective and sensitive enough to detect intracellular Fe^{3+} ions without detrimental effects on the Fe^{3+} based enzymes.

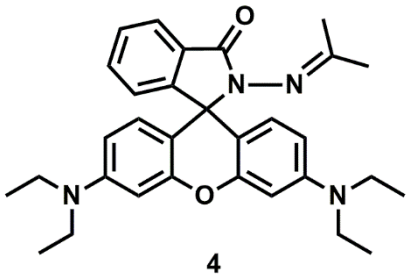

4

Sensing of Fe^{3+} within living cells has been demonstrated by Zhang *et al.* using a novel rhodamine based "turn on" fluorescent probe (sensor 4). The probe showed 120-fold enhancement in the fluorescence emission upon addition of Fe^{3+} ions, whereas other metal ions did not increase the fluorescence emission, except Cu^{2+}, which showed ~18-fold increment in the fluorescence intensity.[74]

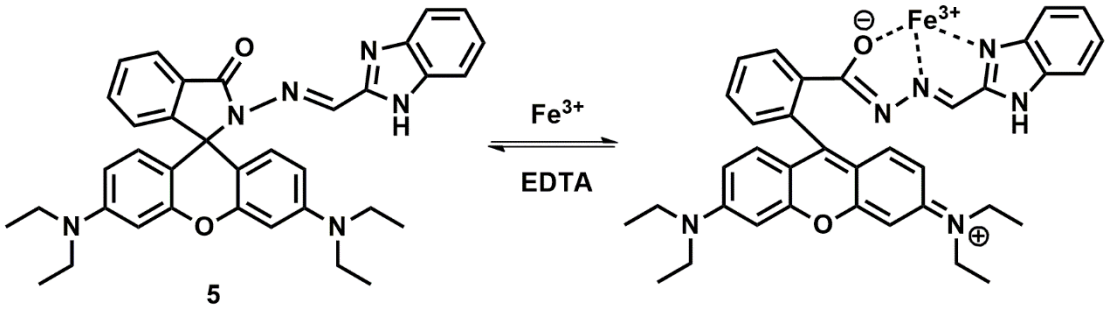

5

A rhodamine benzimidazole conjugate (sensor 5) has been designed by Li *et al* for the detection of Fe^{3+} ions. The sensor 5 showed an extreme selectivity for Fe^{3+} over other metal ions in acetonitrile. Both ESI-MS and Job plot confirmed 1:1 stoichiometry of the complex formed by sensor 5 with Fe^{3+} The binding constant calculated for the complex was $1.01 \times 10^4\ M^{-1}$. The probe exhibited good detection limit 1.5×10^{-8} M for Fe^{3+}.[75]

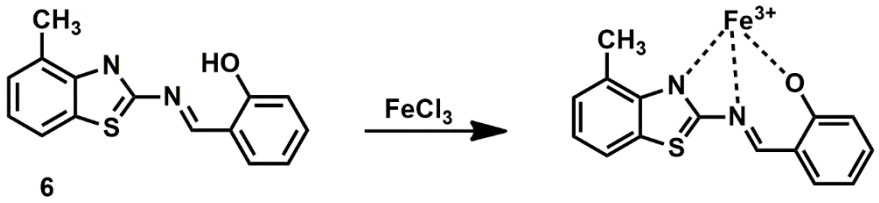

6

Pitchumani *et al.* have developed a benzothiazole derivative based Schiff-base fluorescent chemosensor, (sensor 6) for Fe^{3+} ions. Upon mixing with Fe^{3+} in ACN/Water (1/1, v/v) mixture, a dramatic enhancement of fluorescence is observed. No interference of competitive metal ions was observed in the detection process of Fe^{3+}. Formation of 1:1 complex between sensor 6 and Fe^{3+} was confirmed by The Job plot experiment. The association constant in ACN/H_2O mixture (50% v/v) is found to be $3.6 \times 10^6\ M^{-1}$ and the detection limit is 0.89 nM.[76]

1.4.2 Colorimetric and fluorescent sensors for Cu^{2+} ion

In the past several colorimetric sensors were developed for simple in-field naked eye recognition and semi-quantitative analysis of Cu^{2+} ion. This

simplicity in the detection process is the primary reason for the present emphasis in search of efficient colorimetric sensors for Cu^{2+} ion.

In my thesis work, I have developed new types of Schiff base with electron-withdrawing quinoline moieties, which shows its good affinity towards Cu^{2+} ion. The reason for choosing a system as mentioned above is: C=N double bond in Schiff bases include π electrons and nitrogen in quinoline rings provide feasibility for chelation to copper metal ions. This coordination with Cu^{2+} ion would increase the ICT (intramolecular charge transfer) transition or cause the LMCT (ligand-to-metal charge-transfer) transition, which could be used for Cu^{2+} ion detection with a distinct color change.[18,46,47] Few different types of Schiff-base copper chemosensors are presented below.

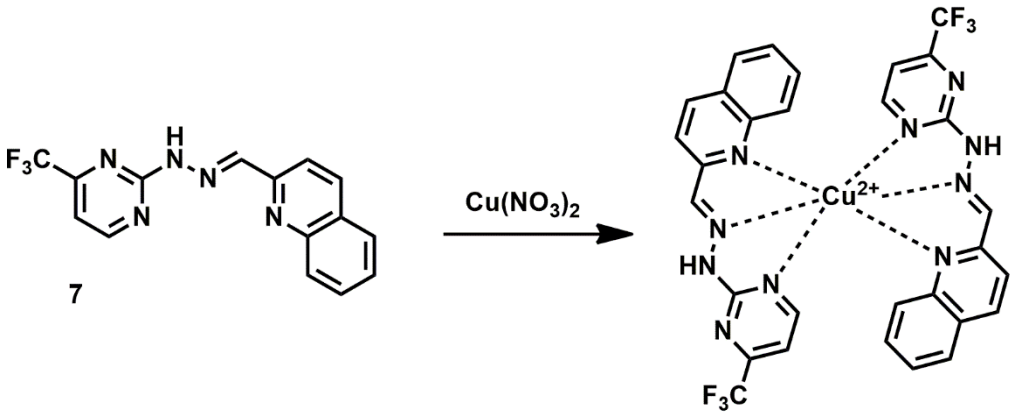

Kim *et al.* reported new pyrimidine derivatives as selective chemosensor (sensor 7) for the Cu^{2+} ion. The electron-withdrawing group, $–CF_3$, attached to the pyrimidine derivatives enhanced ICT to give an entirely different colorimetric response in *bis-Tris* buffer/DMF (4 /1, v/v, pH = 7).[77] The Schiff-base unit with quinoline moieties and electron-withdrawing substituted pyrimidine showed good receptor functionality.

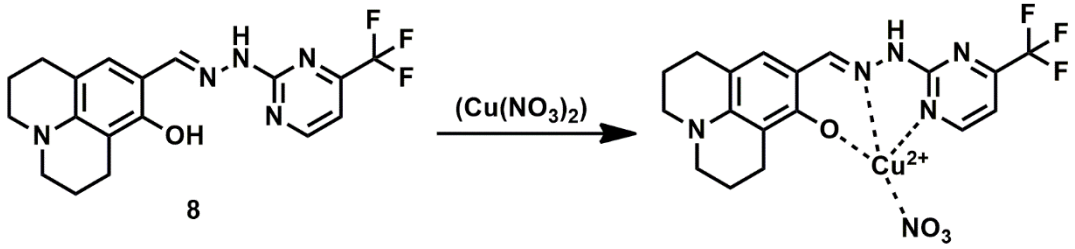

This is another 8-hydroxyjulolidine derivatives based chemosensor 8 appended with pyrimidine , that enabled efficient tridentate complexation with Cu^{2+} in the preference to other metal ions, has been developed by Kim *et al.*[78] The pyrimidine moiety played a vital role in metal ion binding. The substitution of $–CF_3$ attached to the pyrimidine group greatly affected the binding ability of the sensor 8. Upon complexation with Cu^{2+} the color of the solution turned to orange in *bis-Tris* buffer/THF (1/1, v/v), which is attributed to predominant large ICT and slight LMCT charge transfer. The complexation mode and the corresponding transition mechanism were elucidated by the ab initio calculations.

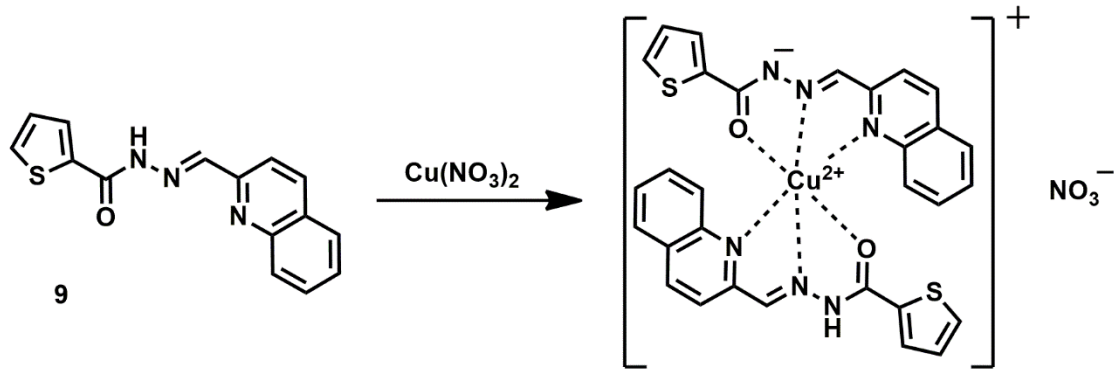

Kim *et al.* have reported a quinoline based Schiff base colorimetric probe (sensor 9) that utilizes the ICT process for the selective detection of Cu^{2+} in *bis–tris* buffer/DMSO (95/5, v/v). According to Kim *et al.*, the formation of the push-pull Cu^{2+}-probe complex upon metal ion binding led to the change in the π electron delocalization that changed the absorption spectrum. Colorimetric response is observed for sensor 9 to Cu^{2+} ions in solution which caused the red-

shift. Based on the theoretical calculation, they conclude that a large ICT and slight LMCT beget by chelation of chemosensor to Cu^{2+}.[79]

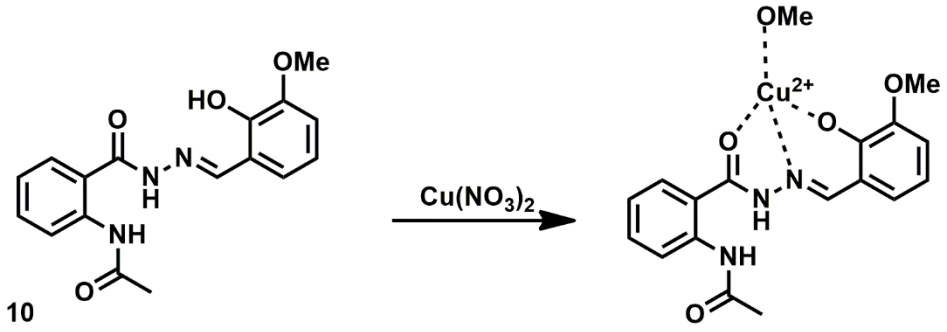

Patra *et al.* have developed a new flexible Schiff base fluorescent colorimetric probe *N*′-(2-hydroxy-3-methoxybenzylidene)-2-(benzamido)-benzohydrazide (sensor 10) that selectively senses Cu^{2+} and Ni^{2+} among transition metal ions.[80] The color change from pale yellow to intense yellow for both metal ions and a significant fluorescence enhancement of the **chemosensor** was observed only in the presence of Ni^{2+} ions whereas interaction with Cu^{2+} causes fluorescence quenching in methanol–*tris*-HCl buffer (10 mM, pH 7.2) solution (1/1, v/v). According to Patra et al chemosensing behaviour of the sensor 10 towards Cu^{2+} and Ni^{2+} ions can be applied to the formation of molecular logical devices.

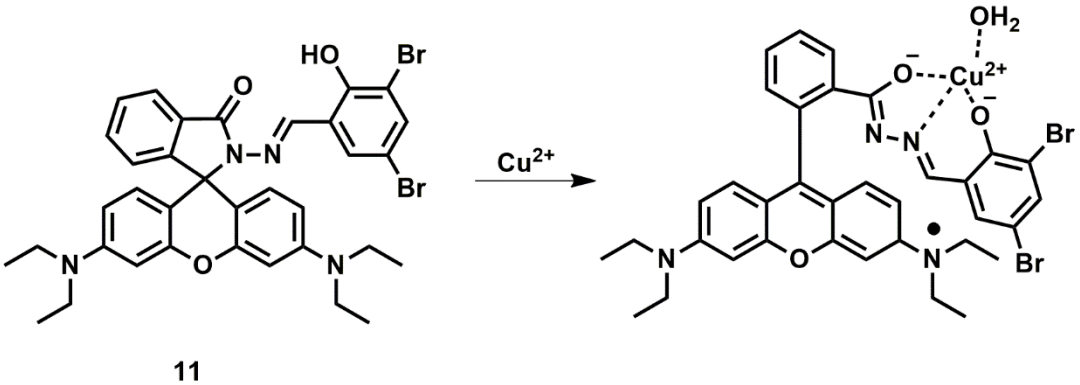

Zhao *et al.* reported a rhodamine-based Schiff-base as a dual chemosensor for VO^{2+} and Cu^{2+} metal ions. This chemosensor (sensor 11) can

selectively detect VO^{2+} *via* fluorescence "off–on" type switching with a high quantum yield and exhibits chromogenic behavior for Cu^{2+} ions with a distinct color change from colorless to pink in DMSO–*Tris*–HCl (7/3, v/v, pH 7.4) solution.[81] The complexation shifts the chemical equilibrium towards the rhodamine spirolactam ring-opened form and results in a new and profound spectral band developed at 518 nm. The binding stoichiometry of sensor 11 with Cu^{2+} and VO^{2+} was found to be 1:1.

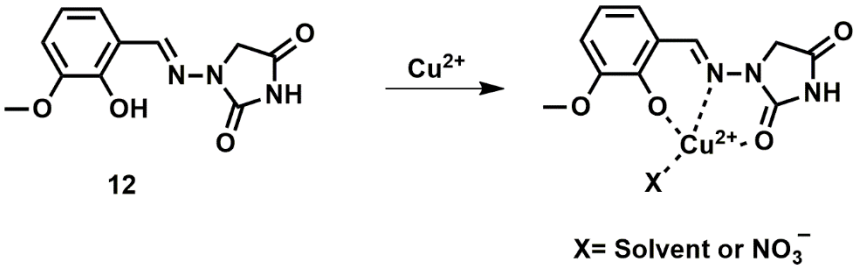

12

A novel salicylaldehyde moiety based Schiff-base (sensor 12) with chromophore unit aminohydantoin have been developed by Kim *et al*.[82] This dual chemosensor detects Zn^{2+} ion by a substantial fluorescence enhancement and Cu^{2+} ion by the colorimetric change from colorless to pink in acetonitrile/buffer solution (95/5; v/v pH 7.0). The electron donating group attached to salicylaldehyde moiety cause an enhancement of ICT transitions, which resulted in the red shift (340.51 to 427.71 nm) with vivid color change due to the coordination between Cu^{2+} ion and chemosensor.

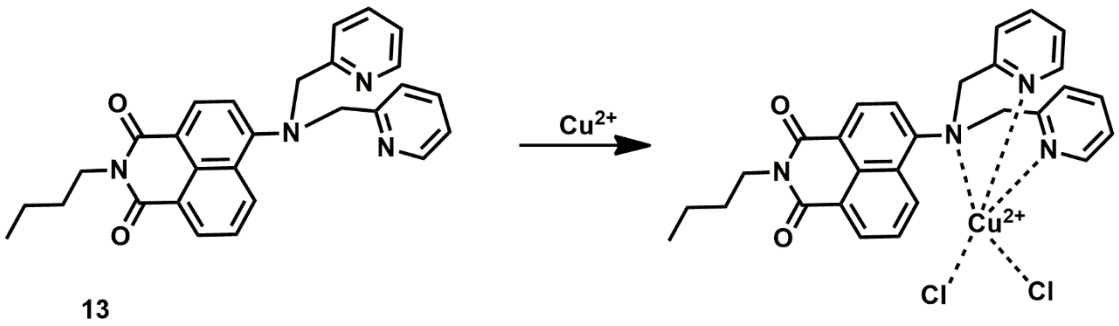

13

A novel fluorescent probe (sensor 13) with naphthalimide as fluorophore and di(2- picolyl)amino unit as receptor has been reported by Wang *et al*.[83] In acetonitrile/H_2O solution, Cu^{2+} ions induced significant blue shift in the absorption maximum of the probe due to the coordination of Cu^{2+} with the tertiary amine conjugated to the naphthalimide. The observed blue shift on the absorption maximum was due to the decrease in the electron donating tendency of the tertiary amine to the naphthalimide fluorophore. The formation of a 1:1 Cu^{2+}-sensor complex significantly quenched the fluorescence of the probe by the paramagnetic Cu^{2+}.

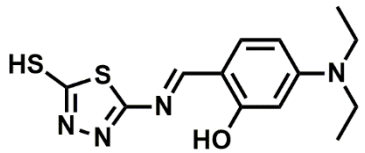

14

A *bis*-rhodamine fluorescent probe 14 has been found useful for the determination of Cu^{2+} with the quenching of fluorescence. In ethanol-water(3/2, v/v, pH 7.4) the fluorescent 14 selectively coordinated to Cu^{2+}, leads to great fluorescence quenching with color changed from canary yellow to brown attributes to naked eyes detection. The fluorescence quantum yield of the ligand was found to be 0.52. The detection limit of the probe for Cu^{2+} in was 5.721×10^{-7} mol/L. Job plot revealed the 1:1 binding mode of the sensor with Cu^{2+} is 1:1 with corresponding binding constant 2.67×10^4 M^{-1}, according to Qi *et al*.[84]

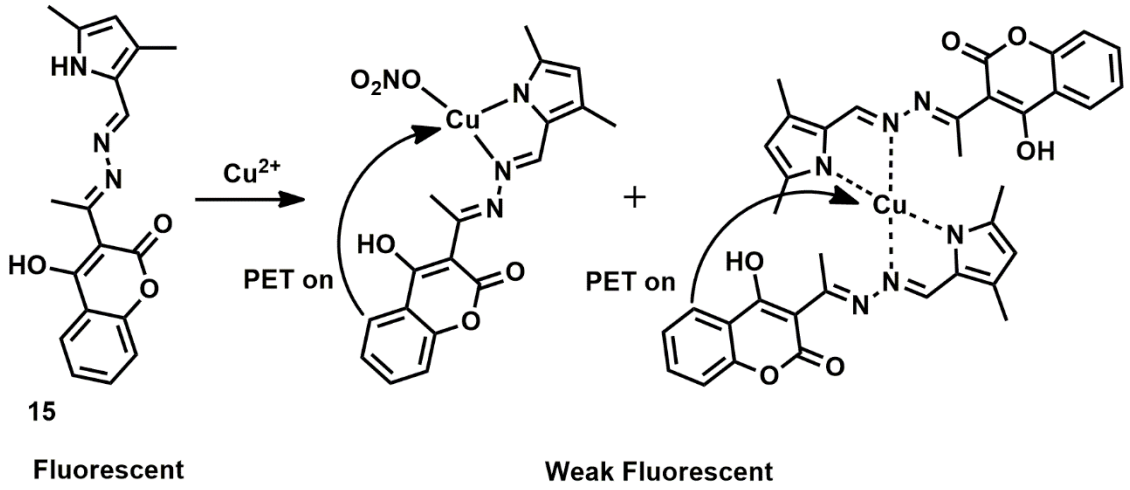

Lui *et al* have developed a new fluorescent molecular chemosensor fabricated by conjugation of coumarine derivative with pyrrole.[85] This Schiff base 15 containing pyrrole displayed great affinity with Cu^{2+} over other metal ions. Upon adding water in increasing fraction, this probe 15 showed a stoke shift from green to orange emissions is attributed to its special AIRE effect. Surprisingly, a significant quenching of both emissions by Cu^{2+} makes 15 a highly efficient fluorescent probe for Cu^{2+} in both solution and aggregation states. The limit of detection of Cu^{2+} by 15 was 32.8 nM.

Chattopadhyay *et al* have reported a salen type Schiff base (sensor 16) as a fluorescence "turn off" chemosensor for Cu^{2+} in 1 mM HEPES buffer-ethanol (50% v/v) solution.[86] The addition of Cu^{2+} to 16 quenched the fluorescence and is scrutinized by Stern-Volmer plot which consider the presence of both static and dynamic quenching phenomena. Further, it was highly selective to Cu^{2+} over other metal ions due to good association constant $1.51 \times 104M^{-1}$ of the probe towards Cu^{2+} ions with a 1:1 binding mode. The detection limit of 16 was found to be as low as 10.55 nM.

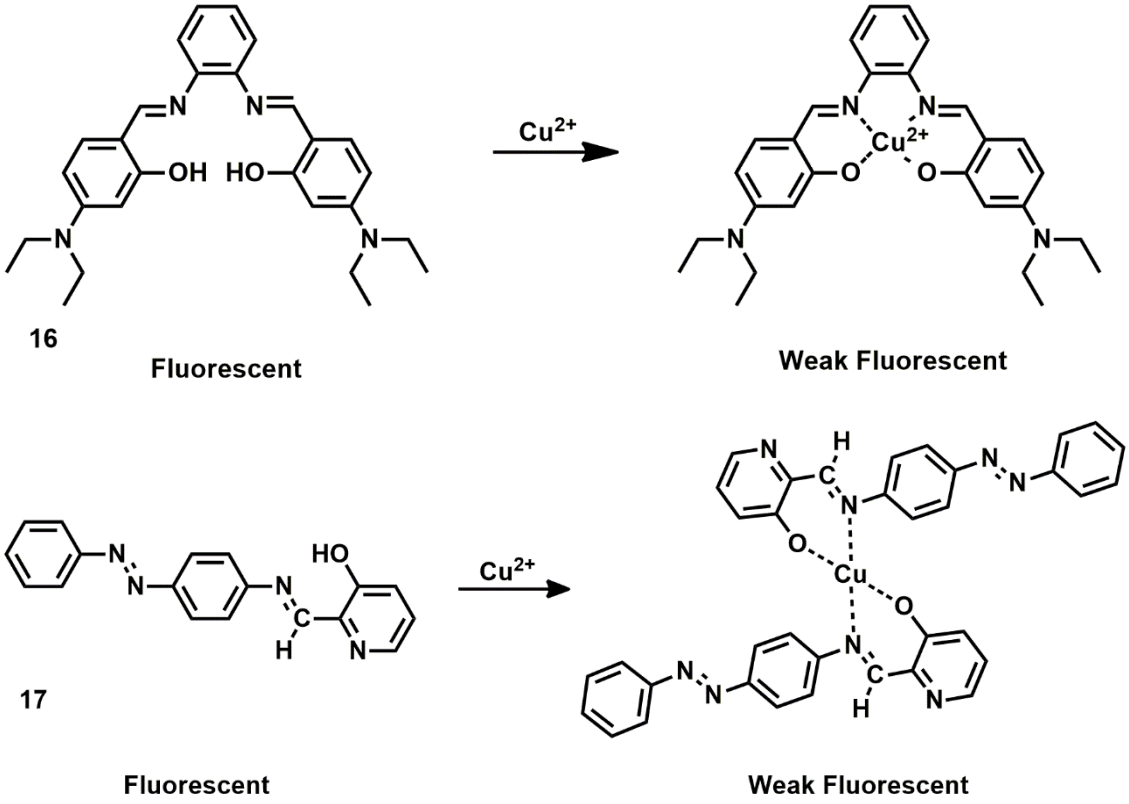

A highly sensitive Cu^{2+} chemosensor 17 based on Azo dye containing Schiff base molecular framework synthesized by Jayabharathi *et al.* displayed an excellent selectivity for Cu^{2+} over the different metal ions such as Ni^{2+}, Hg^{2+}, and Co^{2+} when examined in ethanol.[87] The interaction of Cu^{2+} moderately quenched the fluorescence emission of probe was considered as a result of formation of a non-fluorescent ground state complex and the paramagnetic effect caused by spin-orbit coupling. The probe formed a 1:2 complex with Cu^{2+}.

1.4.3 Colorimetric sensors for Hg^{2+} ion

Mercury is one of the most common toxic metals with its increased release in the environment and its exposure to the body orally or dermally causes harmful effects on human health.[88] Due to the deleterious effect associated with mercury, the development of new colorimetric chemosensors with adequate selectivity to detect mercury has been given considerable

attention over the last few decades.[22] Few different types of mercury chemosensors have been described below:

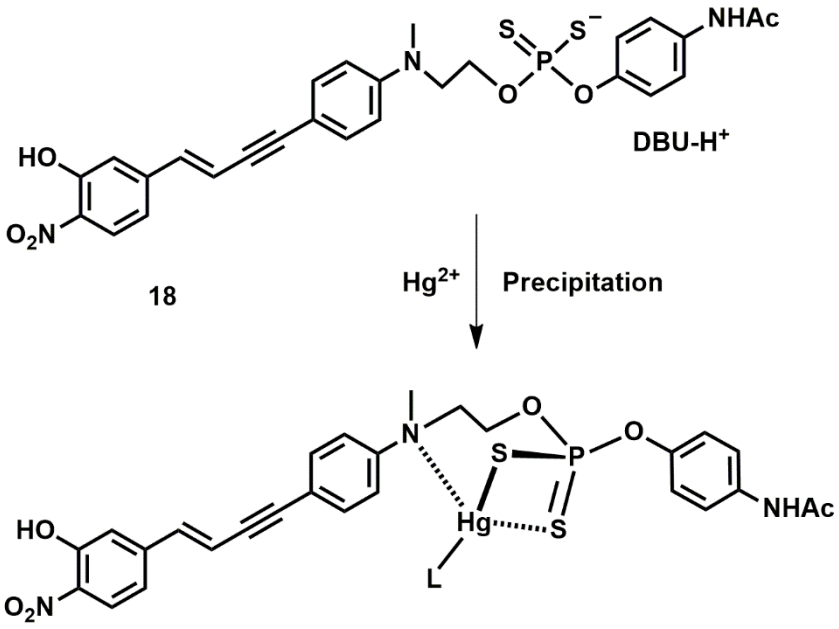

Janda *et al.* synthesized a chemosensor (sensor 18) containing phosphorodithioate and an adjacent amine group, which participates in charge transfer upon addition of Hg^{2+} and causes an instant change in the color of the solution from yellow to red, which is visible to the naked eye.[89] Although chemosensor solution showed a color change in the presence of a number of other metal ions, only Hg^{2+} causes immediate red color and bleaching the aqueous solution by precipitation of a 2:1 complex formed between sensor 18 and Hg^{2+}. The affinity of sensor 18 is highest for Hg^{2+} (dissociation constant, K_d =1.6 × 10^{-9} M) among all other metal ions, thus shows good selectivity for Hg^{2+} with an adequate detection limit of 1 μM of Hg^{2+}.

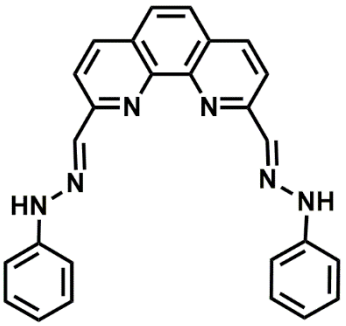

19

Sie *et al.* have reported a 1,10-phenanthroline based Schiff-base (sensor 19) as a colorimetric chemosensor for Hg^{2+} and Cu^{2+} in water containing 0.5% DMSO (v/v).[90] The addition of Hg^{2+} and Cu^{2+} to 19 causes a dramatic color change from yellow to red and yellow to orange respectively. From the absorption titration, the association constants for sensor 19-Hg^{2+} and sensor 19-Cu^{2+} were determined as 5.62×10^7 M^{-1} and 1.26×10^7 M^{-1}, respectively. A Job plot showed a 1:1 stoichiometric complexation of sensor 19 with Hg^{2+} and Cu^{2+} ions and was further confirmed by mass spectrometry. The detection limit of sensor 19 was determined as 0.19 ppm for Hg^{2+} ion and 0.39 ppm for Cu^{2+} ion.

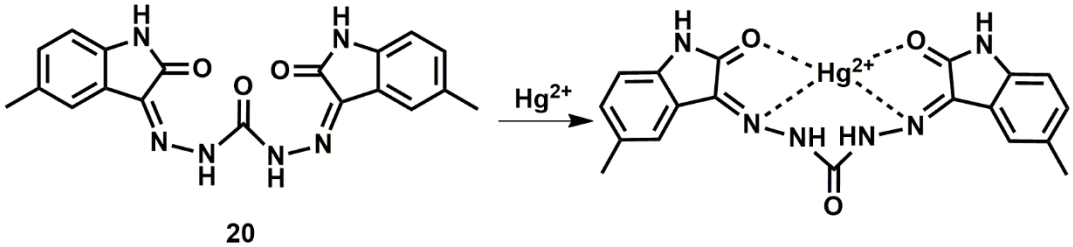

20

Trivedi *et al.* has developed an isatin based Schiff-base (sensor 20) chemosensor that enabled efficient complexation with Hg^{2+} in the preference to a variety of other common metal ions.[91] The color of the solution turned yellow to pink in DMSO upon complexation with Hg^{2+}, which is attributed to

MLCT charge transfer. TD-DFT calculations elucidated the complexation mode and the corresponding transition mechanism.

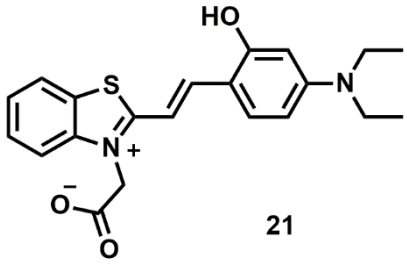

21

Palomares *et al.* has synthesized a chemosensor 21 consists of benzothiazolium as an acceptor and aniline as donor and for colorimetric selective detection of Hg^{2+} in EtOH/HEPPES buffer (1/10, v/v).[92] The addition of Hg^{2+} changes the color of the solution of 21 causes from pink to green which is attributed to ~100 nm blue-shift in the wavelength of maximum absorption. The sensor response to Hg^{2+} pH depended is optimal at pH 7. The stoichiometry of the complex formed between sensor **21**: Hg^{2+} is 1:1 as revealed by Job plot and the value of association constant calculated was 1.0×10^7 M^{-1}.

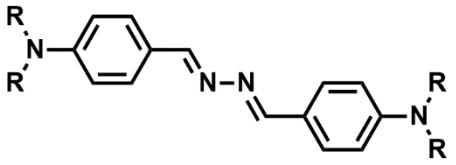

22. R= CH_2CH_3
23. R= C_6H_5

Hu *et al.* has designed chemosensors 22 and 23 for selective colorimetric detection of Hg^{2+}.[93] Addition of Hg^{2+} to 22 and 23 (ACN solution) results in a color changes from light yellow to red that is caused by ~100 nm red-shift in the wavelength of maximum absorption. The red color of solutions of 22/23 and Hg^{2+} disappearance upon addition of thiourea indicating the binding reversibility of sensor to Hg^{2+}. Job plot reveal formation of 1:1 complexes. ^1H NMR studies confirm that it is amine nitrogen atom which makes coordination to Hg^{2+}.

References

1 E. D. Harris, in *Encyclopedia of Metalloproteins*, eds. R. H. Kretsinger, V. N. Uversky and E. A. Permyakov, Springer New York, New York, NY, 2013, pp. 718–723.

2 W. Leong and B. Lönnerdal, in *Iron Physiology and Pathophysiology in Humans*, eds. G. J. Anderson and G. D. McLaren, Humana Press, 2012, pp. 81–95.

3 P. L. Fox and W. Churchill, *BioMetals*, 2003, **16**, 9–40.

4 S. Krupanidhi, A. Sreekumar and C. B. Sanjeevi, *Indian J. Med. Res.*, 2008, **128**, 448–461.

5 G. J. Anderson and C. D. Vulpe, *Cell. Mol. Life Sci.*, 2009, **66**, 3241–3261.

6 M. W. Hentze, M. U. Muckenthaler, B. Galy and C. Camaschella, *Cell*, 2010, **142**, 24–38.

7 M. Wessling-resnick, *Annu. Rev. Nutr.*, 2010, **30**, 105–122.

8 B. Halliwell, *J. Neurochem.*, 1992, **59**, 1609–1623.

9 D. Galaris, V. Skiada and A. Barbouti, *Cancer Lett.*, 2008, **266**, 21–29.

10 S. Swaminathan, V. A. Fonseca, M. G. Alam and S. V Shah, *Diabetes Care*, 2007, **30**, 1926–1933.

11 C. Clara and P. Erika, *Curr. Opin. Pediatr.*, 2011, **23**, 14–20.

12 R. Crichton, *Iron Metabolism – From Molecular Mechanisms to Clinical Consequences*, John Wiley & Sons, 4th edn., 2016.

13 X. Chen, X. Tian, I. Shin and J. Yoon, *Chem. Soc. Rev.*, 2011, **40**, 4783–4804.

14 S. Hu, P. Fürst and D. Hamer, *New Biol.*, 1990, **2**, 544—555.

15 P. Verwilst, K. Sunwoo and J. S. Kim, *Chem. Commun.*, 2015, **51**, 5556–5571.

16 S. R. Patil, J. P. Nandre, P. A. Patil, S. K. Sahoo, M. Devi, C. P. Pradeep, Y. Fabiao, L. Chen, C. Redshaw and U. D. Patil, *RSC Adv.*, 2015, **5**, 21464–21470.

17 J. Li, Y. Zeng, Q. Hu, X. Yu, J. Guo and Z. Pan, *Dalt. Trans.*, 2012, **41**, 3623–3626.

18 G. J. Brewer, *Curr. Opin. Chem. Biol.*, 2003, **7**, 207–212.

19 R. A. Løvstad, *Biometals*, 2004, **17**, 111–113.

20 Y. Shao, J. Wang, H. Wu, J. Liu, I. A. Aksay and Y. Lin, *Electroanalysis*, 2010, **22**, 1027–1036.

21 V. L. Goodman, G. J. Brewer and S. D. Merajver, *Endocr. Relat. cancer*, 2004, **11**, 255–263.

22 E. M. Nolan and S. J. Lippard, *Chem. Rev.*, 2008, **108**, 3443–3480.

23 T. Stafilov and I. Karadjova, *Maced. J. Chem. Chem. Eng.*, 2009, **28**, 17–31.

24 A. P. S. Gonzáles, M. A. Firmino, C. S. Nomura, F. R. P. Rocha, P. V Oliveira and I. Gaubeur, *Anal. Chim. Acta*, 2009, **636**, 198–204.

25 N. Pourreza and R. Hoveizavi, *Anal. Chim. Acta*, 2005, **549**, 124–128.

26 J. Otero-Romaní, A. Moreda-Piñeiro, A. Bermejo-Barrera and P. Bermejo-Barrera, *Anal. Chim. Acta*, 2005, **536**, 213–218.

27 M. Wang, K.-H. Leung, S. Lin, D. S.-H. Chan, D. W. J. Kwong, C.-H. Leung and D.-L. Ma, *Sci. Rep.*, 2014, **4**, 6794.

28 J. S. Becker, A. Matusch, C. Depboylu, J. Dobrowolska and M. V Zoriy, *Anal. Chem.*, 2007, **79**, 6074–6080.

29 T. Kato, S. Nakamura and M. Morita, *Anal. Sci.*, 1990, **6**, 623–626.

30 T. Poursaberi, L. Hajiagha-Babaei, M. Yousefi, S. Rouhani, M. Shamsipur, M. Kargar-Razi, A. Moghimi, H. Aghabozorg and M. R. Ganjali, *Electroanalysis*, 2001, **13**, 1513–1517.

31 A. A. Ensafi, T. Khayamian, A. Benvidi and E. Mirmomtaz, *Anal. Chim. Acta*, 2006, **561**, 225–232.

32 J. Liang, S. Huang, D. Zeng, Z. He, X. Ji, X. Ai and H. Yang, *Talanta*, 2006, **69**, 126–130.

33 M. Ralle and S. Lutsenko, *BioMetals*, 2009, **22**, 197–205.

34 C. J. Fahrni, *Curr. Opin. Chem. Biol.*, 2007, **11**, 121–127.

35 M. Morello, A. Canini, P. Mattioli, R. P. Sorge, A. Alimonti, B. Bocca,

G. Forte, A. Martorana, G. Bernardi and G. Sancesario, *Neurotoxicology*, 2008, **29**, 60–72.

36 N. Kapp, D. Studer, P. Gehr and M. Geiser, in *Electron Microscopy: Methods and Protocols*, ed. J. Kuo, Humana Press, Totowa, NJ, 2007, pp. 431–447.

37 A. W. Czarnik, in *Interfacial Design and Chemical Sensing*, eds. T. E. Mallouk and D. J. Harrison, American Chemical Society, Washington, DC, 1994, pp. 314–323.

38 M. Y. Chae and A. W. Czarnik, *J. Am. Chem. Soc.*, 1992, **114**, 9704–9705.

39 V. Dujols, F. Ford and A. W. Czarnik, *J. Am. Chem. Soc.*, 1997, **119**, 7386–7387.

40 B. Valeur and I. Leray, *Coord. Chem. Rev.*, 2000, **205**, 3–40.

41 D. T. Quang and J. S. Kim, *Chem. Rev.*, 2010, **110**, 6280–6301.

42 C. Suksai and T. Tuntulani, *Chem. Soc. Rev.*, 2003, **32**, 192–202.

43 R. Martínez-Máñez and F. Sancenón, *Chem. Rev.*, 2003, **103**, 4419–4476.

44 H. Tsukube and S. Shinoda, *Chem. Rev.*, 2002, **102**, 2389–2404.

45 L. Pu, *Chem. Rev.*, 2004, **104**, 1687–1716.

46 M. Inouye, K. ichi Hashimoto and K. Isagawa, *J. Am. Chem. Soc.*, 1994, **116**, 5517–5518.

47 A. Metzger and E. V Anslyn, *Angew. Chemie Int. Ed.*, 1998, **37**, 649–652.

48 K. Niikura, A. Metzger and E. V Anslyn, *J. Am. Chem. Soc.*, 1998, **120**, 8533–8534.

49 S. L. Wiskur and E. V Anslyn, *J. Am. Chem. Soc.*, 2001, **123**, 10109–10110.

50 Z. Zhong and E. V Anslyn, *J. Am. Chem. Soc.*, 2002, **124**, 9014–9015.

51 A. S. Pimentel, C. R. W. Guimarães and Y. Miller, 2013, **2013**, 2–4.

52 A. Krylov, T. L. Windus, T. Barnes, E. Marin-Rimoldi, J. A. Nash, B. Pritchard, D. G. A. Smith, D. Altarawy, P. Saxe, C. Clementi, T. D. Crawford, R. J. Harrison, S. Jha, V. S. Pande and T. Head-Gordon, *J.*

Chem. Phys., 2018, **149**, 180901.

53 G. Ambrosi, M. Formica, V. Fusi, L. Giorgi, E. Macedi, M. Micheloni, P. Paoli, R. Pontellini and P. Rossi, *Inorg. Chem.*, 2010, **49**, 9940–9948.

54 B. Kaur, N. Kaur and S. Kumar, *Coord. Chem. Rev.*, 2018, **358**, 13–69.

55 M. R. Wasielewski, *Chem. Rev.*, 1992, **92**, 435–461.

56 F. Scandola, M. T. Indelli, C. Chiorboli and C. A. Bignozzi, *Top. Curr. Chem.*, 1990, 73–149.

57 G. J. Kaoarnos, *Fundamentals of photoinduced electron transfer*, VCH, New York, 1993.

58 R. A. Bissell, A. Prasanna de Silva, H. Q. Nimal Gunaratne, P. L. Mark Lynch, G. E. M. Maguire, C. P. McCoy and K. R. A. Samankumara Sandanayake, *Top. Curr. Chem.*, 1993, 223–264.

59 P. Ghosh, P. K. Bharadwaj, J. Roy and S. Ghosh, *J. Am. Chem. Soc.*, 1997, **119**, 11903–11909.

60 K. Kubo., in *Advanced Concepts in Fluorescence Sensing Part A: Small Molecule Sensing*, eds. C. D. Geddes and J. R. Lakowicz, Springer, New York, 1st edn., 2005, vol. 9, pp. 219–243.

61 D. Rehm and A. Weller, *Isr. J. Chem.*, 1970, **8**, 259–271.

62 P. Carol, S. Sreejith and A. Ajayaghosh, *Chem. – An Asian J.*, 2007, **2**, 338–348.

63 M. Caricato, C. Coluccini, D. A. Vander Griend, A. Forni and D. Pasini, *New J. Chem.*, 2013, **37**, 2792–2799.

64 E. Hrishikesan and P. Kannan, *Inorg. Chem. Commun.*, 2013, **37**, 21–25.

65 E. M. Lee, S. Y. Gwon and S. H. Kim, *Spectrochim. Acta Part A Mol. Biomol. Spectrosc.*, 2014, **120**, 646–649.

66 R. Rani, K. Paul and V. Luxami, *New J. Chem.*, 2016, **40**, 2418–2422.

67 J. R. Lakowicz, *Principles of Fluorescence Spectroscopy*, Springer, New York, 3rd edn., 2006.

68 K. E. Sapsford, L. Berti and I. L. Medintz, *Angew. Chemie Int. Ed.*, 2006, **45**, 4562–4589.

69 Z. X. Han, X. B. Zhang, Z. Li, Y. J. Gong, X. Y. Wu, Z. Jin, C. M. He,

L. X. Jian, J. Zhang, G. L. Shen and R. Q. Yu, *Anal. Chem.*, 2010, **82**, 3108–3113.

70 C. Y. Li, Y. Zhou, Y. F. Li, C. X. Zou and X. F. Kong, *Sensors Actuators B Chem.*, 2013, **186**, 360–366.

71 L. Lan, Q. Niu, Z. Guo, H. Liu and T. Li, *Sensors Actuators B Chem.*, 2017, **244**, 500–508.

72 Z. Guo, Q. Niu and T. Li, *Spectrochim. Acta Part A Mol. Biomol. Spectrosc.*, 2018, **200**, 76–84.

73 M. H. Lee, T. Van Giap, S. H. Kim, Y. H. Lee, C. Kang and J. S. Kim, *Chem. Commun.*, 2010, **46**, 1407–1409.

74 M. Zhang, Y. Gao, M. Li, M. Yu, F. Li, L. Li, M. Zhu, J. Zhang, T. Yi and C. Huang, *Tetrahedron Lett.*, 2007, **48**, 3709–3712.

75 J. Li, Q. Hu, X. Yu, Y. Zeng, C. Cao, X. Liu, J. Guo and Z. Pan, *J. Fluoresc.*, 2011, **21**, 2005.

76 T. Nandhini, P. Kaleeswaran and K. Pitchumani, *Sensors Actuators B Chem.*, 2016, **230**, 199–205.

77 M. S. Kim, S. Y. Lee, J. M. Jung and C. Kim, *Photochem. Photobiol. Sci.*, 2017, **16**, 1677–1689.

78 H. J. Jang, T. G. Jo and C. Kim, *RSC Adv.*, 2017, **7**, 17650–17659.

79 C. H. Min, S. Na, J. E. Shin, J. K. Kim, T. G. Jo and C. Kim, *New J. Chem.*, 2017, **41**, 3991–3999.

80 A. K. Manna, K. Rout, S. Chowdhury and G. K. Patra, *Photochem. Photobiol. Sci.*, 2019, **18**, 1512–1525.

81 D. Jiang, X. Xue, G. Zhang, Y. Wang, H. Zhang, C. Feng, Z. Wang and H. Zhao, *J. Mater. Chem. C*, 2019, **7**, 3576–3589.

82 M. S. Kim, T. G. Jo, M. Yang, J. Han, M. H. Lim and C. Kim, *Spectrochim. Acta Part A Mol. Biomol. Spectrosc.*, 2019, **211**, 34–43.

83 H. Wang, L. Yang, W. Zhang, Y. Zhou, B. Zhao and X. Li, *Inorganica Chim. Acta*, 2012, **381**, 111–116.

84 B. Cao, Q. Hu, Y. Huang, C. Jia and Q. Zhang, *Chem. Res. Chinese Univ.*, 2013, **29**, 419–423.

85 Y. Wang, H. Wu, W. N. Wu, S. J. Li, Z. H. Xu, Z. Q. Xu, Y. C. Fan, X.

L. Zhao and B. Z. Liu, *Sensors Actuators B Chem.*, 2018, **260**, 106–115.

86 B. Mondal, S. Lohar, S. Pal, A. Maji and P. Chattopadhyay, *J. Indian Chem. Soc.*, 2015, **92**, 1–8.

87 J. Jayabharathi, V. Thanikachalam, M. V. Perumal and N. Srinivasan, *Spectrochim. Acta Part A Mol. Biomol. Spectrosc.*, 2011, **83**, 200–206.

88 A. P. de Silva, D. B. Fox, A. J. M. Huxley and T. S. Moody, *Coord. Chem. Rev.*, 2000, **205**, 41–57.

89 J. J. La Clair and K. D. Janda, *Org. Lett.*, 1999, 1996–1999.

90 Y. Sie, C. Li, C. Wan, J. Chen, C. Hu, H. Yan and A. Wu, *Inorganica Chim. Acta*, 2017, **467**, 325–329.

91 A. Krishna, V. Tekuri, M. Mohan and D. R. Trivedi, *Sensors Actuators B. Chem.*, 2019, **284**, 271–280.

92 S. Tatay, P. Gaviña, E. Coronado and E. Palomares, *Org. Lett.*, 2006, **8**, 3857–3860.

93 Y. Fu, H. Li and W. Hu, *European J. Org. Chem.*, 2007, **2007**, 2459–2463.

Chapter 2

Experimental Methods

This chapter comprises the experimental techniques which have been used to accomplish the research work present in this thesis. I will mainly describe the basic theory, working principle, and instrumental setup details of the spectrophotometer, spectrofluorimeter, infrared spectrometer, nuclear magnetic resonance spectrometer, and mass spectrometer. A discussion on the usage of density function theory is also provided in detail.

2.1 Steady state absorption measurement using spectrophotometer

Ultraviolet (UV) and visible (Vis) radiation constitutes a portion of electromagnetic spectrum with wavelength region ranges from 190 nm to 800 nm. Photons of this region possess sufficient energy for the promotion of electrons in atoms and molecules from a ground state energy level to a state of higher energy level.[1]

In case of atoms, highly narrow spectral bands are observed as a result of the electronic transitions. The energy difference between these levels is highly characteristic to the wavelengths corresponding to these narrow bands.[2,3] However, for molecules, super imposition of vibrational and rotational energy levels on the electronic energy levels causes broadening of absorption bands as shown in typical Jablonski diagram (see Figure 2.1).[4] Here for simplicity, I neglected the rotational energy levels in the illustrated Jablonski diagram.

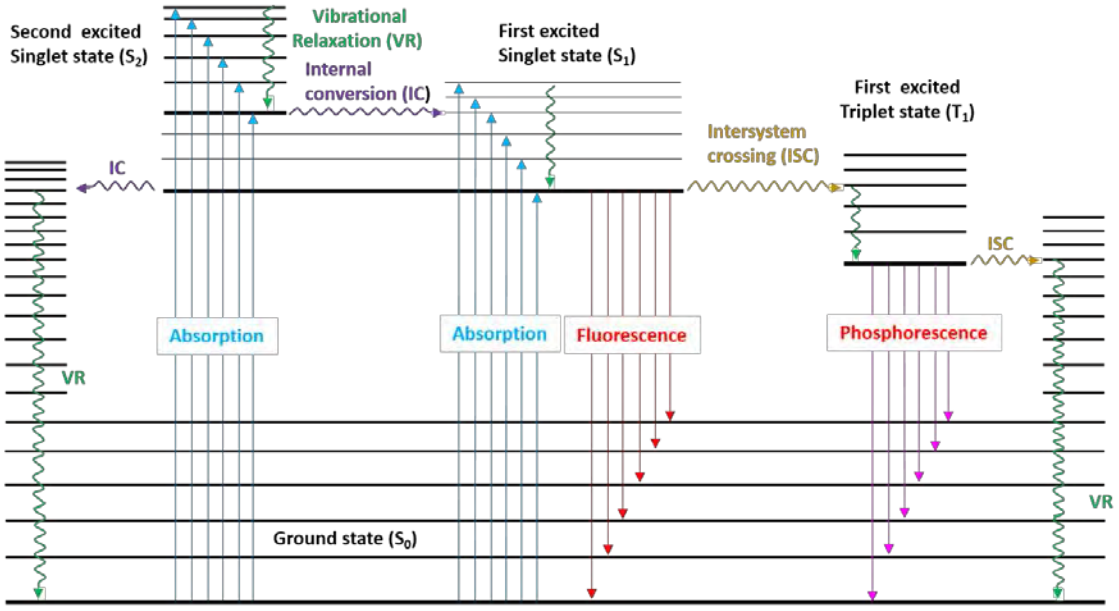

Figure 2.1 Jablonski diagram

The solvent-solute interactions present in the solution also contribute to the broadening of absorption spectra to great extent. There are several other parameters like temperature and pH which affect the absorption profile of a

molecule. The electronic energy levels of a chromophore come closer in the presence of conjugation which not only results in a bathochromic shift but also intensify the absorption band. UV-Visible spectra of chromophores produce only a few broad bands. Therefore, the amount of qualitative information provided by UV-Visible spectroscopy is limited and as a consequence makes the complete identification of an unknown molecule impossible. The most relevant equation associated with the absorbance of a material is the Beer-Lambert law[5] which is described as,

$$A(\lambda) = log\frac{I^0}{I} = \varepsilon(\lambda)cl \qquad \ldots\ldots\ldots (2.1)$$

Where A is absorbance or optical density, I^0 and I denotes the intensity of incident light and intensity of light transmitted through the solution. $\varepsilon(\lambda)$ is the molar absorption coefficient (in L mol^{-1} cm^{-1}), c is the concentration (in mol L^{-1}) of absorbing species and l is the absorption path length (in cm).

For carrying out steady state absorption measurements in this thesis, I have used a commercial spectrophotometer, Schimadzu 2450 from Japan which is a conventional dual-beam spectrophotometer. The basic optical system design of daul-beam spectrophotometer (see Figure 2.2) consist of light source, monochromator (see Figure 2.3), sample holder, detector and other necessary optical accessories. A deuterium-discharge lamp is used as source of UV radiation (180-400 nm) whereas a tungsten-filament lamp is used for visible region (400-800 nm). The light is passes through a filter and Monocromator which disperse the radiations in to its component wavelengths. A rotating chopper having transparent, mirror, and opaque parts was placed in the optical path. This chopper rotates at an optimal speed in a synchronized way which switches the path of light between a reference and sample to the photomultiplier tube (PMT). This alternate the measurements of transmitting photons from reference and sample occur several times per second, thus correcting the drift

in lamp intensity. The UV-Visible spectrum is recorded as a XY-plot where X-axis is wavelength of absorbed radiation and Y-axis represent the absorbance.

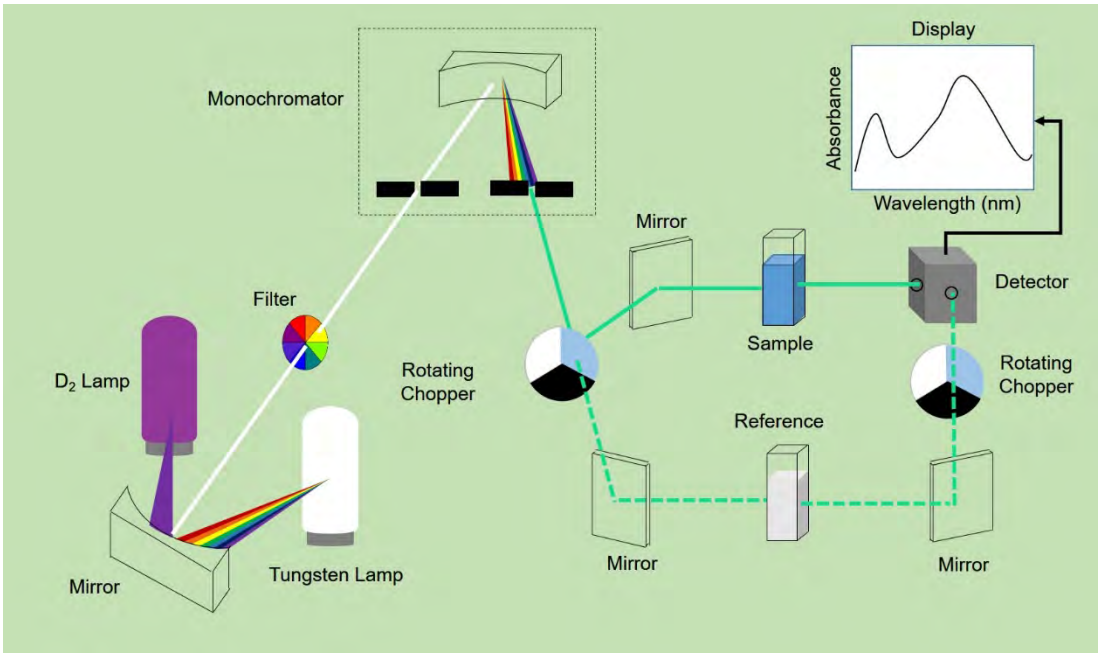

Figure 2.2 Schematic representation of a dual beam UV-Visible spectrophotometer.

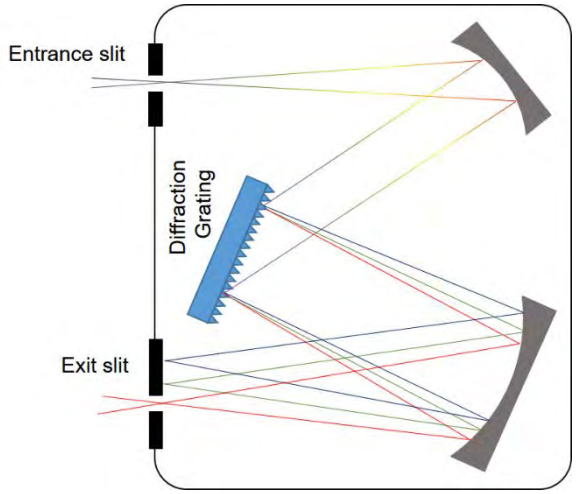

Figure 2.3 Schematic diagram of optical representation of monochromator.

2.2 Steady state fluorescence measurement using spectrofluorimeter

Following the absorption of light, molecules undergo several processes while returning from excited electronic state to the ground electronic state.[6,7] Molecules emitting light from an excited singlet state while coming back to the ground state results in fluorescence, are called fluorophores. Excitation can send a fluorophore to some higher vibrational levels of either S_1 or other higher electronic levels.

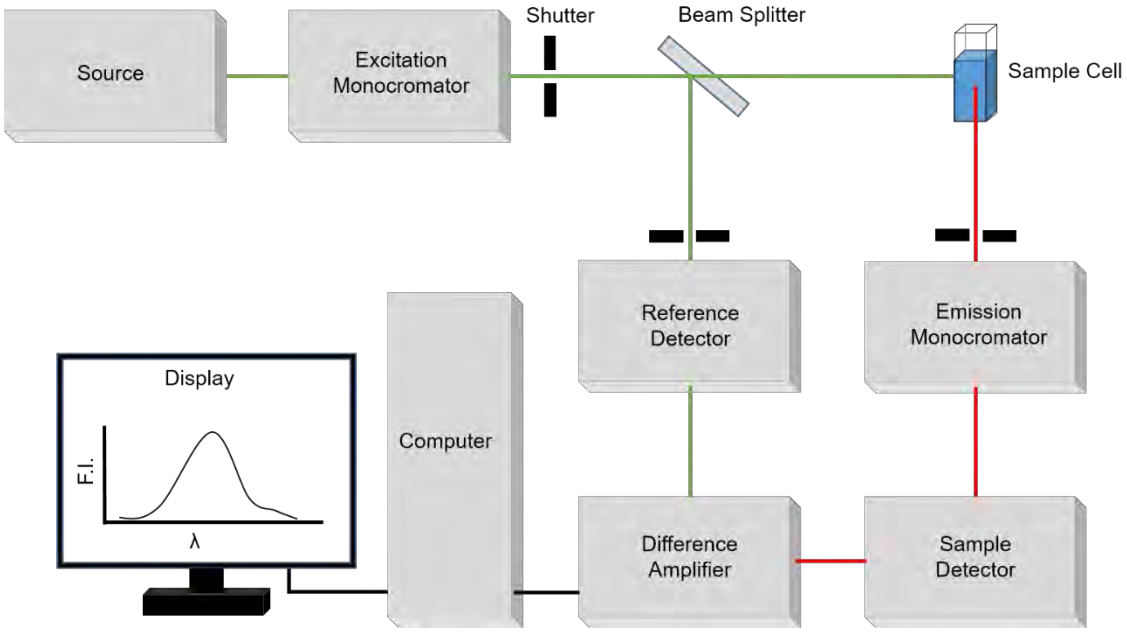

Figure 2.4 Schematic diagram of Spectrofluorimeter. (Acronym: F.I.= fluorescence Intensity)

Apart from some exceptional cases, these molecules quickly relaxed back to lowest vibrational level of S_1 electronic states by a non-radiative process called internal conversion.[8] Therefore, we usually get fluorescence spectra as a result of radiative relaxation from the lowest vibration level of S_1 electronic state to the ground electronic state S_0.

A commercial spectrofluorimeter (Fluoromax-4, Jobin Yvon, USA) was used for steady state fluorescence measurements. A schematic representation of basic components of spectrofluorimeter is illustrated in Figure 2.4. The general setup of spectrofluorimeter equipped with a 75-450 W high-pressure

xenon lamp which is a more intense continuous source of exciting light, an excitation monochromator, a beam splitter, a sample chamber, shutters, an emission monochromator, and photomultiplier tubes to collect the emitted photons. A beam splitter is placed in the path of excitation light which reflects part of the excitation light to a reference cell. A drift in the intensity of the light source is corrected by division of the intensity from the sample by that of the reference. The spectrometer has an amplifier which automatically quantify the signal from PMT. The output is usually recorded as a plot of wavelength distribution against the number of fluorescence photons generated by a fluorophore.

2.3 Infrared spectrometer

Infrared (IR) spectroscopy is one of the most common and widely used spectroscopic techniques. IR spectroscopy deals with the absorption of electromagnetic radiation in infrared region. The molecular absorption of infrared radiation takes place by quantized vibrational and rotational energy transition to higher energy states as shown in Figure 2.5.[9] Thus IR spectrum is also referred as vibrational rotational spectrum.

Unlike UV spectra, which contain only few broad absorption bands, IR spectra have comparatively many sharp absorption bands and therefore provide different structural parameters of a molecule. Different bands observed in an IR spectrum correspond to specific bonds present in a molecule. Thus, IR spectroscopy is largely used for the detection of functional groups and identification of molecules.[10] For the IR active molecules, electric dipole moment of the molecules must change as a result of the vibration that occurs when IR radiation is absorbed. Dipole moment is a vector quantity and depends on the orientation of the molecule and the photon electric vector.

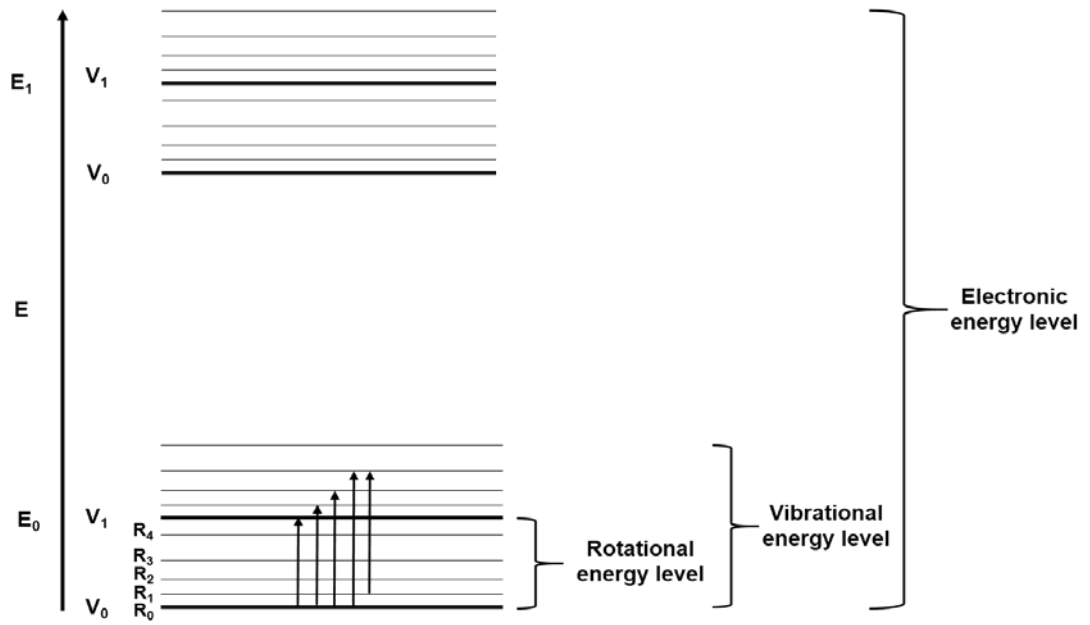

Figure 2.5 Schematic diagram of energy levels for a molecule and possible rotational-vibrational transitions.

The transition probability between two states is given by transition moment integral, which is written as[11]

$$\langle \psi_i | \hat{M} | \psi_f \rangle \quad \ldots\ldots\ldots (2.2)$$

Here i and f represent initial and final states, respectively. ψ is the wave function and $\hat{M}$ is the dipole moment. The intensity of IR radiation of absorption, I_{IR} is related to the transition moment integral as

$$I_{IR} \propto \langle \psi_i | \hat{M} | \psi_f \rangle \quad \ldots\ldots\ldots (2.3)$$

A commercial IR spectrometer (Bruker Tensor 27 IR, USA) was used for IR measurements, which a design of optical pathway has produced a pattern called interferogram. It is a plot of intensity versus time (a time domain signal), which can be converted into frequency domain by using a mathematical operation known as Fourier transformation (FT). This type of instruments is called Fourier transform infrared spectrometer or FT-IR.

A schematic layout of basic FT-IR spectrometer is illustrated in Figure 2.6 which consists of an IR source, interferometer, sample compartment, IR

detector, electric amplifier, Analog to digital convertor, and a computer.

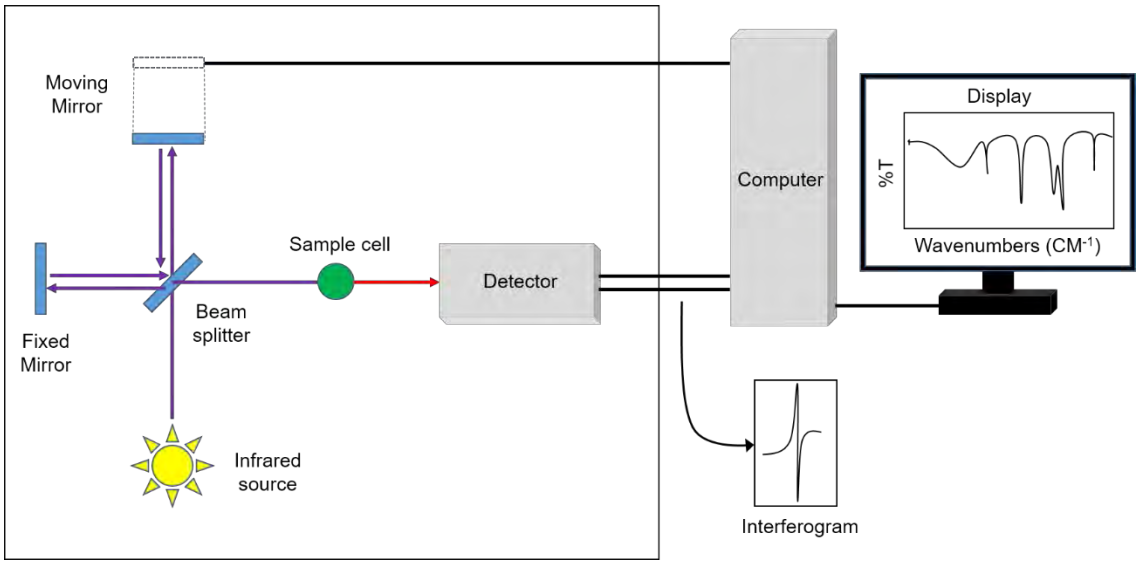

Figure 2.6 Schematic representation of basic component of FT-IR spectrometer. (Acronym: %T= Percentage Transmittance)

Infrared radiation source is usually produced by a Nernst filament or globar lamp. An interferometer is employed to process the energy sent to the sample. In the interferometer, the IR radiations pass through a beam splitter, which separate the incoming beam into two perpendicular beams one in same direction, and another is oriented at 90^{o}. One beam which is oriented at 90^{o} goes to a fixed mirror and is reflect to the beam splitter. The undeflected beam also return to the beam splitter after reflecting to a moving mirror. The moving mirror is used to vary the path travelled by the second beam. When both beams return and combine at the beam splitter, the different path length traveled by the beams causes constructive and destructive interferences. The combined beam containing this interference pattern is called interferogram. This interferogram contains all of the radiative energy and a wide range of wavelength coming from the source. As it passes through the samples, the samples simultaneously absorb all the wavelength. A detector collected the signal from the modified interferogram comprises details about the radiation intensity absorbed at every wavelength. A computer then uses a reference laser beam to compare it with the modified interferogram to generate a processed

interferogram that contains all of the information in time domain. A computer also extracts all absorbed frequency components by implemented Fourier transformation from time domain to frequency domain and reconstruct typical infrared spectrum.

2.4 Nuclear magnetic resonance spectrometer

NMR is another most important and powerful spectroscopic method which gives us information about the types of magnetically distinct atoms as well as the nature of the chemical environment adjacent to every distinct atom type. The magnetic property of atomic nuclei play a key role in NMR spectroscopy.[12] NMR activity is exhibited by atomic nuclei having either odd atomic number, odd mass number or both and hence possesses magnetic moment and a spin angular momentum. The basic principle of NMR is described as a condition when the frequency of the rotating magnetic field becomes equal to the frequency of the processing nucleus. This condition is called resonance and is governed by the following equation:[13]

$$\upsilon = \left(\frac{\gamma}{2\pi}\right) B_0 \qquad \ldots\ldots\ldots (2.4)$$

Here υ the frequency of radiation is absorbed during the transition from one spin state to the other, γ is magnetogyric ratio, and $B_0$is applied magnetic field. The basic components of a NMR spectrometer is shown in Figure 2.7 which includes a strong magnet with a homogeneous field whose field strength can be varied as much as 20 ppm with the help of sweep generator by changing the current through it. This instrument also equipped with a transmitter coil provided in the gap between magnet poles and attached to the radio frequency transmitter. A receiver coil is provided perpendicular to the transmitter coil which is connected to the radio frequency receiver or detector which is further connected to a recorder.

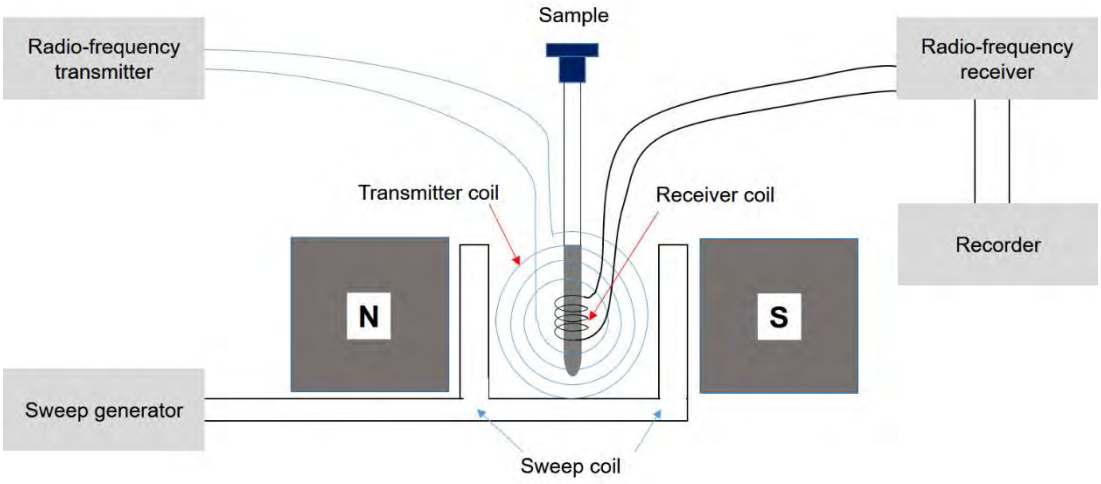

Figure 2.7 Schematic diagram of NMR spectrometer.

The sample cell (NMR tube) filled with 0.4 ml of sample is placed inside a sample holder and is irradiated by constant radio frequency beam generated by radio frequency transmitter. By increasing the strength of the magnetic field, the precession frequency of every proton increase. When the precession frequency of any proton becomes equal to incident radio frequency, they are said to be in resonance and absorption of energy takes place. As a result, a signal is received by the detector which is amplified and recorded as a peak. Proton NMR (^{1}H NMR) and ^{13}C NMR are the two famous NMR techniques.

2.5 Mass spectrometer

Mass spectrometry is a powerful and robust analytical technique used to quantify target compound, to identify unknown sample, and to solve the structure of different molecules.[14] Q–Tof Premier™ API tandem mass spectrometer is used for our studies in this thesis. The basic configuration of a quadrupole-Time of Flight (Q-TOF) mass spectrometer consists of an ion source, a quadrupolar mass filter, a quadrupolar collision cell, a TOF analyzer, reflectrons, detector, a data system or personal computer, and other necessary optics accessories as shown in Figure 2.8.

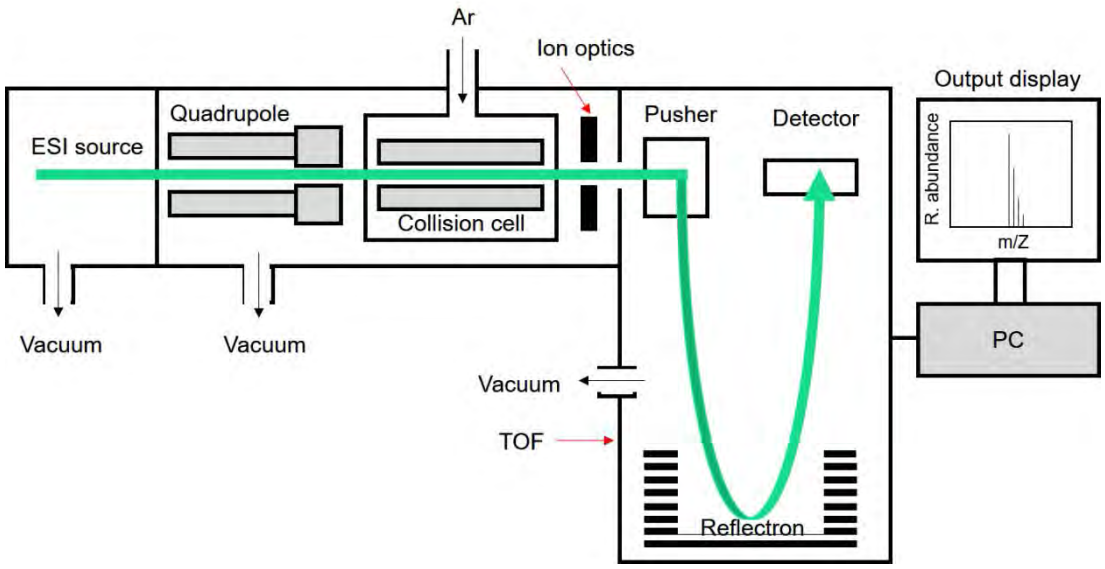

Figure 2.8 Schematic representation of quadrupole-Time of Flight (Q-TOF) mass spectrometer.

Many types of ion source can be interfaced with a Q-TOF mass spectrometer but for our studies we used an ion source based on electrospray ionization - a soft ionization technique whose schematic working mechanism is illustrated in Figure 2.9. Ions produce in the high pressure ion source enters in to a mass filter where ions are selected by their *m/z* ratio.[15] The ions are then accelerated to a higher kinetic energy before entering the collision cell where the ions undergoes collision with a neutral gas (Ar / N_2) and subjected to collision induced dissociation (CID). Both the quadrupoles are working in radiofrequency (RF) mode only. After leaving the collision cell, ions pass through an ion optics where ion beam is shaped in to nearly parallel beam. This parallel ion beam enters in to the orthogonal time-of-flight mass analyzer, where this ion beam first passes through a pusher. Pusher accelerate the ions beam and make them travel through the flight tube. There is a reflectron (ion mirror) placed at the opposite end of the flight tube that reflects the ions towards the detector. The mass spectrum data is recorded with the help of computer which a graph plotted relative abundance as Y-axis and *m/z* as X-axis.

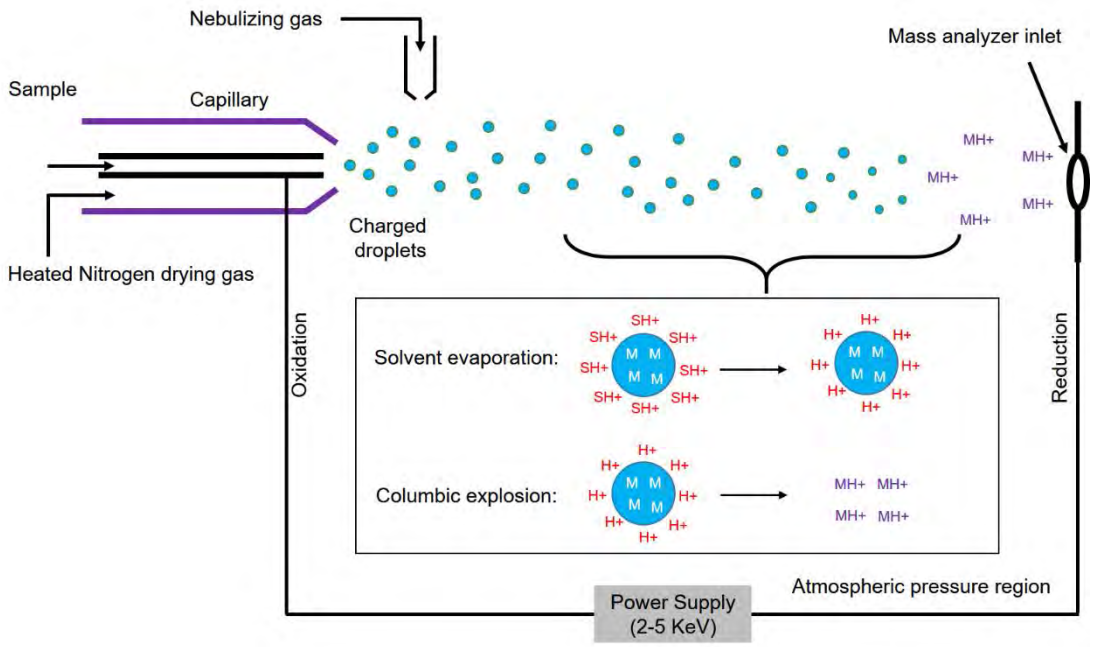

Figure 2.9 Schematic representation of Electrospray Ionization chamber

This hybrid configuration achieved by the addition of two quadrupole and a TOF give this instruments a combination of high mass accuracy and high sensitivity at the same time.

For theoretical mass calculations we have used a freeware software tool called “molecular weight calculator” version 6.50, which generates an isotopic distribution for the molecular formula we entered. We then try to overlap these theoretical mass distribution with our experimental mass distribution.

2.6 Quantum mechanical calculations

To compute the molecular properties efficiently, by means of computational methods have become one of the growing field of interest. It is an efficient and successful approach to compute molecular structures, vibrational frequencies, and total energy of the system. A deep insight of the chemical properties such as reactivity of the ligands in a structural framework, mechanism of complex formation and its effect on physical properties such as absorbance and fluorescence require an efficient computational methodology.

Therefore, one should always keep in mind to achieve better accuracy at a reasonable computational cost while choosing the computational methods. In this thesis, we have computed ground state properties of the concern chemical systems by solving a time-independent Schrödinger equation within the framework of non-relativistic and Born-Oppenheimer approximations.

$$\hat{H}\Psi = E\Psi \qquad \ldots\ldots\ldots (2.5)$$

Here H is a Hamiltonian operator and Ψ is a wave function that describes the state of the system.

Density functional theory (DFT) is one of the efficient computational method and has become a widely accepted tool for understanding many atomic-level intricate processes and therefore, its application is growing rapidly. Hohenberg and Kohn, in 1964 formulized two captivating theorems[16] that helped DFT to achieve a status of completely established theory. The first theorem[17] states that the ground-state electron density of a nondegenerate system , $\rho(r)$, determines the external potential, $v(r)$. The total number of electrons of a system is determined by $\rho(r)$ via normalization. The second theorem states that the ground-state density of a nondegenerate system can be computed variationally with a given trial density. These two theorems proposed by Hohenberg and Kohn are the heart of the DFT:

$$\delta\left[E[\rho] - \mu\left(\int \rho(r)dr - N\right)\right] = 0 \qquad \ldots\ldots\ldots (2.6)$$

Here the functional, $E[\rho]$ is independent of the external potential for a particular system of interest and can be inserted into the above equation (only if its form is known) to obtain the exact energy and density of that particular system. μ is the Lagrangian multiplier and is also known as the chemical potential of a system.Thus, for the Schrödinger equation 2.5, energy functional, $E[\rho]$can be defined as the sum of three terms:

$$E[\rho] = T[\rho] + V_{ext}[\rho] + V_{ee}[\rho] \quad \ldots\ldots\ldots (2.7)$$

Here $T[\rho]$is the kinetic energy, V_{ext} is the external potential and V_{ee} is electron-electron interaction.

The formulation of the kinetic energy functional, explicitly in terms of density is much more difficult and need some approximations. Similarly, the functional form of the electron-electron interaction terms is unknown. The dependence of the external potential term on the density is trivial and shown as:

$$V_{ext}[\rho] = \int \hat{V}_{ext}\, \rho(r) dr \quad \ldots\ldots\ldots (2.8)$$

In 1965, Kohn and Sham, [16] have successfully come forward with their new formulation of replacing the kinetic energy functional $T[\rho]$ of the interacting system with that of non-interacting ones and introduced the orbitals into the picture thereby computing the kinetic energy with good accuracy. The formulation is simple since these orbitals determines the density or vice-versa and functional form can be written as

$$T_s[\rho] = -\frac{1}{2}\sum_{i}^{N} \langle \phi_i | \nabla^2 | \phi_i \rangle \quad \ldots\ldots\ldots (2.9)$$

Here $T_s[\rho]$ is the kinetic energy functional of a non-interacting system.

$$\rho(r) = \sum_{i}^{N} |\phi_i|^2 \quad \ldots\ldots\ldots (2.10)$$

Considering the classical Coulomb interaction (Hartree energy), $V_H[\rho]$a significant component of electron-electron interaction, energy functional of equation 2.7 can be rearranged as;

$$E[\rho] = T_s[\rho] + V_{ext}[\rho] + V_H[\rho] + E_{xc}[\rho] \quad \ldots\ldots\ldots (2.11)$$

$$E_{xc}[\rho] = (T[\rho] - T_s[\rho]) + (V_{ee}[\rho] - V_H[\rho]) \quad \ldots\ldots\ldots (2.12)$$

Here $E_{xc}$is the exchange-correlation functional and is simply the sum of the error made in using a non-interacting kinetic energy and the error made in treating the electron-electron interaction classically. Rewriting energy functional (equation 2.11) by substituting the density of non-interacting electrons orbitals (equation 2.10) and applying the variational theorem (equation 2.6). We discover that the orbitals that minimize a system's energy fulfill the following non-linear set of equation

$$\left[-\frac{1}{2}\nabla^2 + v_{ext}(r) + \int \frac{\rho(r')}{|r-r'|}dr' + v_{xc}(r)\right]\phi_i(r) = \varepsilon_i\phi_i(r) \quad \ldots\ldots\ldots (2.13)$$

For a known exact energy functional, the orbitals provides the exact electronic density of ground state *via* equation 2.10 and exact ground state energy *via* equation 2.11.

2.6.1 Exchange-correlation functionals

The utility of density functional theory (DFT) depends on the approximation used for$E_{xc}[\rho]$. To formulate of the exact functional of the E_{xc} is a non-trivial task and in itself is a growing field of research. There are many different type of functional forms available with different suitability targeting the specific study. The judgment of their suitability depends upon the target properties (i.e. how good are the computed results compared to the experimental outcomes).

The Local density approximation (LDA) made a critical assumption that the density of a molecule is uniform throughout the molecule, however, the results obtained from LDA are not very satisfactory that's why this method is not very popular. There are methods which includes a gradient correction (GC) factor that looks to account for non-uniformity of electron density.

As the name suggests, hybrid methods incorporate some of the more useful features from Hartree-Fock methods along with some improvements of DFT mathematics. B3LYP is the most commonly used hybrid methods by

computational chemists. Axel Becke originally implemented this strategy in 1993.[18,19] B3LYP, which stands for Becke, 3 parameters, Lee- Yang-Parr, is one of the most frequently used variant of hybrid functional. The resultant exchange-correlation energy functional is

$$E_{xc} = E_{xc}^{LDA} + a_0(E_x^{HF} - E_x^{LDA}) + a_x \Delta E_x^{B88} + a_c \Delta E_c^{PW91} \quad \ldots\ldots\ldots (2.14)$$

Where a_0= 0.2, a_x = 0.72 and a_c = 0.81. ΔE_x^{B88} and $\Delta E_c^{PW91}$are widely used correction to LDA exchange and correlation energies respectively.[20] Here lower case *x* and *c* refers to determination of electron exchange[21] and electron correlation[22] respectively. This form of Hybrid functional are now widely used in chemical applications.

2.6.2 Basis Set Effects

In quantum chemistry, a basis set is a set of functions which are combined as linear combination (generally as a part of quantum chemical calculation) to create molecular orbital. These functions are typically centered on atoms as atomic orbitals. Quantum mechanical calculations are generally carried out using a finite set of basis functions. We used basis set 6-31+G.(d,p) and def2-TZVP for all the calculations discussed in this thesis.

2.6.3 Solvent effects

Understanding the effect of solvents is an important aspect in photochemistry as solvent properties have profound effects on the electronic absorbance and emission spectra of molecules. In computational chemistry, the use of self-consistent reaction-field (SCRF) continuum method is a common approach to consider these solvent effects where structure of the solvent is not taken into account explicitly. However, the quantitative treatment of the electronic structure of solute and evaluation of polarization effects are the key advantages of the SCRF model. There are several other methods which incorporate solvation effect through SCRF technique and gives special

attention to the calculation of Gibb's energy of solvation. The Polarizable Continuum Model (PCM) has been considered as a reliable tool for the description of electrostatic solute-solvent interactions among all the SCRF methods.[23] In this model, a solvent is considered as a dielectric continuum and the solute molecule placed in a cavity formed by an envelope of spheres. A dipole in the solute molecule induces a dipole in the dielectric (solvent) medium. The polarization of dielectric generates an electric field applied to the solute molecule by the solvent dipole and hence, modifying its electron density. This solute molecule-solvent interaction leads to net stabilization of the system. The way of efficiently modeling the solvent effects is the use of density functional theory (DFT) within continuum models for solvation.[24]

References

1 T. Owen, *Fundamental of Modern UV-Visible Spectroscopy*, Agilent Technology, Germany, 2000.

2 N. V Tkachenko, in *Optical spectroscopy: Methods and instrumentations*, Elsevier Science, Amsterdam, 1st edn., 2006, pp. 89–106.

3 C. N. Banwell, *Fundamentals of Molecular Spectroscopy*, McGraw-Hill, London, 3rd edn., 1983.

4 A. Jablonski, *Nature*, 1933, **131**, 839–840.

5 A. Rodger, in *Encyclopedia of Biophysics*, ed. G. C. K. Roberts, Springer Berlin Heidelberg, Berlin, Heidelberg, 2013, pp. 184–185.

6 J. R. Lakowicz, *Principles of Fluorescence Spectroscopy*, Springer, New York, 3rd edn., 2006.

7 B. Valeur, *Molecular Fluorescence: Principles and Applications*, Wiley-VCH, Weinheim, 2001.

8 T. Itoh, *Chem. Rev.*, 2012, **112**, 4541–4568.

9 L. J. Bellamy, *The infrared spectra of Complex Molecules*, John Wiley, New York, 3rd edn., 1975.

10 C. J. Pouchert, *Aldrich FT-IR Spectra*, Aldrich Chemical Co., Milwaukee, WI, 2nd edn., 1997.

11 and P. H. S. Nakanishi, K., *Infrared Absorption Spectroscopy*, Holden-Day, San Francisco, 2nd edn., 1998.

12 P. Crews, J. Rodriguez and M. Jaspars, *Organic Spectroscopy*, Oxford University Press, New York, 1998.

13 J. B. Lambert, H. F. Shurvell, D. A. Lightner and R. G. Cooks, *Introduction to Organic Spectroscopy*, PrenticeHall, Upper Saddle River, NJ, 1998.

14 E. de Hoffmann and V. Stroobant, *Mass Spectrometry Principles and Applications*, John Wiley & Sons, Ltd., West Sussex, England, 2007.

15 S. Banerjee and S. Mazumdar, *Int. J. Anal. Chem.*, 2012, 40.

16 R. M. Dreizler and E. K. U. Gross, *Density Functional Theory*, Springer-Verlag, Berlin, 1990.

17 W. Kohn and L. J. Sham, *Phys. Rev.*, 1965, **140**, A1133--A1138.

18 A. D. Becke, *J. Chem. Phys.*, 1993, **98**, 5648–5652.

19 A. D. Becke, *J. Chem. Phys.*, 1993, **98**, 1372–1377.

20 A. D. Becke, *Phys. Rev. A*, 1988, **38**, 3098–3100.

21 C. Lee, W. Yang and R. G. Parr, *Phys. Rev. B*, 1988, **37**, 785–789.

22 S. H. Vosko, L. Wilk and M. Nusair, *Can. J. Phys.*, 1980, **58**, 1200–1211.

23 J. Tomasi, B. Mennucci and R. Cammi, *Chem. Rev.*, 2005, **105**, 2999–3094.

24 R. J. Hall, M. M. Davidson, N. A. Burton and I. H. Hillier, *J. Phys. Chem.*, 1995, **99**, 921–924.

Chapter 3

Selective visual detection of Fe^{3+} at PPM level through 4-(pyridin-2-ylmethylene)amino)phenol (PYAP)

Md. Serajul Haque Faizi, Shradhey Gupta, Vaisakh Mohan K., **Vipin Kumar Jain**, Pratik Sen. *Sensors and Actuators B,* 2016, **222**, 15–20.

A new turn-on fluorescence sensor 4-((pyridin-2-ylmethylene)amino)-phenol (PYAP) has been developed for the detection of Fe^{3+}in methanol. About 200-fold increase in fluorescence intensity was observed for PYAP in presence of 2 equiv of Fe^{3+}. However, other metal ions e.g., Na^{+}, K^{+}, Ba^{2+}, Mg^{2+}, Al^{3+}, Cr^{3+},Co^{2+}, Ni^{2+}, Cu^{2+}, Zn^{2+}, Cd^{2+}, Pb^{2+} and Ag^{+} induced only a minor change in the fluorescence property for the PYAP. Interestingly, the detection limit was found to be in ppm level with a rapid response time of minutes. The naked eye low-level detection of Fe^{3+} ion by the occurrence of the red fluorescence makes PYAP a potential Fe^{3+}sensor in methanol. Moreover, the synthesis of this particular chemosensor is facile, scalable to multi gram quantity and also the starting materials are cheap, which makes this suitable for practical application compared to other Fe^{3+}sensors.

3.1 Introduction

The design and synthesis of highly selective chemosensors for metal ions, such as Cu^{2+}, Fe^{3+}, Zn^{2+}, Cd^{2+}, Mn^{2+}, Hg^{2+} and Pb^{2+}, have attracted a great deal of attention in the scientific community.[1–8] Among these important metal ions, the trivalent form of iron (Fe^{3+}) is the most essential trace element in biological systems, and it plays an important role in many biochemical processes at the cellular level.[9–12] It provides oxygen-carrying capacity to heme and acts as a cofactor in many enzymatic reactions involved in the mitochondrial respiratory chain.[13] Iron is indispensable for most of the organisms, and both its deficiency and surplus can induce various disorders in several iron-regulated processes.[14–17] Recent research suggests that Fe^{3+} could also be involved in the under-lying mechanisms of many neurodegenerative diseases, such as Parkinson's disease and Alzheimer's disease.[18]

In view of the wide role of Fe^{3+} ion, it is outmost necessary to efficiently estimate the concentration of iron metal ions. Researchers have developed several traditional methods of measuring iron ions, including atomic absorption spectrometry, inductively coupled plasma mass spectroscopy, inductively coupled plasma-atomic emission spectrometry, voltammetry and etc.[19–22] Although these methods are quantitative, they require sophisticated apparatus, and are not easily employed in on-site analysis. In recent times, fluorescence chemosensing of the metal ions has evolved to an extent with implications leading to very selective and ultrasensitive detection limits.[23–28] Unfortunately, there have been relatively less number of fluorescent chemosensors for detection of Fe^{3+} at ppm level, because of the fluorescent quenching by the paramagnetic nature of Fe^{3+} ion.[29–38] Therefore, the development of new fluorescent sensor for Fe^{3+}, especially those that are very selective, low cost, easily available and easily synthesized, is still a challenge.[39–41] Moreover, the fluorescence based sensing method is simple, inexpensive, rapid and more reliable for the specific ion detection. Thus, the synthesis of new chemosensors

capable of showing selective sensing properties with iron ions at ppm level is inevitable. Recently, Zaichenget al. reported the detection of Fe^{3+} through europium based metalorganic framework fluorescent probe with chelating terpyridine. In the past, there were several successful attempts to develop fluorescence sensor for Fe^{3+} ion.[29-41] However, the reaction schemes for the synthesis of such reported sensors are very complex, require extreme reaction conditions and are also expensive. On the other hand, phenol-based Schiff bases are known as good π-conjugated ligands for metal ions.[42–48] This work is ongoing part of our research interest.[49–52] In the present work, we have synthesized a Schiff base, 4-((pyridin-2-ylmethylene)amino)phenol (PYAP), which shows a very good chemosensing property to Fe^{3+}.

3.2 Experimental

3.2.1 Materials and methods

All the reagents are of analytical grades and used with-out further purification. The metal ion salts used in stock solutions were $NaNO_3$, KNO_3, $Ba(NO_3)_2$, $Mg(NO_3)_2{\cdot}6H_2O$, $Al(NO)_3{\cdot}9H_2O$, $Cr(NO_3)_3{\cdot}9H_2O$, $Co(NO_3)_2{\cdot}6H_2O$, $Ni(NO_3)_2{\cdot}6H_2O$, $Cu(NO_3)_2{\cdot}3H_2O$, $Zn(NO_3)_2{\cdot}6H_2O$, $Cd(NO_3)_2{\cdot}4H_2O$, $Pb(NO_3)_2$, $AgNO_3$ and $Fe(NO_3)_3{\cdot}9H_2O$. Solvents like acetone, acetonitrile, 1-butanol, ethanol and methanol are purchased from Alfa acer Chemical Co. and used as received except methanol was used after distillation over magnesium methoxide [$Mg(OCH_3)_2$]. Pyridine-2-carbaldehyde was purchased from Aldrich Chemical Co. and used as received. 4-Aminophenol purchased from Loba Chemie Pvt. Ltd., India. Infrared spectra were recorded on Perkin-Elmer Lambda 2 spectrometer with KBr discs in the range 4000–400 cm^{-1}. ESI-MS spectra were recorded on a Waters-HAB213 spectrometer. UV–vis absorption spectra of the samples were measured on a commercial spectrophotometer (UV2450, Schimadzu, Japan). Fluorescence spectra were measured on fluorimeter (Fluorolog 3-21, HoribaJobin-Yvon, USA).^{1}H NMR spectra were obtained on either a JEOL JNM LA (400 MHz)

or a JEOL LA 500FT (500 MHz) spectrometer.

3.2.2 General design of experiment

A stock solution of PYAP (0.2 mM) was prepared in acetone, acetonitrile, 1-butanol, ethanol, and methanol. Metal ion solutions (10 mM) of $NaNO_3$, KNO_3, $Ba(NO_3)_2$, $Mg(NO_3)_2 \cdot 6H_2O$, $Al(NO)_3 \cdot 9H_2O$, $Cr(NO_3)_3 \cdot 9H_2O$, $Co(NO_3)_2 \cdot 6H_2O$, $Ni(NO_3)_2 \cdot 6H_2O$, $Cu(NO_3)_2 \cdot 3H_2O$, $Zn(NO_3)_2 \cdot 6H_2O$, $Cd(NO_3)_2 \cdot 4H_2O$, $Pb(NO_3)_2$, $AgNO_3$ and $Fe(NO_3)_3 \cdot 9H_2O$ are prepared in acetone, acetonitrile, 1-butanol, ethanol, and methanol. The solution of each metal salts is diluted in diluted as per requirement of the experiment. A dilute solution of PYAP (10 µM) is prepared in each solvents then the ions were added. Absorbance and emission spectra for each sample prepared were recorded after a 1 min of incubation period.

3.2.3 Synthesis and characterization of PYAP

Synthesis of 4-((pyridin-2-ylmethylene)amino)phenol (PYAP) is summarized in Scheme 3.1. PYAP was prepared by condensation of 4-aminophenol and pyridine-2-carbaldehyde through nucleophilic substitution in a satisfactory yield.

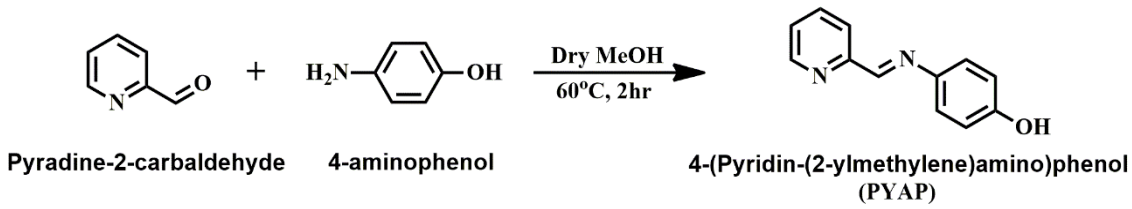

Scheme 3.1 Synthetic route of the imine based chemosensor PYAP

Briefly, pyridine-2-carbaldehyde (0.49 g, 4.50 mmol) was added drop wise to the methanolic solution (20 mL) of 4-aminophenol (0.50 g, 4.50 mmol) at room temperature. The yellow precipitate appeared within a minute and the reaction mixture was stirred for 2 h. The solvent was concentrated, filtered and washed with methanol (2 × 3 mL) and hexane (3 × 10 mL) respectively. A yellow solid powder was obtained which was recrystallized from methanol and

dried in vacuum desiccator. The reaction yield of PYAP was found to be 80% (0.73 g). FT-IR gives the clear evidence for the formation of our desired product; (KBr, cm^{-1}): $\nu_{O\text{-}H}$ 3443, $\nu_{HC\text{-}N}$ 1618, $\nu_{C\text{-}N}$ 1580(FT-IR spectrum of PYAP (see Figure 3.1). After the condensation reaction, the new peak at 1618 cm^{-1} indicates the formation of imine (CH=N) bond. Also, $-NH_2$ peaks of *p*-aminophenol and –C=O peak of pyridine-2-carbaldehyde disappear in the FT-IR spectrum of PYAP. The peak values of –OH, aromatic C-H and aromatic –C=C vibrations are seen at 3443, 3043 and 1542–1493 cm^{-1}, respectively. The purity and structure of PYAP was fully confirmed by ^{1}H NMR, ^{13}C NMR (see Figure 3.2) and ESI-MS spectra (see Figure 3.3). ^{1}H NMR (400 MHz, DMSO-d_6) δ (ppm) 9.64 (OH, br), 8.67 (d, J = 4.4 Hz, 1H), 8.59 (s, 1H, CH=N), 8.12 (t, J = 7.6 Hz, 1H), 7.90 (1H, t, J = 7.6 Hz), 7.46 (1H, t, J = 6.4 Hz) 7.29 (2H, d, J = 6.8 Hz), 6.83 (d, J = 6.8 Hz, 2H). ^{13}C NMR (100 MHz, DMSO-d_6, ppm): δ(ppm)= 115.83, 120.68, 122.93, 125.06, 136.87, 141.51, 149.54, 154.56, 156.94, 157.06. ESI-MS ($M+H^+$): Calculated 199.09; found 199.04. Melting point of PYAP is measured to be 195–197 °C. The reaction is facile, scalable to multi gram quantity and the starting materials are cheap.

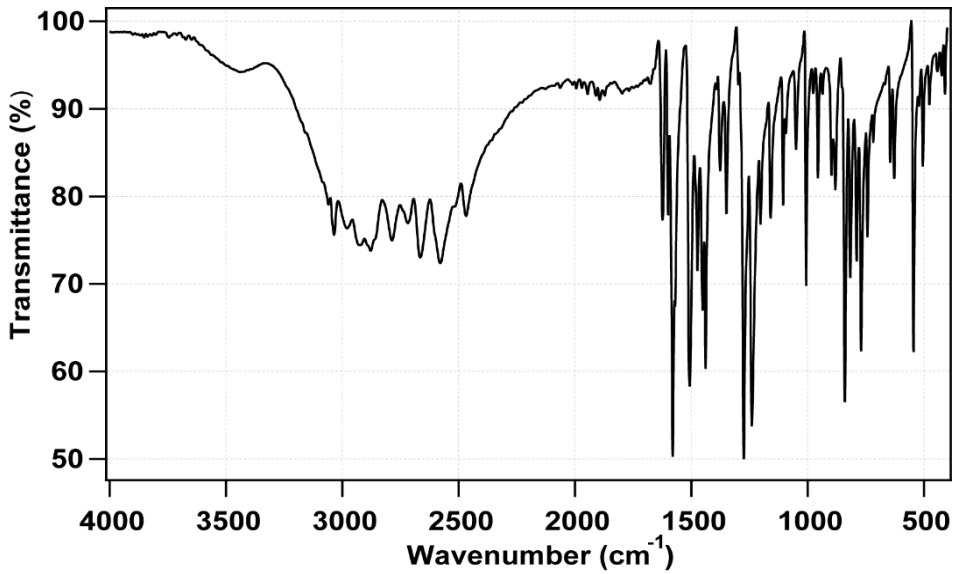

Figure 3.1 FT-IR spectrum of PYAP

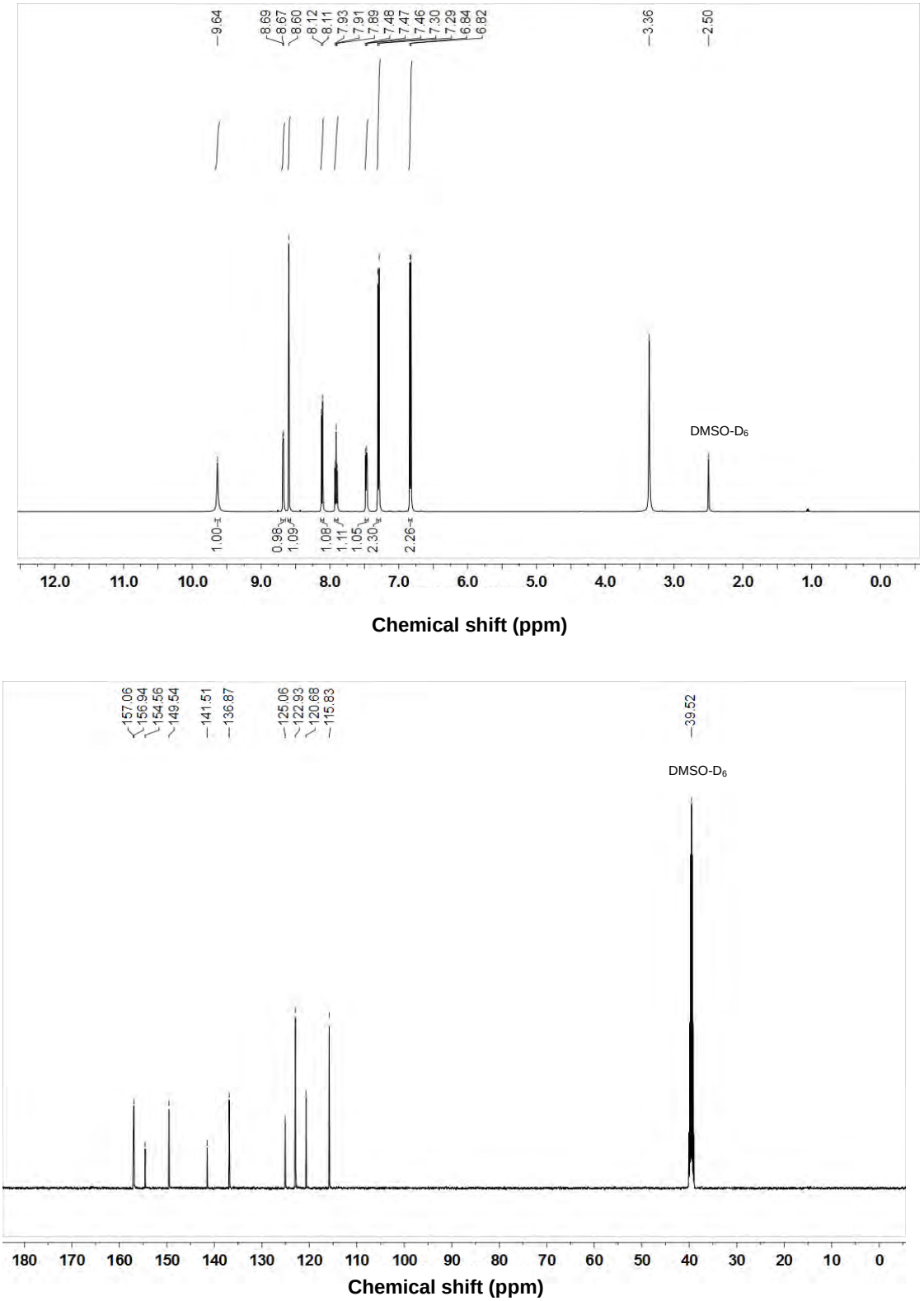

Figure 3.2 ^{1}H NMR spectrum of PYAP taken in DMSO-d_6. (b) ^{13}H NMR spectrum of PYAP taken in DMSO-d_6.

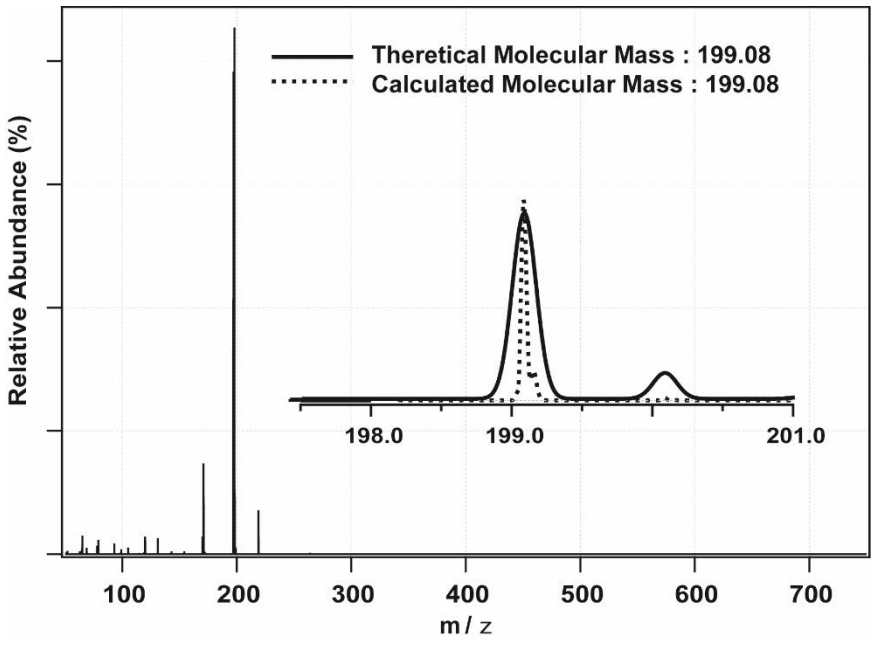

Figure 3.3 ESI-MS spectrum of PYAP (Inset: Theoretical mass spectrum).

3.3 Results and discussion

3.3.1 Synthesis and structural characterization of PYAP

The targeted sensor 4-((pyridin-2-ylmethylene)amino)phenol (PYAP) was easily synthesized by reaction of p-aminophenol and pyridine-2-carbaldehyde by the procedure as given in Scheme 3.1. Which are readily condensed at room temperature to give desired product. The structure of the sensor PYAP was well characterized by FT-IR, ESI-MS, ^{1}H NMR, ^{13}H NMR analysis.

3.3.2 Selectivity and sensitivity experiment for PYAP towards Fe^{3+}

The absorption spectrum of PYAP in methanol shows a maximum at 345 nm with an extinction coefficient of 11,000 M^{-1} cm^{-1}, which is weakly fluorescent under irradiation at 300 nm with an emission maximum at 380 nm as shown in Figure 3.4. Except for all other metal ions, only the addition of $Fe(NO_3)_3$ (20 µM) in the methanolic solution of PYAP (10 µM) shifted the absorption spectrum maxima of the solution to 415 nm. And the pale yellow color of the ligand containing solution becomes dark yellow (Figure 3.5).

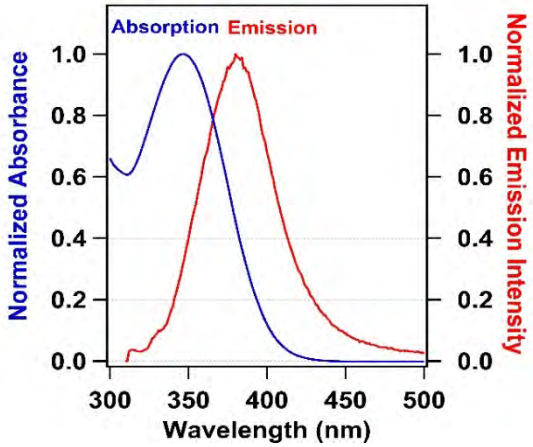

Figure 3.4 Normalized absorption and emission spectra of PYAP in methanol.

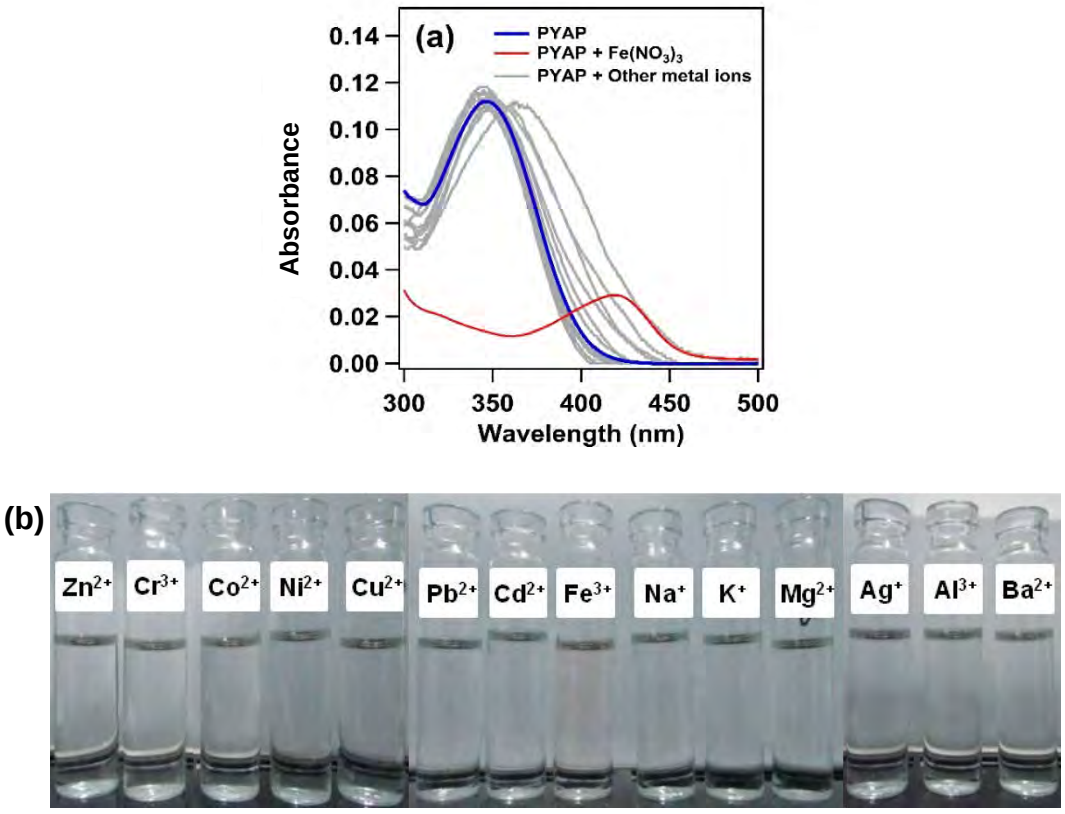

Figure 3.5 (a) Absorption spectra of PYAP (10 µM) in the presence of different metal ions such as Na^{+}, K^{+}, $Ba2^{+}$, Mg^{2+}, Al^{3+}, Cr^{3+}, Co^{2+}, Ni^{2+}, Cu^{2+}, Zn^{2+}, Cd^{2+}, Pb^{2+}, Ag^{+} and Fe^{3+} (metal ions as their NO^{3-} salts and metal concentration is 20 µM) in methanol. (b) The photographic image of metal ion (20 µM) solutions with chemosensor (PYAP, 20 µM) under room light.

However, importantly, we have not observed any appreciable color change or change in the absorption spectrum of PYAP (10 µM) on addition of 2 equivalent of other metal ions (e.g., Na^{+}, K^{+}, Ba^{2+}, Mg^{2+}, Al^{3+}, Cr^{3+},Co^{2+},

Ni^{2+}, Cu^{2+}, Zn^{2+}, Cd^{2+}, Pb^{2+} and Ag^{+}) as shown in Figure 3.5(b). This makes the PYAP molecule a selective sensor for Fe^{3+}. Upon the gradual addition of Fe^{3+} (0.0–2.5 equiv) to PYAP (10 µM) solution, the new band appears at 415 nm and its absorbance keep on increasing with a concomitant decrease in the 345 nm band with a clear isosbestic point at 395 nm Figure 3.6 (a).

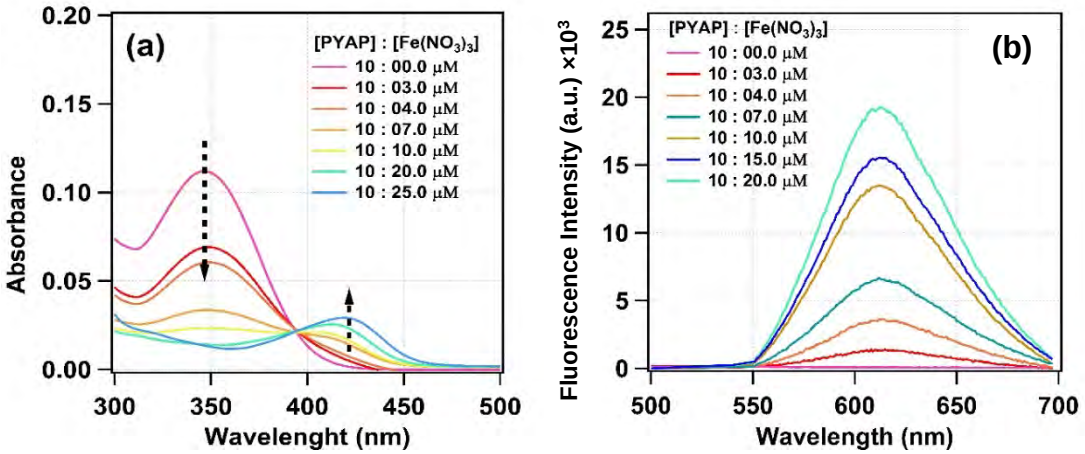

Figure 3.6 (a) UV-Visible absorption spectra of PYAP in the presence of different concentrations of Fe^{3+} ion in methanol. (b) Fluorescence spectra of PYAP (10 µM) at different concentration of Fe^{3+} recorded in methanol (excitation at 395 nm).

This clearly indicates that a new species has formed during the titration of PYAP with Fe^{3+}. The changes in the UV–Vis spectrum of the solutions can be interpreted as the electronic rearrangement in PYAP through coordination with Fe^{3+}. On the other hand, the change in the emission property of PYAP on addition of Fe^{3+} is found to be much more prominent. The emission spectrum of PYAP in methanol shows a less intense peak at 380 nm upon excitation at 300 nm Figure 3.4. A new fluorescence band appears at 612 nm (excited at 395 nm) upon gradual addition of Fe^{3+} in PYAP solution and is depicted in Figure 3.6(b), in contrary to the other metal ions (Na^{+}, K^{+}, Ba^{2+}, Mg^{2+}, Al^{3+}, Cr^{3+}, Co^{2+}, Ni^{2+}, Cu^{2+}, Zn^{2+}, Cd^{2+}, Pb^{2+} and Ag^{+}) under investigation, which is detectable by naked eye under UV irradiation as shown in Figure 3.7.

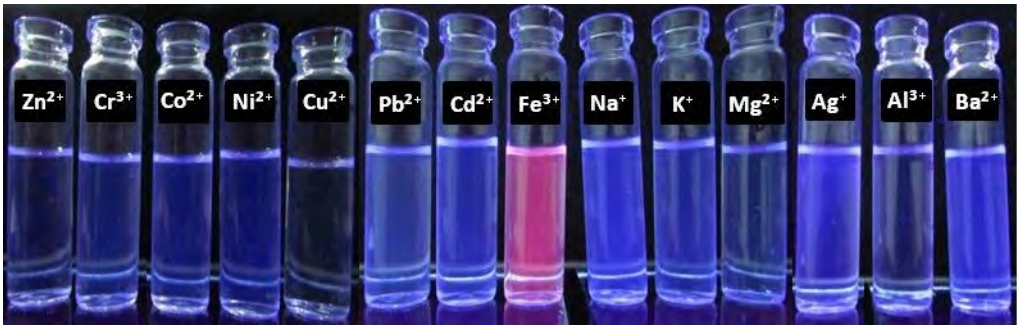

Figure 3.7 The photographic image of metal ions (20 µM) solutions with ligand (PYAP, 10 µM) under UV light illumination

In presence of 2.5 equiv Fe^{3+}, the change in fluorescence intensity is found to be about 200 times, makes this molecule as a unique selective and sensitive sensor for Fe^{3+} (Figure 3.8).

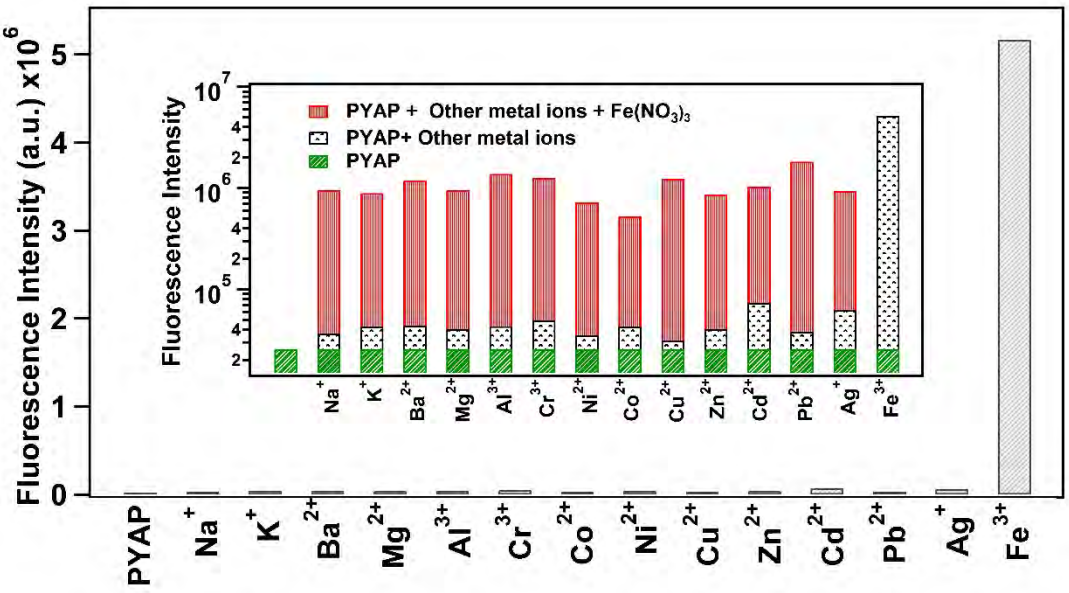

Figure 3.8 Comparison of fluorescence intensity of PYAP (10 µM) in the absence and presence of 2 equivalents of different metal ions such as Na^+, K^+, Ba^{2+}, Mg^{2+}, Al^{3+}, Cr^{3+}, Co^{2+}, Ni^{2+}, Cu^{2+}, Zn^{2+}, Cd^{2+}, Pb^{2+}, Ag^+ and Fe^{3+} (metal ions as their $NO3^-$ salts) in methanol.

Also, we have shown that the presence of other metal ions does not influence much the fluorescence property of Fe^{3+}–PYAP complex (inset of Figure 3.8). These results clearly indicate that the sensing of Fe^{3+} by PYAP is barely affected by common coexisting metal ions even when the concentration of these ions are 100 times higher than Fe^{3+}.

3.3.3 Solvent dependent experiment

To understand solvent effect, the absorption and emission spectra of PYAP were taken in different solvents as illustrated in Figure 3.9.

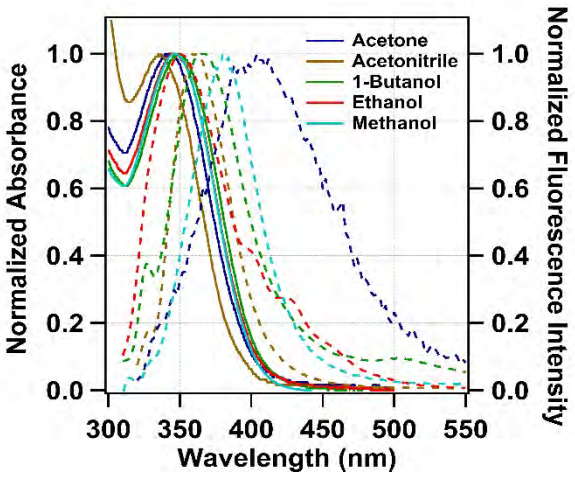

Figure 3.9 Normalized absorption and emission spectra of PYAP in different solvent.

The emission spectra of PYAP depend on the solvent; however, such solvent dependencies have been found small in absorption spectra (solid lines). We have also taken some spectral data to gain an insight into the sensing ability of PYAP towards the Fe^{3+} in different solvents. This is to note that PYAP could also detect Fe^{3+} efficiently in other solvents, e.g., ethanol, 1-butanol, and acetone. On the other hand, in acetonitrile, the sensing ability of PYAP toward Fe^{3+} was not observed in Figure 3.10.

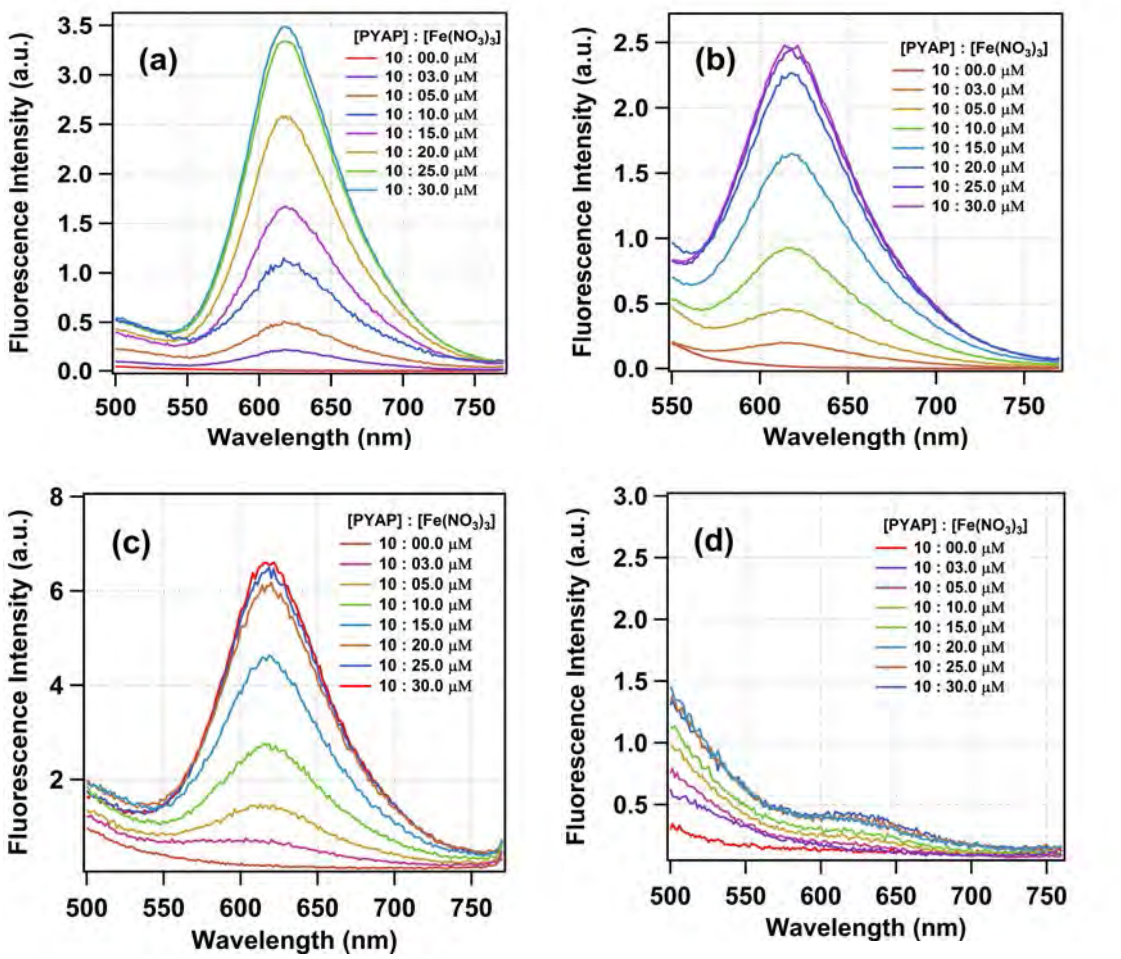

Figure 3.10 Fluorescence spectra of PYAP (10 μM) in the presence of different concentration Fe^{3+} ions in different solvents such as (a) ethanol, (b) 1-butanol, (c) acetone, and (d) acetonitrile (excitation at 395 nm).

3.3.4 Intensive study of PYAP with other metal ions

We have further conducted a study to get a closer look into the sensing propensity of PYAP towards different metal ions other than Fe^{3+}. From our investigation, we found that metal ions like Ag^{+}, Cu^{2+}, and Ni^{2+} also somewhat changes the absorption spectra of PYAP as shown in Figure 3.11[(a), (b), (c)]. However, the fluorescence enhancement in presence of Ag^{+}, Cu^{2+}, Ni^{2+} (see Figure 3.11[(d), (e), (f)]) is negligible compared to Fe^{3+}. This straightforwardly supports the idea of selective sensing of Fe^{3+}, which makes PYAP an excellent chemosensor for Fe^{3+}.

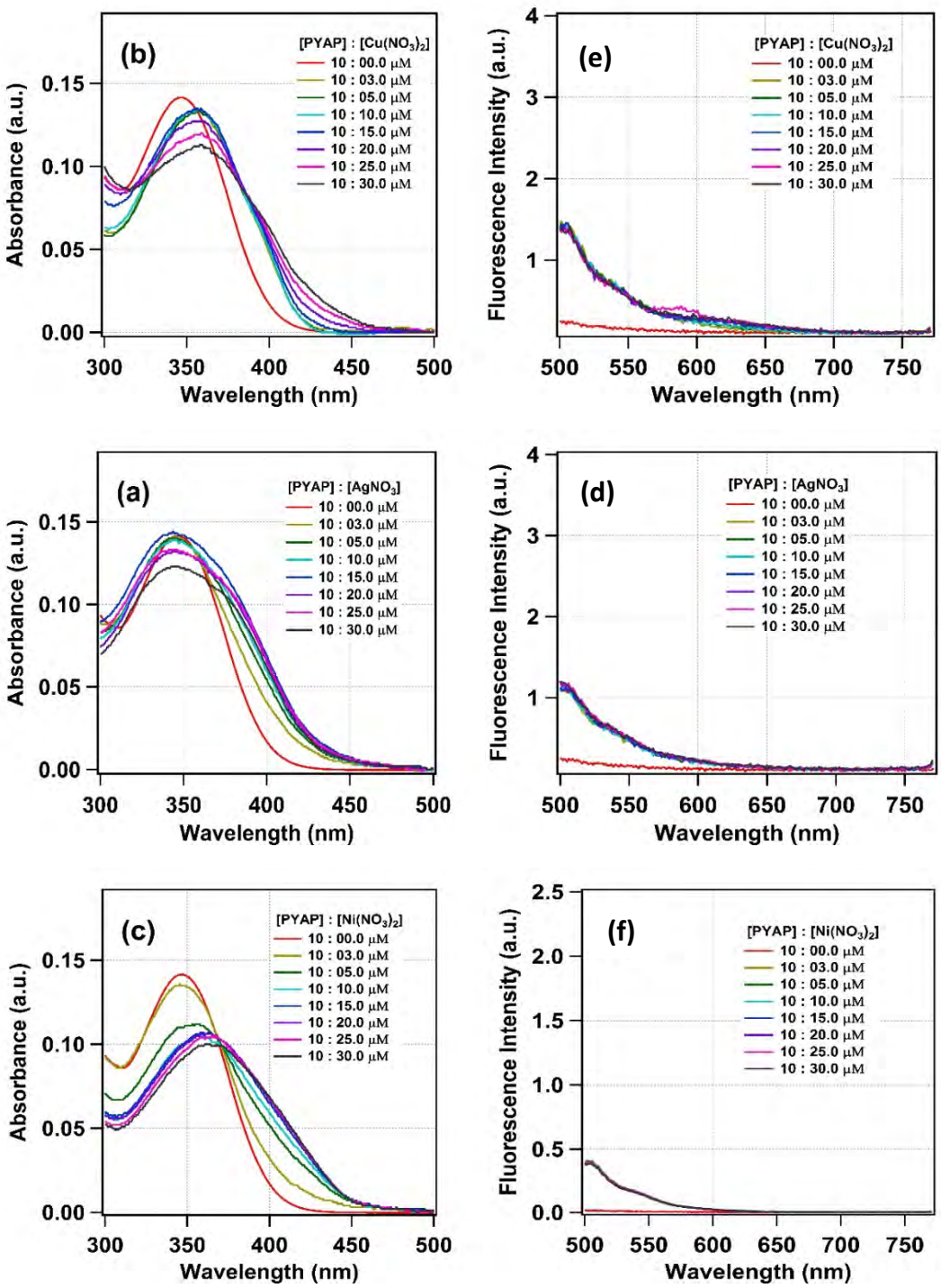

Figure 3.11 Absorption [(a), (b), (c)] and Emission [(d), (e), (f)] spectra of PYAP (10 μM) in the presence of different concentration metal ions such as Ag^{+}, Cu^{2+} and Ni^{2+}in methanol.

3.3.5 Limit of detection and Binding stoichiometry

More importantly, the level of detection was found to be at ppm level as shown in Figure 3.12(a), where we have shown that PYAP can efficiently detect the Fe^{3+} ion in a solution where the concentration of Fe^{3+} is 2 μM. Also, the

ability of this fluorescence sensor to quantitatively detect Fe^{3+} within few minutes, makes it practically applicable.

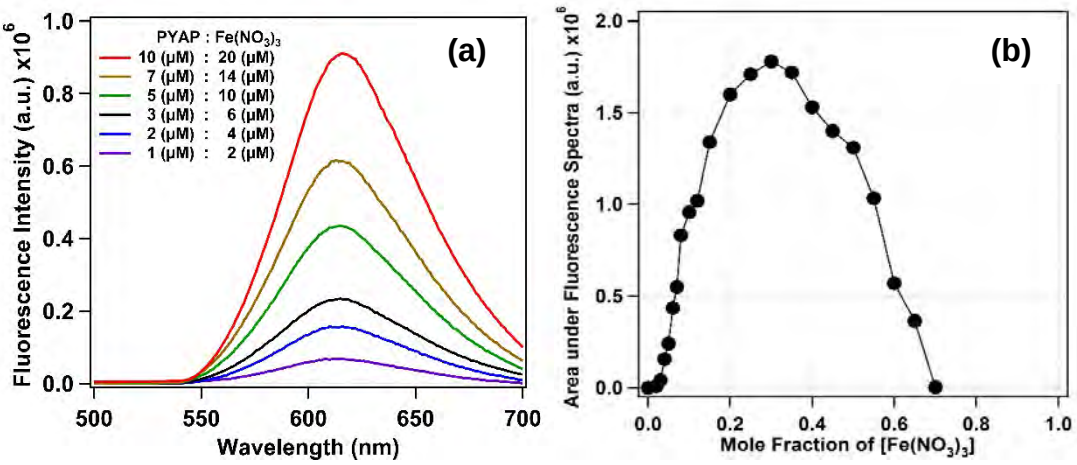

Figure 3.12 (a) Fluorescence spectra of different concentration of PYAP with 2 equivalents of Fe^{3+} in methanol (excitation at 395 nm) displaying at ppm level detection efficiency of PYAP towards $Fe3^{+}$.(b) Job's Plot of PYAP at different concentration of Fe^{3+} recorded in methanol (excitation at 395 nm).

The binding stoichiometry between PYAP and Fe^{3+} has been measured using the Job's plot method through the change in fluorescence intensity, where the concentrations of PYAP and Fe^{3+} were varied, keeping the total concentration constant as shown in Figure 3.12 (b) above. This clearly indicates that 2:1 stoichiometric complex of PYAP and Fe^{3+} is present in the methanol.

3.3.6 Measurement of binding constant

For the binding constant measurement, we have kept the concentration of Fe^{3+} metal ion fixed and measured the change in fluorescence intensity with an increase in the PYAP concentration, where we have observed a monotonous increase of fluorescence intensity (see Figure 3.13)

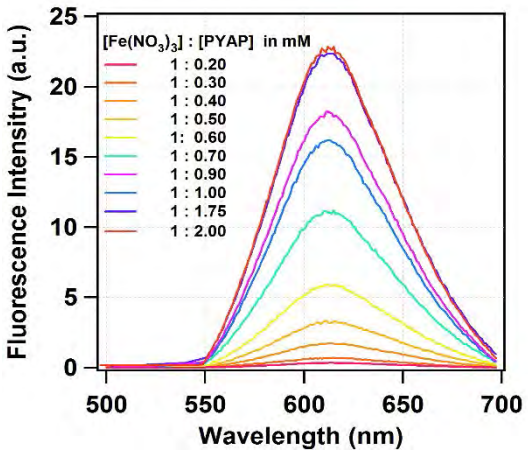

Figure 3.13 Change in fluorescence intensity due to complex formation on gradual increase of PYAP concentration in a solution of fixed Fe^{3+} concentration.

For 2:1 complexation between PYAP and Fe^{3+}, the overall equilibrium can be written as

$$2L + M \rightleftharpoons C \qquad \ldots\ldots\ldots \quad (3.1)$$

Here L is the PYAP; M is the Fe^{3+} ion and C is the complex. Assuming the concentration of free ligand is much higher than the complexes one, the dependence of the fluorescence intensity on the total concentration of PYAP in the system can be written as[53,54]

$$\frac{F}{F_m - F} = \frac{[C]}{[M]} = K[L_T]^2 \qquad \ldots\ldots\ldots \quad (3.2)$$

Here L_T is total concentration of PYAP in the medium. F and F_m are the fluorescence intensity of the sample at the intermediate concentration of ligand and maximum fluorescence intensity when all the metal ions formed complex with the ligand, respectively. By taking logarithm on both sides of equation (3.2), equation (3.2) is again reformulated as,

$$\log\left(\frac{F}{F_m - F}\right) = logK + 2\log[L_T] \qquad \ldots\ldots\ldots \quad (3.3)$$

The binding constant K was determined from the plot of the linear regression of $log\ (F/(F_m - F))$ vs. log [PYAP] (Figure 3.14) as per equation (3.3). The

estimated value of binding constant by fitting is found to be 5.12 ± 0.6 $(mM)^{-2}$ (R^2 value of linear relationship is found 0.987 in fitting).

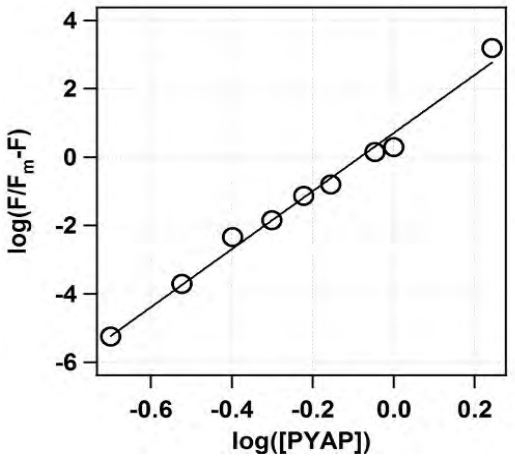

Figure 3.14 Determination of binding constant between PYAP and Fe^{3+} in methanol using a linear regression plot of log ($F/(F_m - F)$) vs. log [PYAP].

3.3.7 Proposed Binding Mode

The study of the job's plot clearly indicates that stoichiometric of the complex formed between PYAP and Fe^{3+} is present in the methanol is 2:1 and is depicted in Figure 3.15.

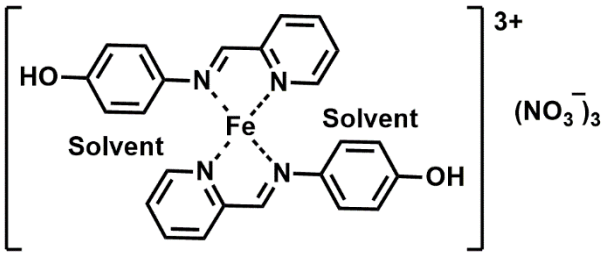

Figure 3.15 Proposed structure of PYAP–Fe^{3+} complex.

^{1}H NMR spectra of PYAP in the absence and presence of Fe^{3+} were recorded at room temperature, as shown in Figure 3.16(a). Upon addition of 0.5 equivalent of Fe^{3+}, the proton signals broaden compared to PYAP protons signals, which indicate the complexation process. We have also recorded an ESI-MS spectrum for PYAP-Iron Complex, which also showed similarities with our theoretical mass-spectrum (see Figure 3.16 (b)).

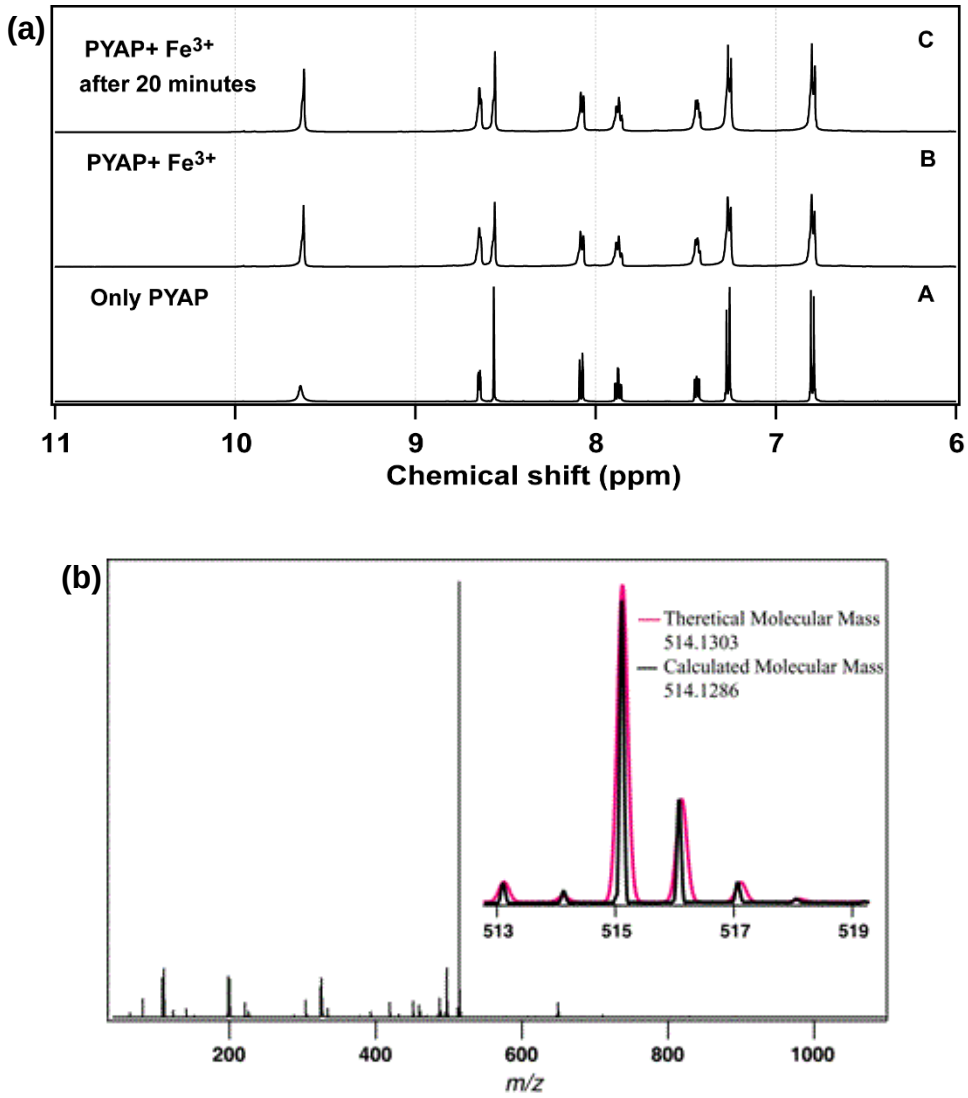

Figure 3.16 (a) ^{1}H NMR spectrum of PYAP taken in DMSO-d_6 (A) Only PYAP (B) PYAP and Iron nitrate taken after 10 minutes and (C) after 20 minutes. (b) ESI-MS spectrum of PYAP-Iron Complex. (Inset: Theoretical mass spectrum).

3.4 Semi-real sample analysis

To address the applicability of the sensor for real sample analysis, we went to one step behind and used it to estimate Fe^{3+} in a semi-real sample. For this we have prepared the following composition of water sample.

Sample 1: 2 μM (Arsenic nitrate) + 1 μM (Cadmium nitrate) + 10 μM (Chromium nitrate) + 10 μM (Copper nitrate) + 5 μM (Nickel nitrate) + 5 μM (Lead nitrate) + 2 μM (Mercury nitrate) + 40 μM (Zinc nitrate) + 10 μM (Iron nitrate) + 1000 μM (Calcium nitrate) + 500 μM (Magnesium nitrate) + 10 μM Starch + 25 μM Amylose, + 10 μM Amylopectin

Sample 2: 2 μM (Arsenic nitrate) + 1 μM (Cadmium nitrate) + 10 μM (Chromium nitrate) + 10 μM (Copper nitrate) + 5 μM (Nickel nitrate) + 5 μM (Lead nitrate) + 2 μM (Mercury nitrate) + 40 μM (Zinc nitrate) + 30 μM (Iron nitrate) + 1000 μM (Calcium nitrate) + 500 μM (Magnesium nitrate) + 10 μM Starch + 25 μM Amylose, + 10 μM Amylopectin

Further, both the samples were concentrated up to 1% from initial volume and added in 10 μM methanolic solution of PYAP such that there is 100 times dilution of the concentrated samples. Soon after the fluorescence spectra of the PYAP in methanol containing the sample 1 and 2 were recorded.

From the fluorescence intensity, the iron concentration in chosen sample was determined by following method:

The overall equilibrium in the complexation of PYAP with Fe^{3+} can be written as

$$M + 2L \leftrightarrows C \qquad \ldots\ldots\ldots \quad (3.4)$$

Where *L* is the PYAP; M is the Fe^{3+} ion and *C* is the complex. The equilibrium constant (*K*) for equation 3.4 can be written as

$$K = \frac{[C]}{[M][L]^2} \qquad \ldots\ldots\ldots \quad (3.5)$$

Assuming, the concentration of complexes formed is directly proportional to fluorescence intensity at 612 nm, one can write

$$Fluorescence\ Intensity\ \alpha\ [C] = K[M][L]^2 \qquad \ldots\ldots\ldots \quad (3.6)$$

The value of *K* is reported in thesis is 5.12 ± 0.6 $(mM)^{-2}$. Thus a plot of fluorescence intensity vs. Fe^{3+} concentration will be linear for a fixed PYAP concentration, which is shown below. The fluorescence intensity obtained for the semi-real sample was appended in the fitted line, and the concentration of

Fe^{3+} was determined for semi-real samples 1 and 2 as 9.5 μM and 32 μM respectively.

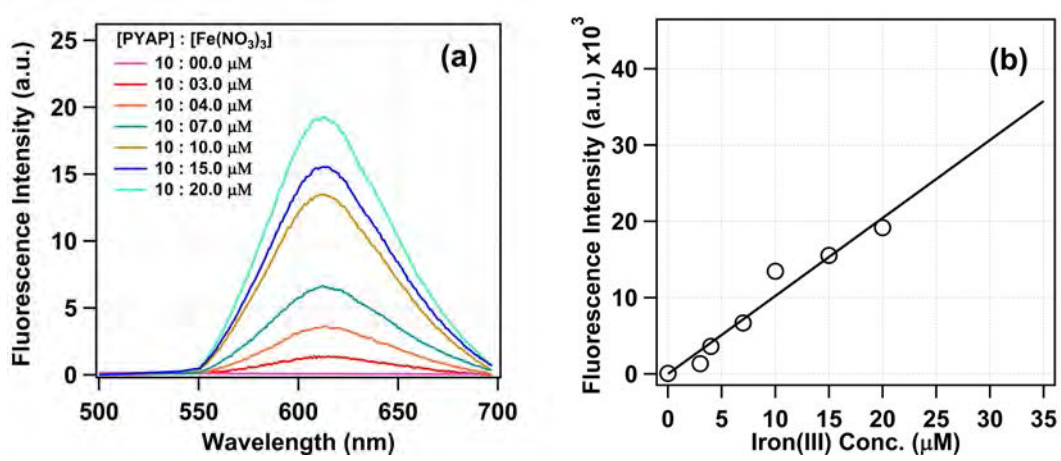

Figure 3.17 (a) (a) Fluorescence spectra of PYAP (10 μM) at different concentration of Fe^{3+} recorded in methanol (excitation at 395 nm). (b) Linear plot of fluorescence intensity against Fe^{3+} concentration.

3.5 Conclusion

In summary, a new highly selective and sensitive chemosensor, PYAP, was synthesized and used for the detection of Fe^{3+} ion with a low detection limit (ppm level) in methanol. Moreover, the response time for the detection was found in minutes time scale. Other metal ions e.g., Na^{+}, K^{+}, Ba^{2+}, Mg^{2+}, Al^{3+}, Cr^{3+},Co^{2+}, Ni^{2+}, Cu^{2+}, Zn^{2+}, Cd^{2+}, Pb^{2+} and Ag^{+} barely influenced the detection of Fe^{3+} by PYAP. As iron is one of the most biologically important elements, this opens up the possibility of using this fluorescent sensor for biological studies and the work on this aspect is in progress in our laboratory.

References

1 M. Dutta and D. Das, *TrAC Trends Anal. Chem.*, 2012, **32**, 113–132.

2 A. Barba-Bon, A. M. Costero, S. Gil, M. Parra, J. Soto, R. Martínez-Máñez and F. Sancenón, *Chem. Commun.*, 2012, **48**, 3000–3002.

3 H. N. Kim, W. X. Ren, J. S. Kim and J. Yoon, *Chem. Soc. Rev.*, 2012, **41**, 3210–3244.

4 G.-C. Kuang, J. R. Allen, M. A. Baird, B. T. Nguyen, L. Zhang, T. J. Morgan, C. W. Levenson, M. W. Davidson and L. Zhu, *Inorg. Chem.*, 2011, **50**, 10493–10504.

5 V. N. Mehta, S. K. Kailasa and H.-F. Wu, *New J. Chem.*, 2014, **38**, 1503–1511.

6 H. S. Hewage and E. V Anslyn, *J. Am. Chem. Soc.*, 2009, **131**, 13099–13106.

7 E. M. Nolan and S. J. Lippard, *Chem. Rev.*, 2008, **108**, 3443–3480.

8 A. P. de Silva, H. Q. N. Gunaratne, T. Gunnlaugsson, A. J. M. Huxley, C. P. McCoy, J. T. Rademacher and T. E. Rice, *Chem. Rev.*, 1997, **97**, 1515–1566.

9 B. D'Autréaux, N. P. Tucker, R. Dixon and S. Spiro, *Nature*, 2005, **437**, 769–772.

10 J.-W. Lee and J. D. Helmann, *Nature*, 2006, **440**, 363–367.

11 H. Weizman, O. Ardon, B. Mester, J. Libman, O. Dwir, Y. Hadar, Y. Chen and A. Shanzer, *J. Am. Chem. Soc.*, 1996, **118**, 12368–12375.

12 J. P. Sumner and R. Kopelman, *Analyst*, 2005, **130**, 528–533.

13 R. R. Crichton, D. T. Dexter and R. J. Ward, *Coord. Chem. Rev.*, 2008, **252**, 1189–1199.

14 N. C. Andrews, *N. Engl. J. Med.*, 1999, **341**, 1986–1995.

15 D. Touati, *Arch. Biochem. Biophys.*, 2000, **373**, 1–6.

16 G. CAIRO and A. PIETRANGELO, *Biochem. J.*, 2000, **352**, 241–250.

17 E. Beutler, V. Felitti, T. Gelbart and N. Ho, *Drug Metab. Dispos.*, 2001, **29**, 495–499.

18 A. S. Dornelles, V. A. Garcia, M. N. M. de Lima, G. Vedana, L. A.

Alcalde, M. R. Bogo and N. Schröder, *Neurochem. Res.*, 2010, **35**, 564–571.

19 J. E. T. Andersen, *Analyst*, 2005, **130**, 385–390.

20 M. E. del Castillo Busto, M. Montes-Bayón, E. Blanco-González, J. Meija and A. Sanz-Medel, *Anal. Chem.*, 2005, **77**, 5615–5621.

21 K. Pomazal, C. Prohaska, I. Steffan, G. Reich and J. F. K. Huber, *Analyst*, 1999, **124**, 657–663.

22 C. M. G. van den Berg, *Anal. Chem.*, 2006, **78**, 156–163.

23 S. Vallejos, P. Estévez, S. Ibeas, A. Muñoz, F. C. García, F. Serna and J. M. García, *Sensors Actuators B Chem.*, 2011, **157**, 686–690.

24 J.-S. Wu, J.-H. Zhou, P.-F. Wang, X.-H. Zhang and S.-K. Wu, *Org. Lett.*, 2005, **7**, 2133–2136.

25 M. A. Hortalá, L. Fabbrizzi, N. Marcotte, F. Stomeo and A. Taglietti, *J. Am. Chem. Soc.*, 2003, **125**, 20–21.

26 M. Chai, D. Zhang, M. Wang, H. Hong, Y. Ye and Y. Zhao, *Sensors Actuators B Chem.*, 2012, **174**, 231–236.

27 L. Zhang, J. Wang, J. Fan, K. Guo and X. Peng, *Bioorg. Med. Chem. Lett.*, 2011, **21**, 5413—5416.

28 Z. Aydin, Y. Wei and M. Guo, *Inorg. Chem. Commun.*, 2012, **20**, 93–96.

29 J. L. Bricks, A. Kovalchuk, C. Trieflinger, M. Nofz, M. Büschel, A. I. Tolmachev, J. Daub and K. Rurack, *J. Am. Chem. Soc.*, 2005, **127**, 13522–13529.

30 Y. Xiang and A. Tong, *Org. Lett.*, 2006, **8**, 1549–1552.

31 X. Zhang, Y. Shiraishi and T. Hirai, *Tetrahedron Lett.*, 2007, **48**, 5455–5459.

32 L. Dong, ChongWu, X. Zeng, L. Mu, S.-F. Xue, Z. Tao and J.-X. Zhang, *Sensors Actuators B Chem.*, 2010, **145**, 433–437.

33 B. Wang, J. Hai, Z. Liu, Q. Wang, Z. Yang and S. Sun, *Angew. Chemie Int. Ed.*, 2010, **49**, 4576–4579.

34 C. R. Lohani and K.-H. Lee, *Sensors Actuators B Chem.*, 2010, **143**, 649–654.

35 J. Mao, L. Wang, W. Dou, X. Tang, Y. Yan and W. Liu, *Org. Lett.*, 2007, **9**, 4567–4570.

36 L.-J. Fan and W. E. Jones, *J. Am. Chem. Soc.*, 2006, **128**, 6784–6785.

37 A. J. Weerasinghe, C. Schmiesing, S. Varaganti, G. Ramakrishna and E. Sinn, *J. Phys. Chem. B*, 2010, **114**, 9413–9419.

38 N. C. Lim, S. V Pavlova and C. Brückner, *Inorg. Chem.*, 2009, **48**, 1173–1182.

39 J. Y. Kwon, Y. J. Jang, Y. J. Lee, K. M. Kim, M. S. Seo, W. Nam and J. Yoon, *J. Am. Chem. Soc.*, 2005, **127**, 10107–10111.

40 S. Sen, S. Sarkar, B. Chattopadhyay, A. Moirangthem, A. Basu, K. Dhara and P. Chattopadhyay, *Analyst*, 2012, **137**, 3335–3342.

41 M. J. C. Marenco, C. Fowley, B. W. Hyland, D. Galindo-Riaño, S. K. Sahoo and J. F. Callan, *J. Fluoresc.*, 2012, **22**, 795–798.

42 L. Salmon, P. Thuéry, E. Rivière and M. Ephritikhine, *Inorg. Chem.*, 2006, **45**, 83–93.

43 D. M. Epstein, S. Choudhary, M. R. Churchill, K. M. Keil, A. V Eliseev and J. R. Morrow, *Inorg. Chem.*, 2001, **40**, 1591–1596.

44 L. Wang, W. Qin, X. Tang, W. Dou and W. Liu, *J. Phys. Chem. A*, 2011, **115**, 1609–1616.

45 S. Dutta, P. Biswas, U. Flörke and K. Nag, *Inorg. Chem.*, 2010, **49**, 7382–7400.

46 C. Ma, A. Lo, A. Abdolmaleki and M. J. MacLachlan, *Org. Lett.*, 2004, **6**, 3841–3844.

47 J. Wang, C. He, P. Wu, J. Wang and C. Duan, *J. Am. Chem. Soc.*, 2011, **133**, 12402–12405.

48 S. Panda, P. B. Pati and S. S. Zade, *Chem. Commun.*, 2011, **47**, 4174–4176.

49 V. Chandrasekhar, S. Das, R. Yadav, S. Hossain, R. Parihar, G. Subramaniam and P. Sen, *Inorg. Chem.*, 2012, **51**, 8664–8666.

50 V. Chandrasekhar, S. M. Wahidur Rahaman, T. Hajra, D. Das, T. Ghatak, S. Rafiq, P. Sen and J. K. Bera, *Chem. Commun.*, 2011, **47**, 10836–10838.

51 V. Chandrasekhar, M. D. Pandey, S. K. Maurya, P. Sen and D. Goswami,

Chem. – An Asian J., 2011, **6**, 2246–2250.

52 M. S. H. Faizi, S. Gupta, V. M. K., V. K. Jain and P. Sen, *Sensors Actuators B Chem.*, 2016, **222**, 15–20.

53 H. A. Benesi and J. H. Hildebrand, *J. Am. Chem. Soc.*, 1949, **71**, 2703–2707.

54 B. Valeur, *Molecular Fluorescence: Principles and Applications*, Wiley-VCH, Weinheim, 2001.

Chapter 4

4-((quinolin-2-ylmethylene)amino)phenol (QMAP) as a potential chemosensor for selective colorimetric detection of Cu^{2+} at PPB level

Mohan, K., V.; Das, N.; **Jain, V. K.**; Khan, T.; Pandey, S. K.; Faizi, M. S. H.; Daniel, J.; Sen, P. *ChemistrySelect*, 2020, **5**, 9435-9442.

This chapter reports a Schiff-base chemosensor, 4-((quinolin-2-ylmethylene)amino)phenol (QMAP) was used as a selective and sensitive colorimetric chemosensor for Cu^{2+} both qualitatively and quantitatively. In presence of Cu^{2+}, QMAP exhibits a distinct color change from colorless to orangish-yellow, which is visible with bare eye. The sensing ability of the QMAP towards Cu^{2+} is found to be independent on the type counter anions and has no hindrance from the presence other metal ions. The limit of detection is estimated as 15.3 ppb. A detail mechanistic study suggests a 2:1 type of complex formation between QMAP and copper and the binding constant is measured to be 3.2×10^{10} M^{-2}. Computational analysis indicate that the color of the complex is probably due to metal to ligand charge transfer.

4.1 Introduction

Copper is the third most abundant trace element in the human body and plays a central roles in many elementary physiological processes.[1–10] Copper acts as an essential cofactor or structural component of many metalloenzymes, including cytochrome *c* oxidase, superoxide dismutase, and tyrosinase.[1] It helps to prevent damage to cells due to its antioxidant action and is necessary for the formation of bone and connective tissue. It is known to have a pivotal role in energy generation, signal transduction, and dioxygen transport.[2] However, an excess amount of copper in the body can cause gastrointestinal, hepatic and renal system disorders.[11,12] Diseases like Alzheimer's disease, Wilson's disease, Prion disease, lateral sclerosis, Parkinson's disease, Menke's disease are closely associated with the disruption of copper homeostasis inside the body.[3–8] Copper is also regarded as one of the toxic environmental pollutants, and it is detrimental to aquatic plants and animals as it is associated with the transport across the cell membrane.[7] Due to the application of copper and copper-related products in medicine, biotechnology, agriculture[8], and industry, the release of copper in the environment become enormous and therefore, it is become necessary to detect and quantify copper in different contexts.

A wide range of methods, which include atomic absorption spectroscopy,[13,14] ion-selective electrodes,[15] inductively coupled plasma mass spectroscopy,[16] inductively coupled atomic emission spectroscopy,[17] voltammetry[18] and X-ray fluorescence,[19] have been used for the detection of metal ions including Cu. Even though these methods provide a good level of detection over a wide range of concentrations, most of them require expensive instruments, well-trained personnel and thorough sample preparation. On contrary, methods based on optical spectroscopy are convenient due to their operational simplicity, high sensitivity, selectivity, and cost-effectiveness.[20–23] In the present study, we have employed a chemosensor for detection and estimation of Cu^{2+} ions in solution, colorimetrically.

Several organic molecules have been reported in the past for their ability of copper detection either by a change in fluorescence or absorption spectrum. Boron-dipyrromethane dyes,[1] diaminomaleonitrile derivatives,[6] spiropyran derivatives,[8] acridine derivatives,[9] pyrene moieties,[24] cresol derivatives[25] are some of the examples of the molecular moieties, which have been proposed for Cu sensing. However, the synthesis of most of them are very difficult and they are costly. Herein we have shown the use of quinoline based molecular system, 4-((pyridin-2-ylmethylene)amino)phenol (QMAP) for the sensing of Cu^{2+} based on the change of the absorption spectrum of the molecule. Quinoline derivatives have been used as competent chemosensors for the selective detection of metals including copper[20,21,23,26–30]. Some quinoline derivatives have also been used to detect alkali metals, alkaline earth metals, and transition metals.[31–35] In the present work, we have synthesized a molecule in which a quinoline moiety is linked to a phenol moiety with a spacer group. The lone pair of electrons on the two nitrogen atoms (one of quinoline moiety and the other of the spacer group) can facilitate the binding of the molecule to a metal ion, in this case, Cu^{2+}. Even though the molecule has been previously synthesized and reported in the literature,[36,37] its ability to act as a copper sensor has not been exploited. We have carried out studies to elucidate the photophysical properties of the molecule and its interaction with Cu^{2+}.

4.2 Materials and methods

4.2.1 Materials

Quinoline-2-carbaldehyde and 4-aminophenol were purchased from Alfa Aesar and Avra, respectively, and used as received. Methanol was purchased from Finar Chemical Ltd., India, and purified through distillation before use. All the metal salts were purchased from Sigma-Aldrich and used without further purification.

4.2.2 Experimental Methods

^{1}H NMR spectra were recorded on commercial NMR spectrometer (JNM LA 400 MHz or LA 500FT 500 MHz, JEOL, Japan). UV-vis absorption spectra of the samples were measured on a commercial spectrophotometer (UV 2450, Schimadzu, Japan). Electrospray ionization mass spectra were recorded on a mass spectrometer (Waters, USA). IR spectra were recorded on a FTIR spectrometer (Vector 22, Bruker, USA) with KBr disc in 4000-600 cm^{-1} range.

4.2.3 Synthesis and characterization of 4-((quinolin-2-ylmethylene) amino)phenol (QMAP)

4-((quinolin-2-ylmethylene)amino)phenol (QMAP) was synthesized by condensation of quinoline-2-carbaldehyde with 4-aminophenol. 4-Aminophenol (0.50 g, 4.59 mmol) was dissolved in 20 mL of methanol followed by addition of quinoline-2-carbaldehyde (0.72 g, 4.59 mmol) Scheme 4.1. The mixture was then heated to reflux for 12 h. The solvent was then concentrated to 10 mL and a yellow precipitate appeared. The yellow precipitate was filtered off and washed with cold methanol (2-3 mL) and hexane (3-10 mL), respectively. The resulting yellow powder was recrystallized from methanol and finally dried in vacuum desiccator. The yield of the compound was found to be 0.90 g, 81%.

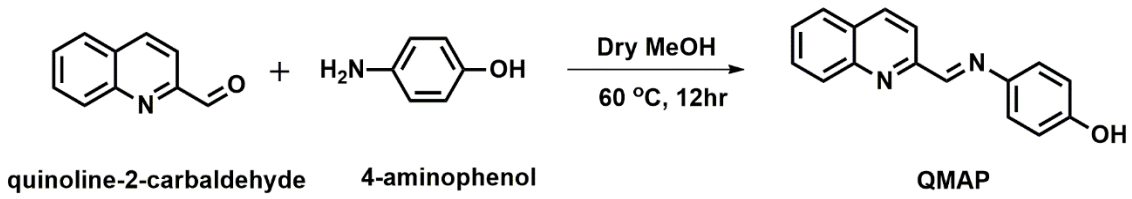

Scheme 4.1 Synthetic scheme of 4-((quinolin-2-ylmethylene)amino)phenol (QMAP)

The purity and structure of QMAP was characterized with ^{1}H NMR, ^{13}C NMR, 2D-COSY NMR, FT-IR and mass spectra (see Figure 4.1, 4.2, 4.3, 4.4, and 4.5). ^{1}H NMR (400 MHz, DMSO-d_6) δ (ppm) 9.64 (s, 1H), 8.79 (s, 1H), 8.465 (d, J = 8.8 Hz, 1H, CH=N), 8.27 (d, 8.4Hz, 1H), 8.10 (d, J = 8.4 Hz, 1H), 8.05 (d, J = 8 Hz, 1H), 7.83 (t, J = 6.8 Hz, 1H), 7.68 (t, J = 6.8 Hz, 1H), 7.4 (d, J =

8.4 Hz, 2H), 6.86 (d, *J* = 8.8 Hz, 2H). ^{13}C NMR (100 MHz, DMSO-d_6, ppm): δ(ppm)= 115.90, 118.02, 123.30, 127.66, 128.09, 128.31, 129.09, 130.17, 136.83, 141.42, 147.41, 154.95, 156.75, 157.43.The stretching frequency at 1578 cm^{-1} in the FT-IR spectrum confirms the formation of imine bond, and after reduction, this peak disappears. The deshielded proton peak at 8.75 ppm also indicates the formation of CH=N and also confirms the required number of proton. The ^{13}C NMR spectrum confirms 12 different carbon atoms. ESI-MS data also confirmed the formation of QMAP and isotopic distribution pattern is also found to be same as of calculated distribution. The melting point of the QMAP was measured to be 235-237 °C.

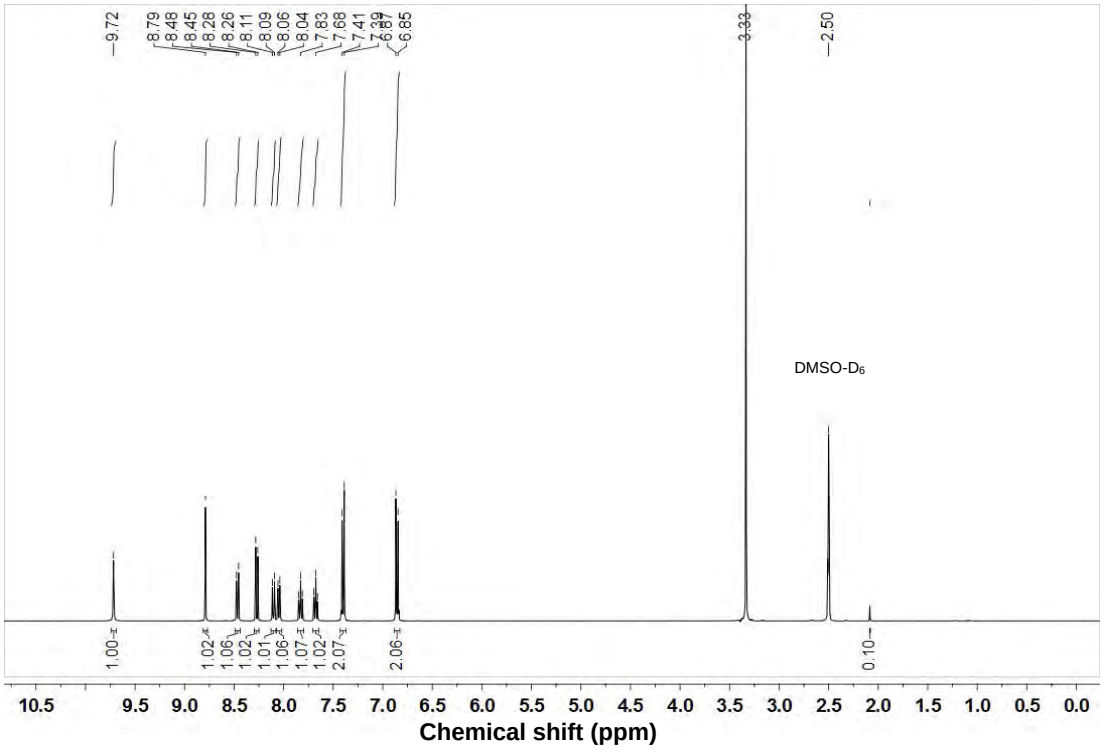

Figure 4.1 (a) ^{1}H NMR spectra of QMAP recorded in DMSO-d_6 at 400 MHz.

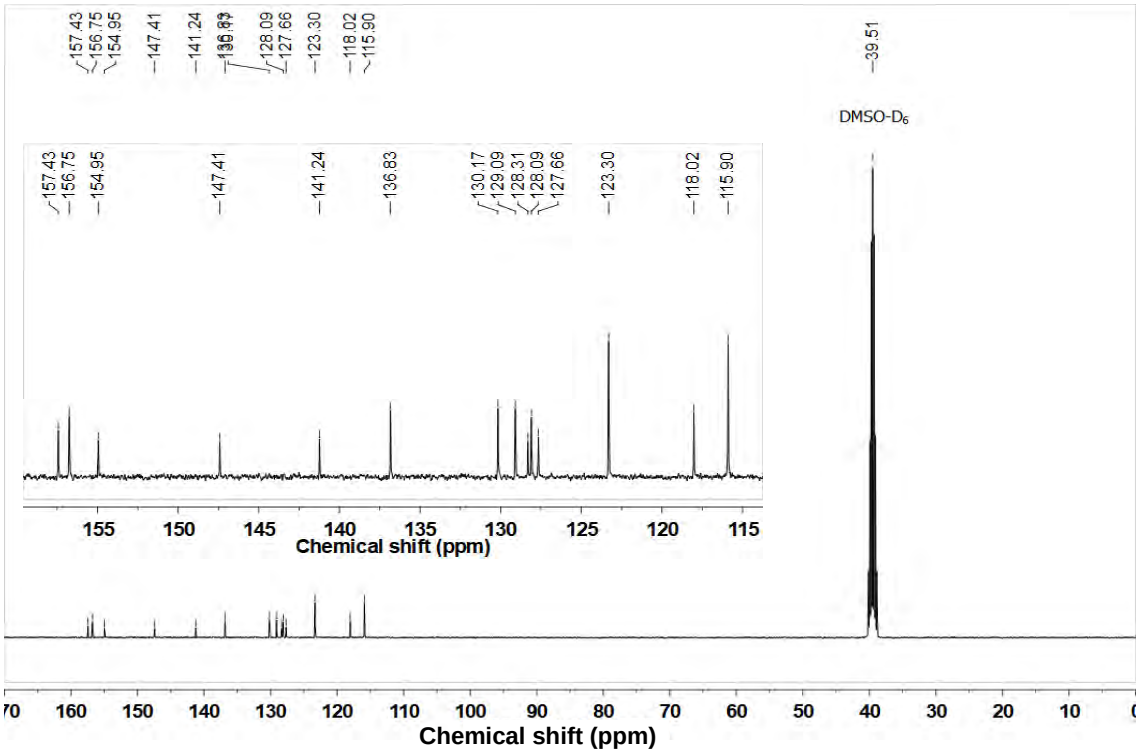

Figure 4.2 ^{13}C NMR spectra of QMAP recorded in DMSO-d_6 at 100 MHz.

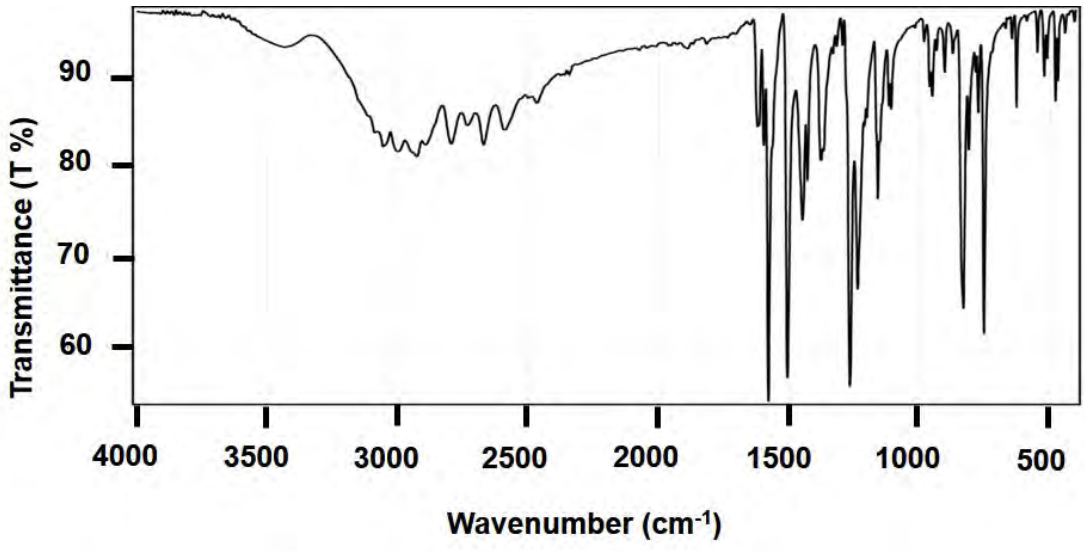

Figure 4.3 Infrared spectra of QMAP recorded in KCl pellet.

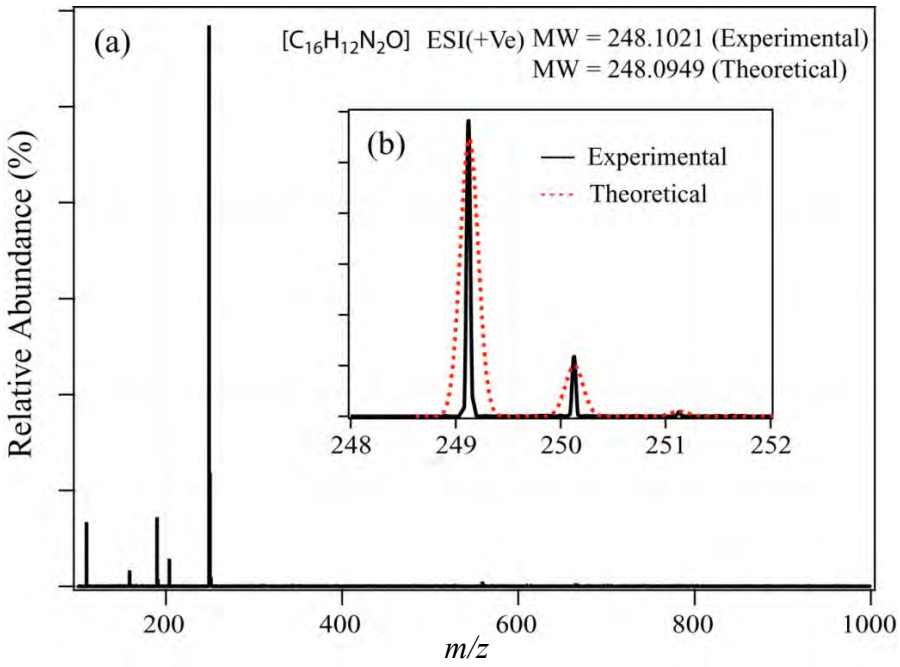

Figure 4.4 ESI-MS spectra of (a) QMAP and (b) Comparison of experimental and theoretical isotopic distribution recorded in MeOH.

4.2.4 Theoretical Calculations

The geometrical optimization, frequency calculation of QMAP and its complex was performed using density functional theory (DFT) on Gaussian 09 program.[38] Here, we have used B3LYP hybrid functional, def2-TZVP basis set and polarizable continuum model (PCM with MeOH as solvent).[39–43] Corresponding orbitals, spin density, and molecular electrostatic potential surface (MESPS) plot were built using the Chemcraft and Jmol programme.[44,45]

4.3 Results and Discussions

4.3.1 QMAP as selective and sensitive Cu^{2+} sensor

The absorption spectrum of QMAP in methanol (see Figure 4.6) consists of two distinct bands centered at 359 nm (ε = 20,800 $M^{-1}cm^{-1}$) and 246 nm (ε = 35,600 $M^{-1}cm^{-1}$), respectively. In the presence of $Cu(NO_3)_2$, the absorption band at 359 nm found to be red shifted by 23 nm along with the formation of a new and distinct band at 558 nm. However, no noticeable change in absorption spectra was observed in the presence of any other metal salts e.g., $NaNO_3$,

KNO_3, $Mg(NO_3)_2$, $Ca(NO_3)_2$, $Al(NO_3)_3$, $Ni(NO_3)_2$, $Co(NO_3)_2$, $Zn(NO_3)_2$, $Cd(NO_3)_2$, $Hg(NO_3)_2$ and $AgNO_3$ (see Figure 4.6), which is also visually detectable (Figure 4.7). This simple observation makes QMAP a potential sensor of Cu^{2+} ion.

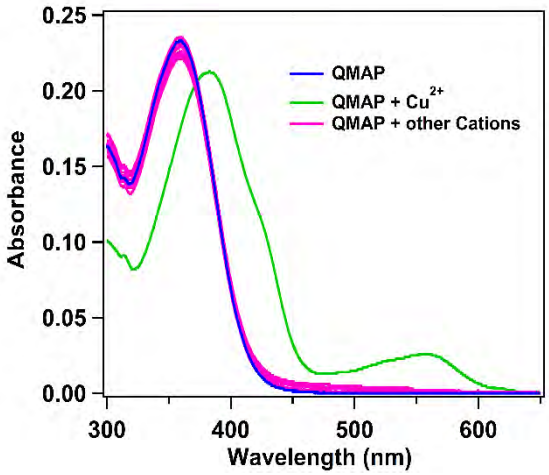

Figure 4.5 UV-Visible absorption spectra of QMAP (10 µM in MeOH) in presence of $Cu(NO_3)_2$ and another salts $NaNO_3$, KNO_3, $Mg(NO_3)_2$, $Ca(NO_3)_2$, $Al(NO_3)_3$, $Ni(NO_3)_2$, $Co(NO_3)_2$, $Zn(NO_3)_2$, $Cd(NO_3)_2$, $Hg(NO_3)_2$ and $AgNO_3$.

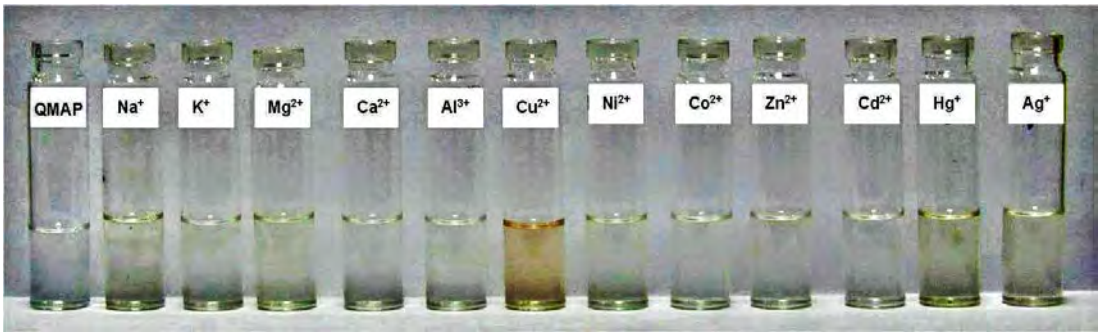

Figure 4.6 Figure 4.7 Photographic image of the color change of QMAP upon addition of different metal ions. A orangish-yellow color is developed only in presence of Cu^{2+}.

A similar experiments were carried out with other copper salts to ensure that the copper sensing ability of QMAP is not limited to its nitrate salt only. The absorption spectrum of QMAP in the presence of copper salts such as $CuSO_4$, $Cu(CH_3COO)_2$ and $CuCl_2$ was recorded, and all those spectra showed similar properties as that of QMAP in the presence of $Cu(NO_3)_2$ (see Figure 4.8(a))

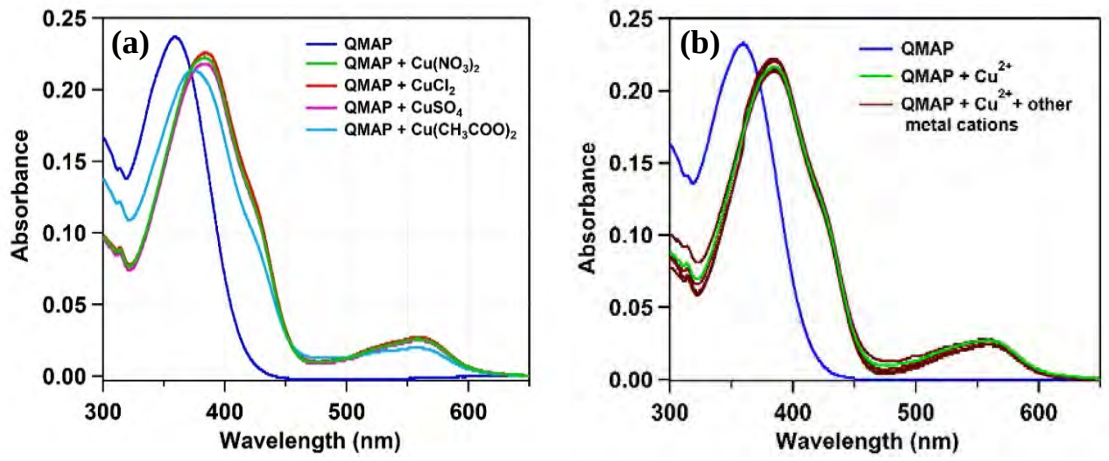

Figure 4.7 (a) UV-Visible absorption spectra of QMAP (10 µM), and QMAP in presence of 1 equivalent $Cu(NO_3)_2$ and other copper salts (SO_4^{2-}, CH3COO$^-$ and Cl^-). (b) UV-Visible absorption spectra of QMAP (10 µM in MeOH) in absence and presence of Cu^{2+} along with 2 equivalents of other metal nitrates salts $NaNO_3$, KNO_3, $Mg(NO_3)_2$, $Ca(NO_3)_2$, $Al(NO_3)_3$, $Ni(NO_3)_2$, $Co(NO_3)_2$, $Zn(NO_3)_2$, $Cd(NO_3)_2$, $Hg(NO_3)_2$ and $AgNO_3$.

To check the effect of other metal ions on the Cu^{2+} sensing ability of QMAP, the absorption spectrum of QMAP/$Cu(NO_3)_2$ system was recorded in the presence of 5 equivalent of other metal nitrates, and the results are shown in Figure 4.8(b). It is clear that the presence of other metal ions does not hamper the selectivity and sensitivity of QMAP towards Cu^{2+}.

4.3.2 Binding Stoichiometry and Limit of Detection

As it is now apparent that QMAP can selectively detect Cu^{2+} in a solution, we look more into the mechanistic aspects of the interaction. To find the stoichiometry of the binding between QMAP and Cu^{2+} ion, we used the Job's plot method. Here, the concentration of QMAP and Cu^{2+} were varied keeping the total concentration constant, and the absorbance at 558 nm was monitored. The corresponding Job's plot is shown in Figure 4.9, which indicate a QMAP:Cu = 2:1 complex formation.

Further, we have carried out a spectroscopic titration by adding $Cu(NO_3)_2$ into the QMAP solution and the resulting spectra are shown in Figure 4.10(a). The concentration of QMAP was maintained at 15.5 µM in this case. The peak of QMAP at 359 nm gradually shifts to 382 nm with the formation of 558 nm absorption band. It should also be noted that the absorption spectra of

the solutions, where the $Cu(NO_3)_2$ concentration is more than 8 µM, overlaps each other and can be concluded that no more binding of Cu(II) ion with QMAP occurs once the Cu^{2+} concentration is more than half as that of QMAP concentration, which is in accordance with the 2:1 binding between QMAP and Cu^{2+} with a high binding constant.

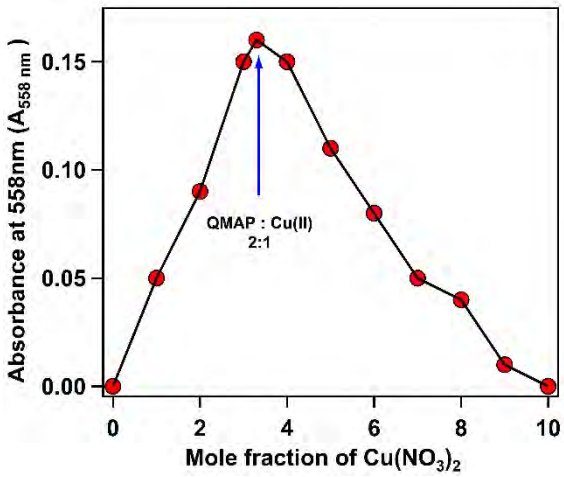

Figure 4.8 Job's plot of QMAP with Cu^{2+} showing a 2:1 QMAP-Cu complex formation.

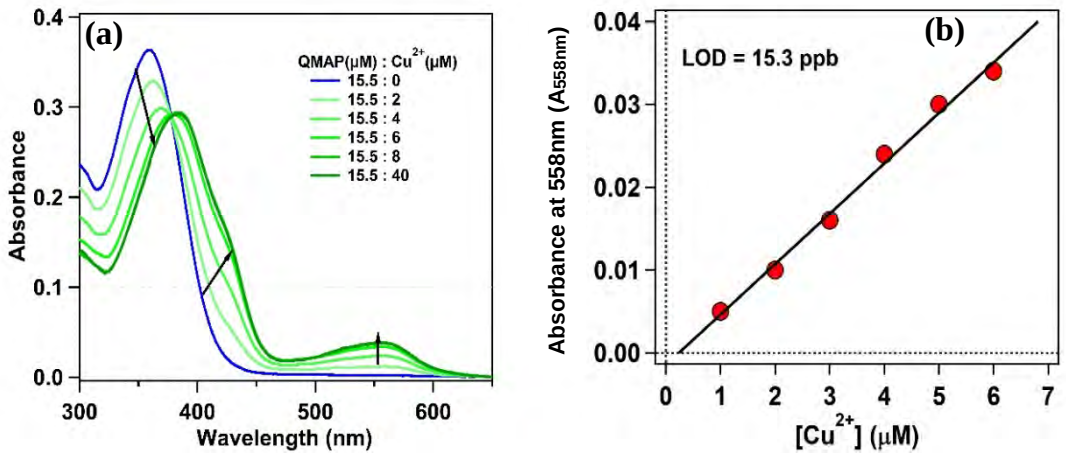

Figure 4.9 (a) Absorption spectra of QMAP with increasing concentration of $Cu(NO_3)_2$. Concentration of QMAP was kept at 15.5 µM and that of $Cu(NO_3)_2$ are 0 µM (red), 2 µM (blue), 4 µM (yellow), 6 µM (violet), 8 µM (pink) and 40 µM (brown). (b). Change in absorbance at 558 nm due to formation of QMAP-Cu complex on gradual addition of Cu^{2+} in QMAP solution and the determination of limit of detection.

Up to 6 µM of Cu^{2+}, the change of absorption with increasing Cu^{2+} concentration is found to be linear in this case, which is used to calculate the

limit of detection (LOD).[46,47] From Figure 4.10(b), we have calculated the LOD to be 15.3 ppb. The value is quite low as compared to the permissible limit of copper in drinking water, which made QMAP a potential sensor in measuring the amount of Cu^{2+} in water.[48]

4.3.3 Binding Constant

The binding constant of the QMAP-Cu complex was estimated by titrating 50 µM $Cu(NO_3)_2$ with QMAP in methanol and monitoring the change in absorbance at 558 nm. It is to emphasize that neither $Cu(NO_3)_2$ nor the QMAP absorbs at 558 nm, whereas, the QMAP-Cu complex does absorb at this wavelength. A plot of absorbance at 558 nm *vs* concentration of QMAP is shown in Figure 4.11. For a 1:2 complexation, the overall equilibrium can be written as $M + 2L \overset{K}{\leftrightarrow} ML_2$, K being the equilibrium constant. Here M represents the metal and L represents the ligand, in this case which are Cu^{2+} and QMAP, respectively, and ML_2 is the QMAP-Cu complex. When, QMAP concentration is not too high, we may assume that $[M_T] \gg [ML_2]$, and under this approximation the concentration of the complex $[ML_2]$ at the equilibrium can be written as

$$[ML_2] = \frac{(2KM_TL_T + 1) - \sqrt{1 + 4KM_TL_T}}{2KM_T} \qquad \ldots\ldots\ldots \quad (4.1)$$

In the above equation, M_T and L_T are the total concentration of the metal and ligand, respectively. The data in Figure 4.11 is fitted with equation 4.1 to and the binding constant is estimated to be 3.2 x 10^{10} M^{-2}.

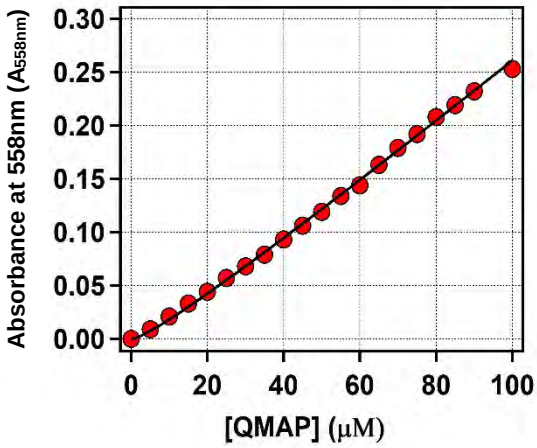

Figure 4.10 Plot of change in absorbance at 558 nm on titration of 50 μM Cu(NO3)2 with QMAP. The solid line is the best fit according to equation 4.1.

4.3.4 Mechanism of the complex formation

As we were unable to crystallize the QMAP-Cu complex, we tried to get some insight about the binding sites through ^{1}H NMR experiments of QMAP in the presence of $Cu(NO_3)_2$ (see Figure 4.12).

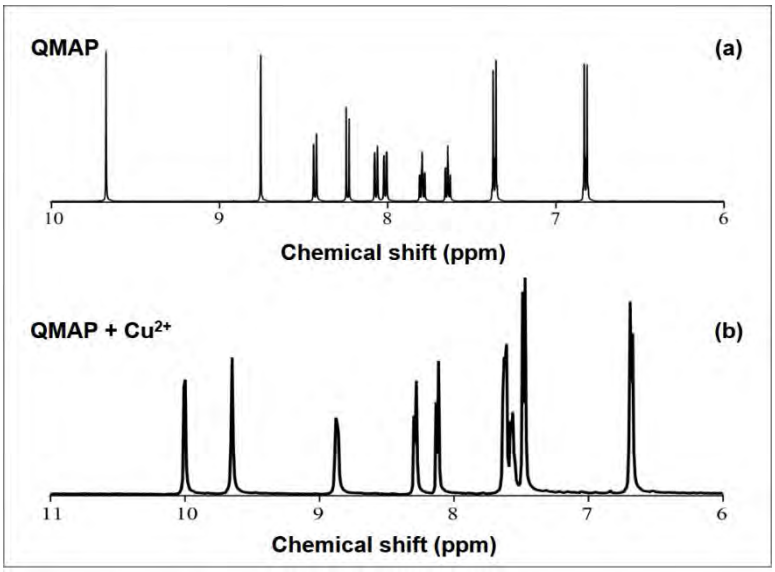

Figure 4.11 ^{1}H NMR spectrum of QMAP taken in DMSO-d_6 (a) Only QMAP (b) PYAP and Copper nitrate.

We observe that the peak corresponding to the proton attached to the carbon atom adjacent to the non-aromatic nitrogen in the molecule has undergone a comparatively higher downfield shift (0.9 ppm). This shift must be because of the binding of Cu^{2+} on the nitrogen atom, which decreases the electron density. The evidence for the binding of Cu^{2+} to nitrogen was also obtained from the infrared spectra of QMAP-Cu complex (Figure 4.13).

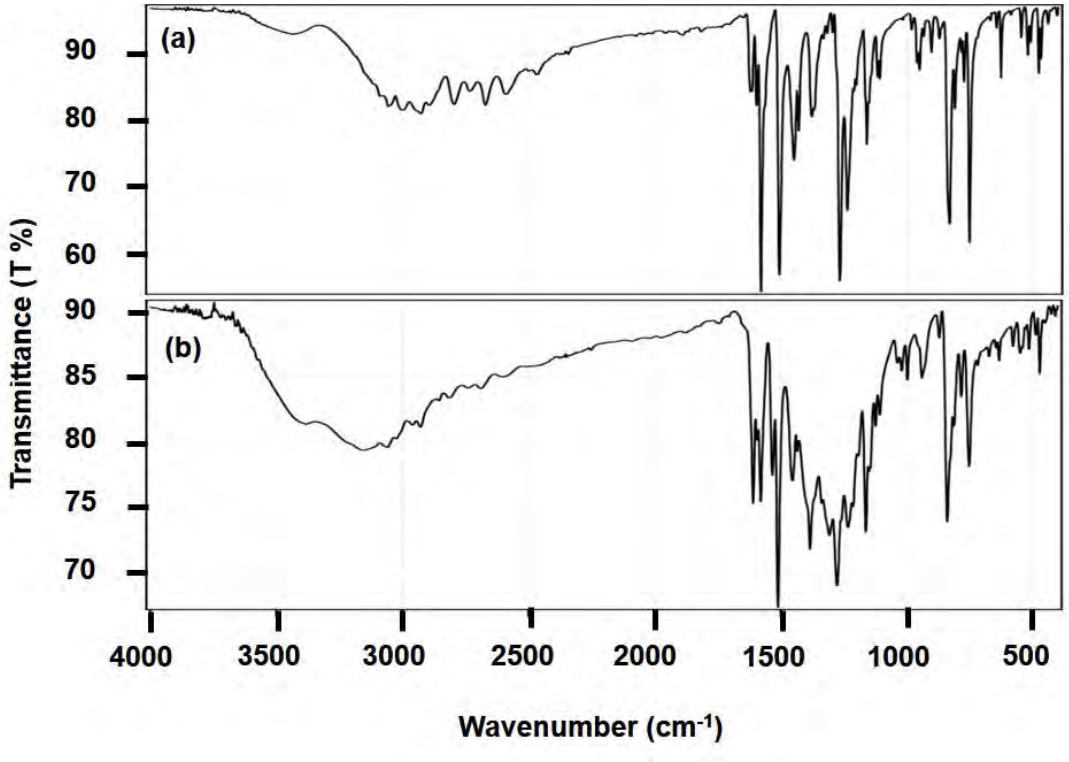

Figure 4.12 Infrared spectra of (a) (QMAP) (b) QMAP-Cu complex recorded in KCl pellet.

The stretching frequency of the non-aromatic C=N bond of QMAP is observed at 1578 cm^{-1}, which decreases to 1508 cm^{-1}. The decrease in frequency can be attributed to the decrease in double-bond character caused by the Cu^{2+} binding. The ESI-MS spectrum further confirmed the proposed composition for the complex. The observed *m/z* value for $[Cu(QMAP)_2]$ is 559.1199 is very similar to the calculated *m/z* value (559.1195) for the complex (see Figure 4.14).

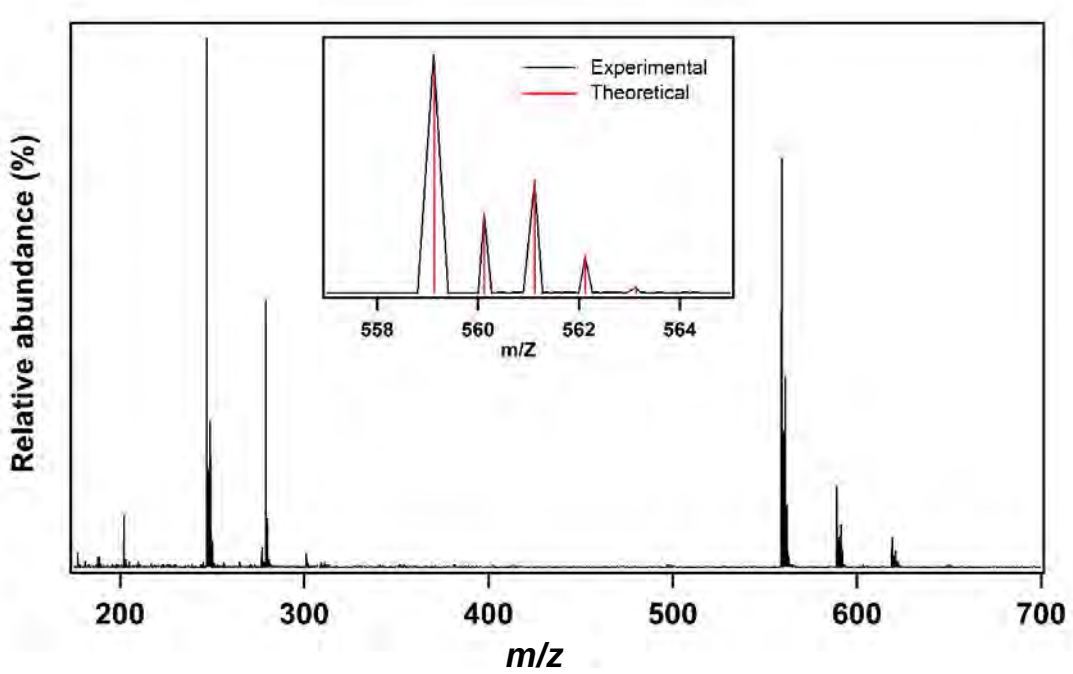

Figure 4.13 ESI-MS spectra of QMAP-Cu complex as $[Cu(QMAP)_2.e]^+$. Inset: Comparison of experimental and theoretical isotopic distribution recorded in MeOH.

Based on this, we propose the structure of QMAP-Cu complex as given in Figure 4.15.

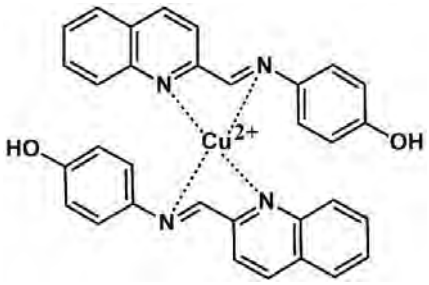

Figure 4.14 Schematic structure of the complex formed between QMAP and copper.

4.3.5 Computational Study

The DFT calculations have been performed for QMAP as well as QMAP-Cu complex to obtain the optimized structures, which are shown in Figure 4.16. The relevant frontier molecular orbitals (FMOs) of the QMAP and QMAP-Cu complex are depicted in Figure 4.17. In QMAP, the HOMOs are positioned mainly over the hydroxyl benzene ring with some contribution from

the quinoline ring. However, the LUMOs are mostly spread over the quinoline ring.

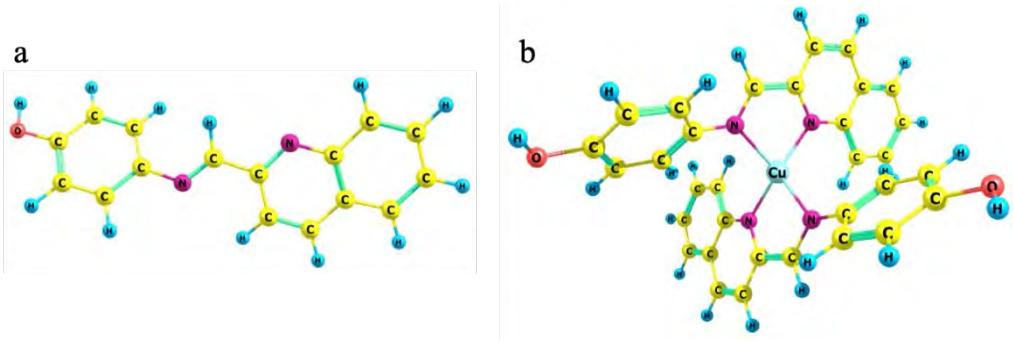

Figure 4.15 Optimized Structures of QMAP and QMAP-Cu complex.

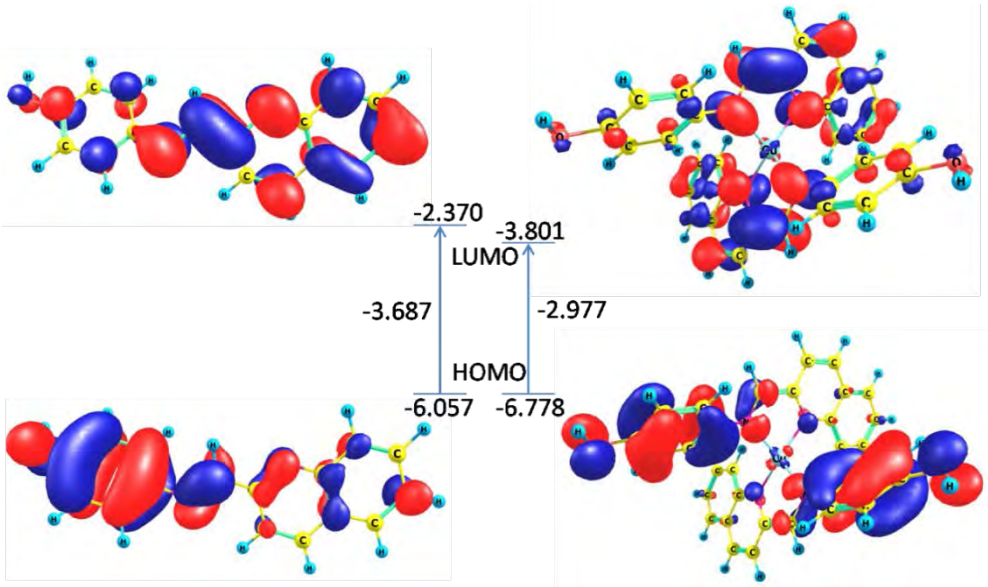

Figure 4.16 The HOMO and LUMO of QMAP and QMAP-Cu complex

Similar to the QMAP, the HOMOs of the QMAP-Cu complex involves the localization of π orbital primarily located over the region of both hydroxyl benzene rings and slightly on the imine groups attached to the hydroxyl benzene rings. Whereas the LUMOs involve the localization of π* orbital positioned over the both quinoline rings and the imine groups.

From the calculation, the HOMO and LUMO energies and their energy gap(ΔE), chemical hardness(η), electronic chemical potential(μ) are calculated

(see Table 4.1). The ΔE value is found to be 3.687 eV for the QMAP and 2.977 eV for the QMAP-Cu^{2+}, respectively. The smaller value of ΔE for QMAP-Cu complex compared to that of the free QMAP, signifies the redshifted absorption band of the complex.

Table 4.1 Result of theoretical calculation for QMAP and QMAP-Cu complex

	System	
	QMAP	**QMAP-Cu complex**
E_{HOMO} **(eV)**	-6.057	-6.778
E_{LUMO} **(eV)**	-2.370	-3.801
ΔE (eV)	3.687	2.977
η (eV)	1.843	1.489
μ (eV)	-4.21	-5.29

Chemical hardness, η, of a chemical species is the measure of resistance in its electronic configuration and can be calculated as $\eta = \Delta E/2$ [35]. Larger the value of ΔE more stable is the system. The η values of QMAP and QMAP-Cu complex are estimated to be 1.843 eV and 1.489 eV, respectively. The electronic chemical potential (μ) is defined as negative of the electronegativity of a system and it can be obtained by $\mu = (E_{HOMO}/E_{LUMO})/2$.[49] The μ can also describe escaping tendency of electron from the equilibrium state. Smaller the value of μ the more stable will be the complex. The μ values of the QMAP-Cu complex and the chemosensor (QMAP) have been determined to be -5.29 eV and -4.21 eV, respectively.

For QMAP and QMAP-Cu complex, the molecular electrostatic potential surface (MESPS) is shown in Figure 4.18. The color code of the MESPS plot has the order red>yellow>green>blue where red and blue represents the most and least electron-rich regions, respectively. From the plot it is clear that for QMAP the most electron rich area is located over the oxygen

atom of hydroxyl group attached to the benzene framework and N atom of the imine group along with the N atom of the quinoline.

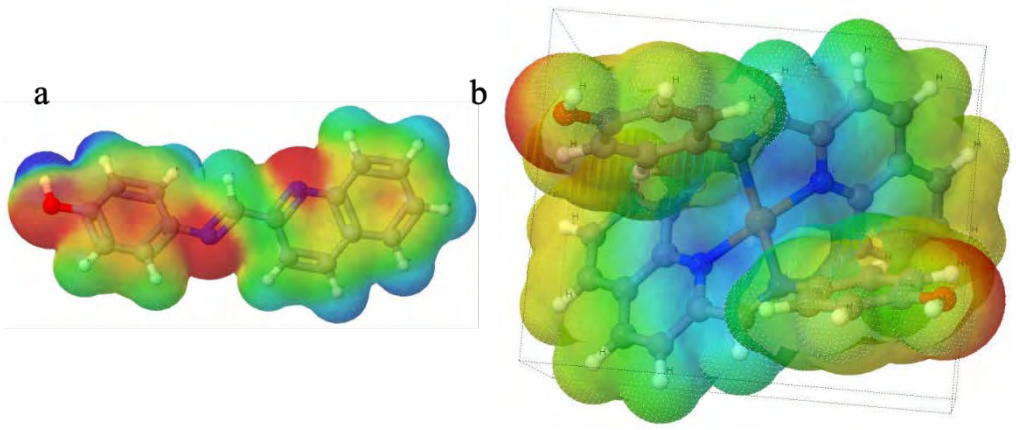

Figure 4.17 Molecular electrostatic potential surface (MESPS) of the QMAP and QMAP-Cu complex.

On the other hand, the most electron deficient region is found over the H atom of the hydroxyl group linked to the benzene and over a few hydrogens of the quinoline rings. In the case of QMAP-Cu complex, the most electron rich region is found to surround over the O atom of the OH groups connected to the benzene rings, while the region around the Cu atom found to be most electron deficient. This result indicate a ligand to metal charge transfer process operational in the QMAP-Cu complex.

4.4 Conclusions

The molecule QMAP was synthesized using a one step process and its ability to selective detection of Cu^{2+} was monitored using UV-Visible absorption spectroscopy. In presence of Cu^{2+} ion, the absorption band of QMAP gets red-shifted by 23 nm and a completely new band around 555 nm formed. The molecule was found to be capable of detecting Cu^{2+} effectively even in presence of other metal ions and was found to sense Cu^{2+} in most of its salts, ca. nitrate, sulphate, chloride and acetate. Spectroscopic titration and the Job's plots suggest a 2:1 binding between QMAP and Cu^{2+} and the binding constant is found to be very high (3.2×10^{10} M^{-2}). Even though the crystal

structure for the QMAP-Cu^{2+} could not be obtained, ^{1}H and ^{13}C NMR, FT-IR, and mass spectrum along with theoretical calculation and MESPS map reveal that the metal is binding to QMAP with the help of the lone pairs on nitrogen and the distinct change in color is due to metal to ligand charge transfer. Overall, a new quinolone based compound is used as a potential sensor of Cu^{2+} with very high binding constant and very low detection limit.

References

1 R. Xie, Y. Yi, Y. He, X. Liu and Z.-X. Liu, *Tetrahedron*, 2013, **69**, 8541–8546.

2 J. Su, J. Xu, Y. Chen, Y. Xiang, R. Yuan and Y. Chai, *Biosens. Bioelectron.*, 2013, **45**, 219–222.

3 W.-L. Chang and P.-Y. Yang, *J. Lumin.*, 2013, **141**, 38–43.

4 X. Wu, P. A. J. Leegwater and H. Fieten, *Int. J. Mol. Sci.*, 2016, **17**, 196.

5 L. Tang, P. Zhou, Z. Huang, J. Zhao and M. Cai, *Tetrahedron Lett.*, 2013, **54**, 5948–5952.

6 H. Zhou, J. Wang, Y. Chen, W. Xi, Z. Zheng, D. Xu, Y. Cao, G. Liu, W. Zhu, J. Wu and Y. Tian, *Dye. Pigment.*, 2013, **98**, 1–10.

7 M. R. Awual, M. Ismael, T. Yaita, S. A. El-Safty, H. Shiwaku, Y. Okamoto and S. Suzuki, *Chem. Eng. J.*, 2013, **222**, 67–76.

8 Y. Shiraishi, N. Saito and T. Hirai, *J. Am. Chem. Soc.*, 2005, **127**, 12820–12822.

9 Y. Wang, L. Shi, H. S. Sun, Z. Shang, J. Chao and W. Jin, *J. Lumin.*, 2013, **139**, 16–21.

10 R. Liu, Z. Chen, S. Wang, C. Qu, L. Chen and Z. Wang, *Talanta*, 2013, **112**, 37–42.

11 E. Madsen and J. D. Gitlin, *Annu. Rev. Neurosci.*, 2007, **30**, 317–337.

12 R. R. Crichton, D. T. Dexter and R. J. Ward, *Coord. Chem. Rev.*, 2008, **252**, 1189–1199.

13 J. B. Willis, *Anal. Chem.*, 1961, **33**, 556–559.

14 A. Maquieira, H. A. M. Elmahadi and R. Puchades, *Anal. Chem.*, 1994, **66**, 3632–3638.

15 M. A. Arnold and M. E. Meyerhoff, *Anal. Chem.*, 1984, **56**, 20–48.

16 D. S. Bushee, *Analyst*, 1988, **113**, 1167–1170.

17 S. S. Berman, J. W. Mclaren and S. N. Willie, *Anal. Chem.*, 1980, 488–492.

18 C. Belmont, M.-L. Tercier, J. Buffle, G. C. Fiaccabrino and M. Koudelka-Hep, *Anal. Chim. Acta*, 1996, **329**, 203–214.

19 H. R. Linder, H. D. Seltner and B. Schreiber, *Anal. Chem.*, 1978, **50**, 896–899.

20 L. Zhang, X. Cui, J. Sun, Y. Wang, W. Li and J. Fang, *Bioorg. Med. Chem. Lett.*, 2013, **23**, 3511–3514.

21 Z. Dong, Y. Guo, X. Tian and J. Ma, *J. Lumin.*, 2013, **134**, 635–639.

22 L. Zhang, D. Duan, X. Cui, J. Sun and J. Fang, *Tetrahedron*, 2013, **69**, 15–21.

23 S. Zhu, W. Lin and L. Yuan, *Dye. Pigment.*, 2013, **99**, 465–471.

24 Y. Cao, L. Ding, W. Hu, L. Wang and Y. Fang, *Appl. Surf. Sci.*, 2013, **273**, 542–548.

25 V. Chandrasekhar, S. Das, R. Yadav, S. Hossain, R. Parihar, G. Subramaniam and P. Sen, *Inorg. Chem.*, 2012, **51**, 8664–8666.

26 Y. Cai, X. Meng, S. Wang, M. Zhu, Z. Pan and Q. Guo, *Tetrahedron Lett.*, 2013, **54**, 1125–1128.

27 K. Ghosh and D. Tarafdar, *Supramol. Chem.*, 2015, **27**, 224–232.

28 R. K. Pathak, J. Dessingou, V. K. Hinge, A. G. Thawari, S. K. Basu and C. P. Rao, *Anal. Chem.*, 2013, **85**, 3707–3714.

29 M. Mac, T. Uchacz, A. Danel and H. Musiolik, *J. Fluoresc.*, 2013, **23**, 1207–1215.

30 L.-K. Zhang, Q.-X. Tong and L.-J. Shi, *Dalt. Trans.*, 2013, **42**, 8567–8570.

31 S. J. Ranee, G. Sivaraman, A. M. Pushpalatha and S. Muthusubramanian, *Sensors Actuators B Chem.*, 2018, **255**, 630–637.

32 D. Wang and X.-J. Zheng, *Inorg. Chem. Commun.*, 2017, **84**, 178–181.

33 C. Wu, J. Wang, J. Shen, C. Zhang, Z. Wu and H. Zhou, *Tetrahedron*, 2017, **73**, 5715–5719.

34 V. Tekuri and D. R. Trivedi, *Anal. Chim. Acta*, 2017, **972**, 81–93.

35 S. B. Roy and K. K. Rajak, *J. Photochem. Photobiol. A Chem.*, 2017, **332**, 505–514.

36 P. Das, A. K. Mandal, U. Reddy G., M. Baidya, S. K. Ghosh and A. Das, *Org. Biomol. Chem.*, 2013, **11**, 6604–6614.

37 B. S. Jursic, F. Douelle, K. Bowdy and E. D. Stevens, *Tetrahedron Lett.*, 2002, **43**, 5361–5365.

38 M. J. Frisch, G. W. Trucks, H. B. Schlegel, G. E. Scuseria, M. A. Robb, J. R. Cheeseman, G. Scalmani, V. Barone, B. Mennucci, G. A. Petersson, H. Nakatsuji, M. Caricato, X. Li, H. P. Hratchian, A. F. Izmaylov, J. Bloino, G. Zheng, J. L. Sonnenberg, M. Hada, M. Ehara, K. Toyota, R. Fukuda, J. Hasegawa, M. Ishida, T. Nakajima, Y. Honda, O. Kitao, H. Nakai, T. Vreven, J. A. Montgomery, J. E. Peralta, F. Ogliaro, M. Bearpark, J. J. Heyd, E. Brothers, K. N. Kudin, V. N. Staroverov, R. Kobayashi, J. Normand, K. Raghavachari, A. Rendell, J. C. Burant, S. S. Iyengar, J. Tomasi, M. Cossi, N. Rega, J. M. Millam, M. Klene, J. E. Knox, J. B. Cross, V. Bakken, C. Adamo, J. Jaramillo, R. Gomperts, R. E. Stratmann, O. Yazyev, A. J. Austin, R. Cammi, C. Pomelli, J. W. Ochterski, R. L. Martin, K. Morokuma, V. G. Zakrzewski, G. A. Voth, P. Salvador, J. J. Dannenberg, S. Dapprich, A. D. Daniels, Ö. Farkas, J. B. Foresman, J. V Ortiz, J. Cioslowski and D. J. Fox, Gaussian 09 (Revision A.02), Gaussian, Inc., Wallingford CT, 2016.

39 A. D. Becke, *J. Chem. Phys.*, 1993, **98**, 5648–5652.

40 P. J. Stephens, F. J. Devlin, C. F. Chabalowski and M. J. Frisch, *J. Phys. Chem.*, 1994, **98**, 11623–11627.

41 K. Kim and K. D. Jordan, *J. Phys. Chem.*, 1994, **98**, 10089–10094.

42 J. Tomasi, B. Mennucci and R. Cammi, *Chem. Rev.*, 2005, **105**, 2999–3094.

43 F. Weigend, *Phys. Chem. Chem. Phys.*, 2006, **8**, 1057–1065.

44 G. A. Zhurko, ChemCraft, http://www.chemcraftprog.com.

45 R. Hanson, M. Howard and E. Willighagen, Jmol: an open-source Java viewer for chemical structures in 3D, http://www.jmol.org.

46 Y. Ding, T. Li, W. Zhu and Y. Xie, *Org. Biomol. Chem.*, 2012, **10**, 4201–

4207.

47 A. Das, S. U. Dighe, N. Das, S. Batra and P. Sen, *Spectrochim. Acta Part A Mol. Biomol. Spectrosc.*, 2019, **220**, 117099.

48 E. L. Que, D. W. Domaille and C. J. Chang, *Chem. Rev.*, 2008, **108**, 1517–1549.

49 R. Vijayaraj, V. Subramanian and P. K. Chattaraj, *J. Chem. Theory Comput.*, 2009, **5**, 2744–2753.

Chapter 5

Synthesis and application of N^1,N^1-diethyl-N^4-(quinolin-2-ylmethyl)benzene-1,4-diamine (RQMBD) for selective and sensitive visual detection of Cu^{2+} at PPB level

An optimum level of Cu^{2+} is crucial for maintaining biological activities in our body. Thus, it is very important to detect the amount of Cu^{2+} in the ingredients take up by us. Over the past few decades, a large number of chemosensors have been developed for selective and quantitative detection of Cu^{2+}. In this work, we have developed a new quinoline based chemosensor following straightforward synthetic procedure from very cheap starting materials that can detect Cu^{2+} visually. A 2:1 binding mechanism of the ligand with Cu^{2+} is proposed using Job's plot. Gigantic binding constant, zero interference from other ions, ppb level sensitivity, and instantaneous detection makes it a good candidate for the Cu^{2+} sensing application.

5.1 Introduction

Optimum amount of the transition metal ions are very important for life and have a crucial effect on several physiological and environmental processes.[1,3] Cu^{2+} is the third most available (after iron and zinc) essential trace element for human and is involved as a cofactor of several enzymes such as cytochrome-C oxidase, tyrosinase, catechol oxidase, bilirubin oxidase, ceruloplasmin, dopamine β monooxygenase and superoxide dismutase.[4-9] It is also crucial for healthy brain function and oxidative metabolism.[9,10] Copper is also essential for infant growth, bone strength, iron transport, cholesterol and glucose metabolism.[11] The deficiency of copper may lead to Menkes disease, anemia, neutropenia, bone abnormalities.[12] However, excess of copper is also not good and results in chronic toxicity associated with Wilson's disease, Parkinson's disease, Prion disease, Alzheimer's disease and various gastrointestinal problems.[6,12-19] Considering its dual behavior in various physiological processes World Health Organization have set the safe limit of daily copper intake as 1.5-3 mg for adults.[20] Copper in drinking water is recommended also as 1-2 mg/liter.[10] Thus, it is very important to detect Cu^{2+} even at a very low concentration to assess the associated health risks.

Till date, various methods are developed for the sensing of Cu^{2+} including absorption spectrometry[21], inductively coupled atomic emission spectrometry[22], ion-selective electrodes[23], surface-plasma resonance detectors[24,25], quantum dot based assays[26] and Anodic stripping voltammetry (ASV).[27] From the viewpoint of cost-effectiveness and routine applications, these techniques are not very suitable even though one gets very high selectivity and sensitivity towards Cu^{2+}. On the other hand, the visual detection of Cu^{2+} employing optical spectroscopy is simple, highly sensitive, cost-effective and also having ppm to sub-ppm level detection limit.[28-32] A number of molecules have been reported for the spectroscopic identification of Cu^{2+} by employing either absorption and/or fluorescence spectroscopy. However, most of the colorimetric sensors for Cu^{2+} suffers from one or the other drawbacks.

Hrishikesan *et al.* reported a *bis*-triazole appended azobenzene chromophore for selective detection of Cu^{2+}. But, the synthesis of the chromophore is very complicated.[33] Kaur *et al.* reported a triazolyl monoazo derivative for Cu^{2+} sensing. In this case, the detection limit is too high.[34] For some other Cu^{2+} sensors, response time is too long.[35,36] Some reported chemosensors also suffers from the interference from other metals.[35-39] As a result, there is still a high demand for a better chemosensor, especially if it can detect Cu^{2+} in ppm level visually in a cost effective

In our study, we have developed a simple colorimetric chemosensor N^1,N^1-diethyl-N^4-(quinolin-2-ylmethyl)benzene-1,4-diamine (RQMBD), which is successfully synthesized by reduction of a Schiff-base as shown in Scheme 5.1. A systematic analysis was done for this chemosensor to investigate its sensing ability for Cu^{2+} ions. Intriguingly, RQMBD gives a visual color change from pale yellow to red, good detection limit and fast response time, with high selectivity and sensitivity towards Cu^{2+}. The rest of the paper presents the details of our study.

5.2 Experimental methods

5.2.1 Material and measurements

All the reagents used were of analytical grades and used without any further purification. Both the starting materials, quinoline 2-carbaldehyde and N^1,N^1-diethylbenzene-1,4-diammine, were purchased from Sigma Aldrich. Various Cu^{2+} salts (nitrate, chloride, bromide, chlorate and sulphate) and nitrate salts of various metal ions (e.g., Na^+, K^+, Ca^{2+}, Mg^{2+}, Fe^{2+}, Mn^{2+}, Co^{2+}, Ni^{2+}, Cu^{2+}, Zn^{2+}, Cd^{2+}, Sr^{2+}, Pb^{2+}) are bought from Sigma Aldrich. HPLC methanol was purchased from Finar Chemical Ltd., and was used after distillation for various solution preparation. UV-Vis absorption and emission spectra of the samples were measured on a commercial spectrophotometer (UV2450, Schimadzu, Japan) and fluorimeter (Fluoromax, Horiba Jobin-Yvon, USA), respectively. NMR spectra were obtained on a commercial NMR spectrometer

(400 MHz, JOEL, Japan). ESI-MS spectra were recorded on a triple quadrupole mass spectrometer (Waters-HAB213 spectrometer, USA). All the experiments are done at 25°C.

5.2.2 Synthesis and characterization of *N,N*-diethyl(quinolin-2-ylmethyl)-benzene-1,4-diamine (RQMBD)

The chemosensor, RQMBD, was synthesized in two steps as summarized in Scheme 5.1. In the first step, N^1,N^1-diethyl-N^4-(quinolin-2-ylmethylene)benzene-1,4-diamine (QMBD) was synthesized by condensation of quinolone-2-carbaldehyde and N^1,N^1-diethylbenzene-1,4-diammine through nucleophilic substitution reaction. The details of this synthesis is reported in our previous publication.[40]

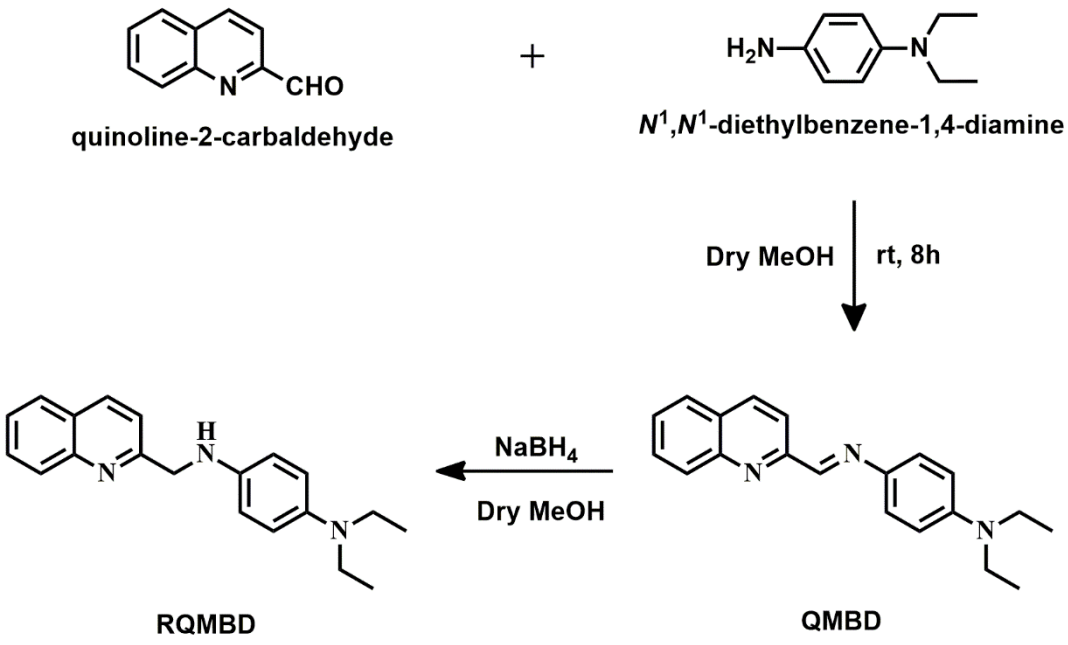

Scheme 5.1 Synthetic scheme for N^1,N^1-diethyl-N^4(quinolin-2-ylmethyl)benzene-1,4-diamine (RQMBD)

Simple reduction of this compound by sodium borohydride produces N^1,N^1-diethyl-N^4-(quinolin-2-ylmethyl)benzene-1,4-diamine (RQMBD), which is obtained as a yellowish compound. It was then washed with cold methanol and then with hexane. The pure compound was obtained by column chromatography with a yield of 78%. The compound is characterized by NMR

(Figure 5.1 and 5.2) and mass spectra (Figure 5.3). (^{1}H NMR (400 MHz, DMSO-d_6, ppm) δ: 8.38(d, *J*=8.8 Hz, 1H), 8.23(d, *J*=8.4 Hz, 1H), 8.14(d, *J*=8.4 Hz, 1H), 7.85(d, *J*=8.4 Hz, 1H), 7.75(t, *J*=8.4 Hz, 1H), 7.568(t, *J*=9.6 Hz, 2H), 7.41(d, *J*=9.2 Hz, 2H), 6.69(d, *J*=9.2 Hz, 2H), 5.26(s, 2H), 4.42(s, 1H), 3.04(dd, 12Hz, 4Hz, 4H), 1.08(t, 8Hz, 6H). ^{13}C NMR (100 MHz, DMSO-d_6, ppm): δ= 161.52, 147.49, 136.56, 130.03, 128.95, 128.04, 125.97, 123.68, 119.73, 116.39, 113.66, 111.56, 45.31, 43.87, 13.04. ESI-MS: *m/z*: found [M + H^+] = 306.19, molecular formula $C_{20}H_{23}N_3$, requires [M + H^+] = 306.19.

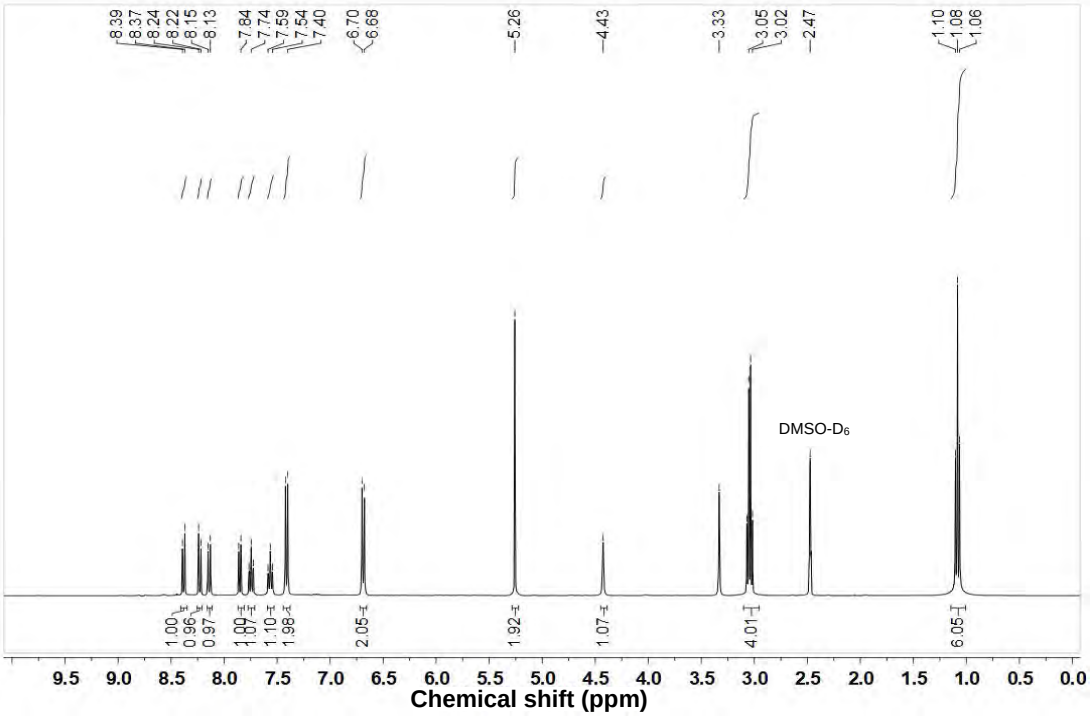

Figure 5.1 ^{1}HNMR spectrum of RQMBD in DMSO-d_6

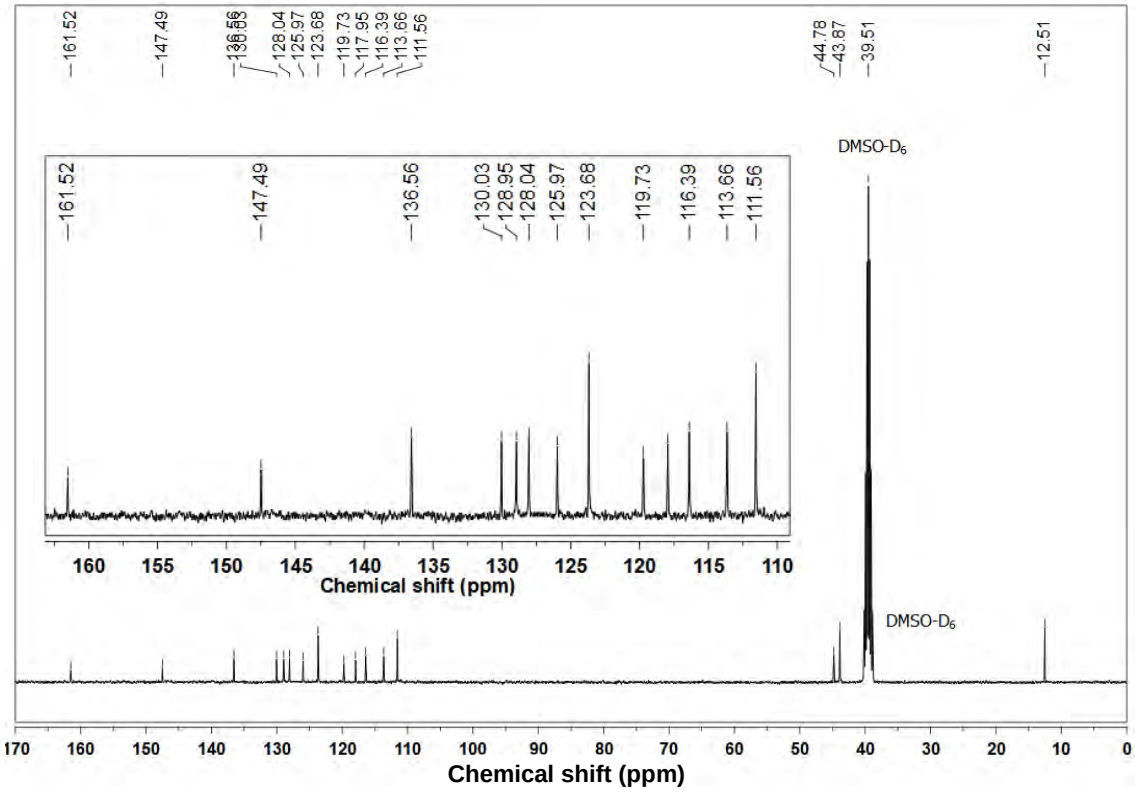

Figure 5.2 ^{13}C NMR of RQMBD in DMSO-d_6.

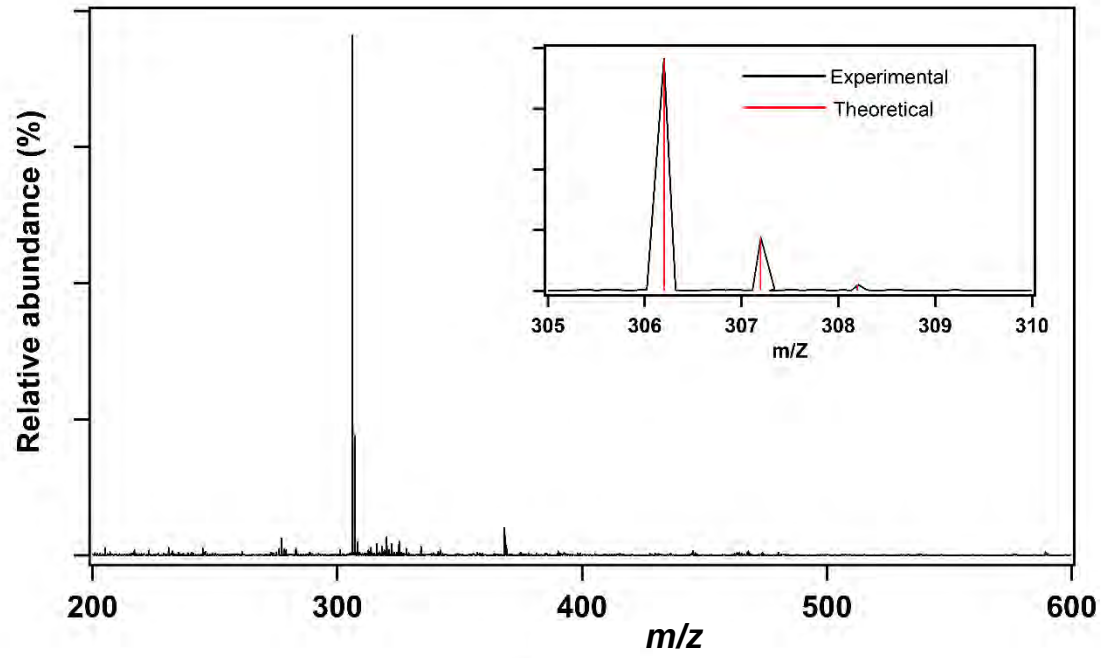

Figure 5.3 . ESI-MS spectrum of RQMBD

5.2.3 General procedures

A stock solution of the chemosensor (0.2 mM RQMBD) was prepared in methanol. Metal ion solutions (2 mM) of $NaNO_3$, KNO_3, $Ca(NO_3)_2$, $Mg(NO_3)_2.6H_2O$, $Fe(NO_3)_3.9H_2O$, $Mn(NO_3)_2$, $Co(NO)_2.6H_2O$, $Ni(NO_3)_2.6H_2O$, $Cu(NO_3)_2.3H_2O$, $Zn(NO_3)_2.6H_2O$, $Sr(NO_3)_2.4H_2O$, $Cd(NO_3)_2.4H_2O$, $Pb(NO_3)_2$, $CuCl_2.2H_2O$, $CuBr_2.2H_2O$, $Cu(ClO_4)_2.6H_2O$, and $CuSO_4.5H_2O$, were prepared in MeOH. The stoke solutions of all metal ions are then diluted according to the experimental requirements and then added to the solution of RQMBD, which was diluted to 40 µM with MeOH. All spectral data were measured after 1 minute of the sample preparation.

5.3 Result and discussion

5.3.1 Spectroscopic characterization of RQMBD

The steady state absorption and emission studies were conducted for RQMBD in methanol at 20 µM concentration. It shows an absorption maximum at ~350 nm with an extinction coefficient of 16000 M^{-1} cm^{-1}. Upon exciting at 350 nm, it shows an emission maximum centered around 445 nm as illustrated in Figure 5.4. We did not observe any apparent change in absorbance of RQMBD with time, indicating no degradation of the chemosensor in the solution phase.

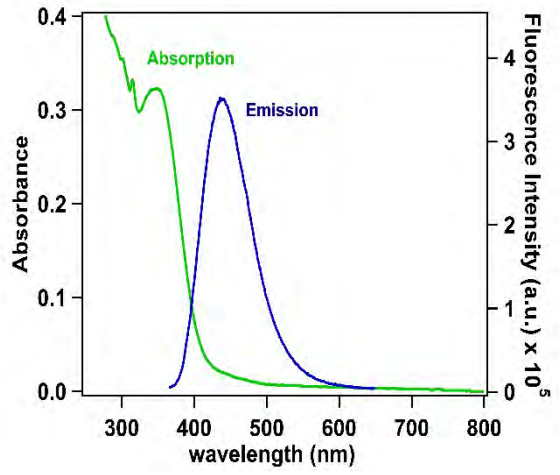

Figure 5.4 Absorption (black) and emission (red) spectra of RQMBD in methanol

5.3.2 RQMBD as selective and sensitive Cu^{2+} sensor

Two equivalent methanolic solutions of different metal ions (Na^{+}, K^{+}, Mg^{2+}, Ca^{2+}, Mn^{2+}, Co^{2+}, Ni^{2+}, Zn^{2+}, Sr^{2+}, Cd^{2+}, Cu^{2+}, Pb^{2+} and Fe^{2+}) were added separately to 20 µM methanolic solution of RQMBD. We did not observe any change in color of the sensor solution on addition of metal salts except for Cu^{2+}, for which the pale yellow color of the solution turns to red instantaneously as shown in Figure 5.5.

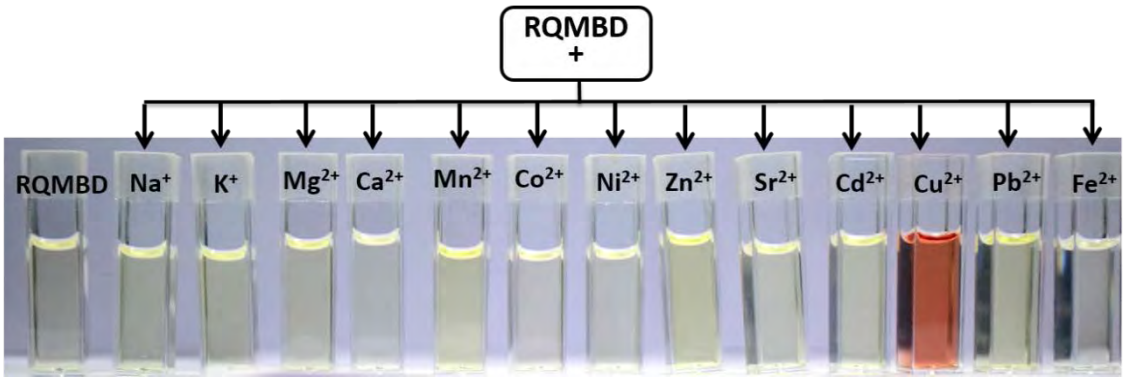

Figure 5.5 Photographic image of the color change of RQMBD upon addition of different metal ions.

The absorption maxima shifted to 375 nm from 350 nm with a new band appearing around 550 nm. The appearance of new band around 550 nm is the reason for the colorimetric transition from pale yellow to red upon addition of Cu^{2+} in RQMBD. From fluorescence study, we see that, Cu^{2+} quenches the fluorescence intensity of RQMBD when excited at 350 nm. Addition of other metals ion induce either a little or no change in the absorption and emission spectra of RQMBD as shown in Figure 5.6(a) and 5.6(b), respectively. Especially Ni^{2+}, Cd^{2+} and Co^{2+}, which are also well-known quencher, does not quench the emission of RQMBD at all. This makes RQMBD a potential Cu^{2+} sensor. The different spectrophotometric and spectrofluorimetric response of RQMBD only towards Cu^{2+} implies that there is some specific interaction between Cu^{2+} and RQMBD. For other metal ions, the interaction between metal

ions and RQMBD is either totally absent or too low to detect.

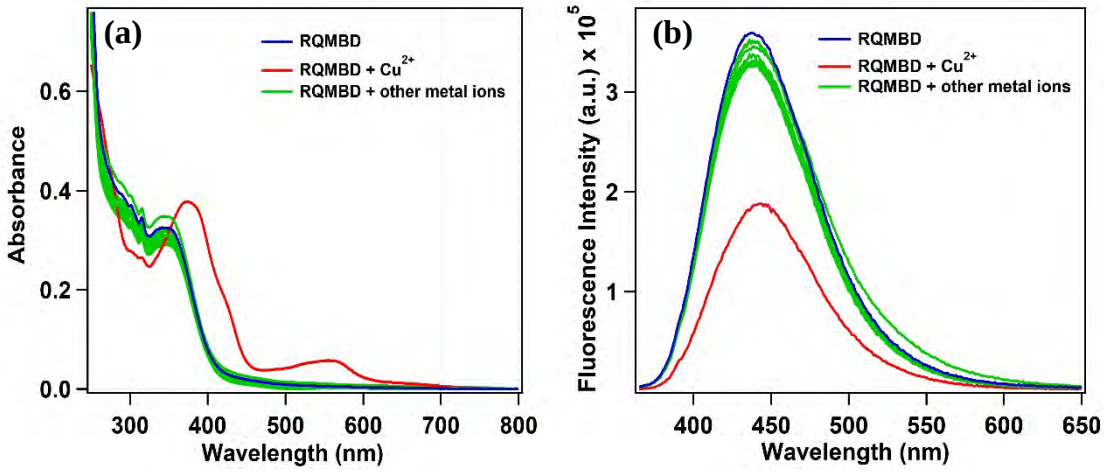

Figure 5.6 Spectral analysis of selectivity of RQMBD towards various metal ions (a) UV-visible absorption spectra of RQMBD (20 µM in methanol) in the presence of 2 equivalent of various metal ions. (b) Emission spectra of RQMBD (20 µM in methanol) in the presence of 2 equivalent of various metal ions, when excited at 350 nm.

Further we have done a competitive experiment by measuring the absorption and emission of one equivalent of RQMBD with one equivalent of Cu^{2+} in presence of 20 equivalents of different metal salts. From the Figure 5.7(a) and (b) we can see that there is no change in the absorption profile or emission profile of RQMBD + Cu^{2+} system even in presence of 20 equivalent of other metal ions.

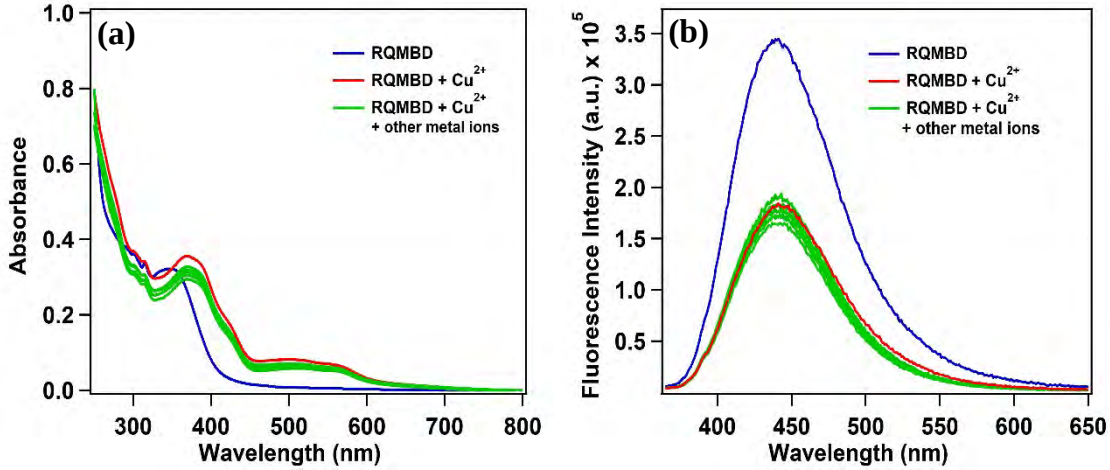

Figure 5.7 (a) UV-Visible absorption and (b) emission spectra of RQMBD (20 µM) and RQMBD-Cu^{2+} complex in the presence of other metal ions (Na^{+}, Mg^{2+}, K^{+}, Ca^{2+}, Fe^{2+}, Mn^{2+}, Co^{2+}, Ni^{2+}, Zn^{2+}, Sr^{2+}, Cd^{2+} and Pb^{2+}) in excess (400 µM).

Therefore, we conclude that our sensor can detect Cu^{2+} selectively and sensitively even in presence of excess concentration of other co-existing metal salts.

We have illustrated this analysis in a bar diagram (Figure 5.8), though our sensor is not quenched that much like some previous reports.[2,32] but from the viewpoint of interference, our sensor does have an edge over most of the reported Cu^{2+} sensor.

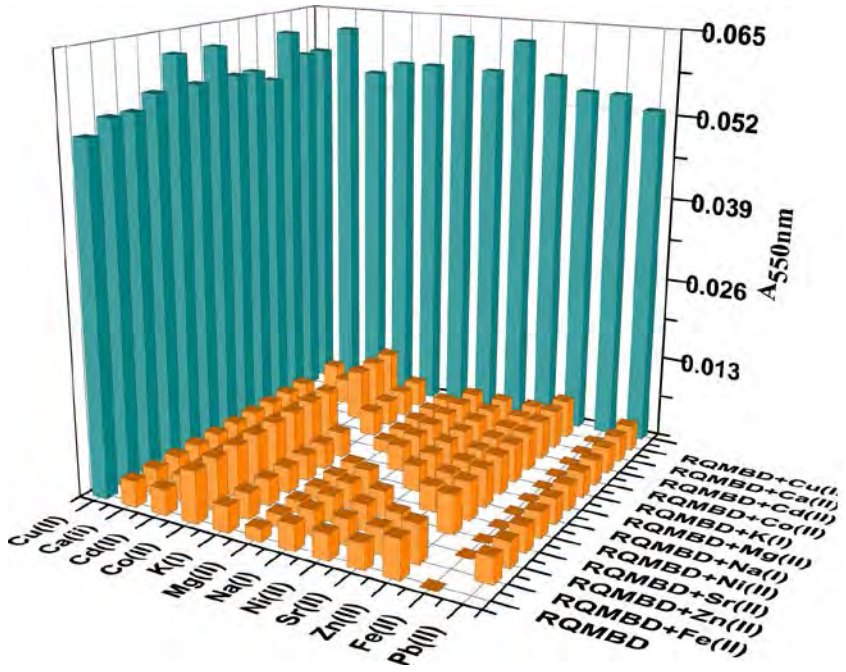

Figure 5.8 Bar diagram showing the selectivity and sensitivity of RQMBD on Cu^{2+} over other cations using absorbance at 550nm

5.3.3 Role of counter ion in the sensing ability

The spectroscopic behavior of RQMBD with different salts of Cu^{2+} (perchlorate, chloride, sulphate, and bromide) remains same as that of $Cu(NO_3)_2$ suggesting that there is no role of counter ions upon the sensing as illustrated in Figure 5.9.

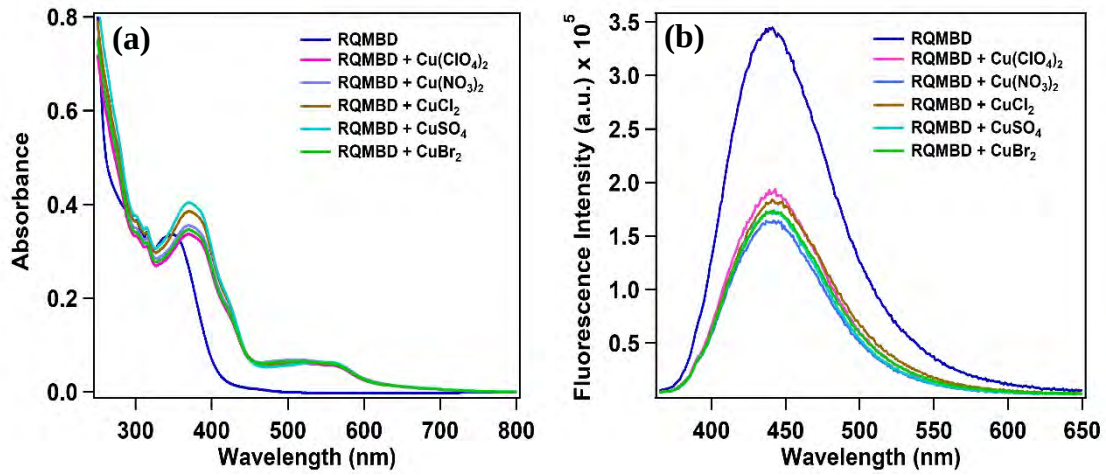

Figure 5.9 (a) UV–Visible absorption and (b) emission spectra of RQMBD (20 μM) in methanol in absence and presence of 20 μM different salts of Cu^{2+} (perchlorate, nitrate, chloride, sulphate and bromide)

5.3.4 Spectrophotometric titration experiment and the binding mechanism

To find the binding stoichiometry between RQMBD and Cu^{2+}, we have used Job's method by monitoring the absorbance at 550 nm. Here we have varied the concentration of RQMBD and Cu^{2+} keeping their total concentration fixed at 40 μM. The Job's plot (Figure 5.10) clearly indicate the formation of a 1:2 ratiometric complex between Cu^{2+} and RQMBD. Accordingly, we propose a structure of the copper-RQMBD as depicted in Figure 5.11.

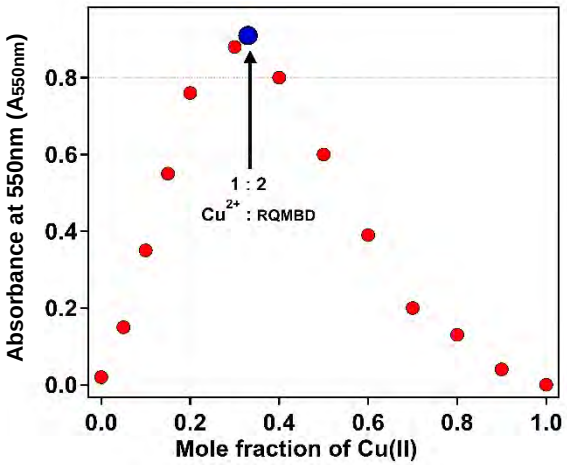

Figure 5.10 Job's plot of RQMBD with Cu^{2+} showing a 1:2 Cu^{2+}-RQMBD complex formation.

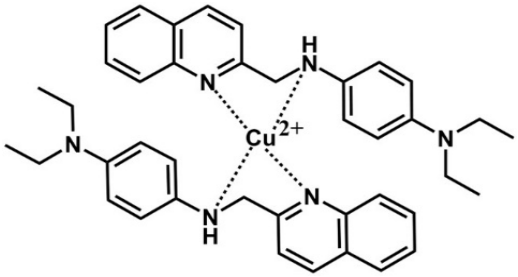

Figure 5.11 Proposed structure of the complex between RQMBD and Cu^{2+}.

To find the binding constant of the complex, we titrated RQMBD with Cu^{2+}. Upon gradual addition of Cu^{2+} (0 µM to 40 µM), in the methanolic solution of RQMBD (20 µM), the absorption band at 350 nm gradually shifts towards 375 nm with a new band developing around 550 nm (Figure 5.12(a)). A clear isosbestic point is observed around 350 nm suggesting a gradual formation of the complex. It is clear that the titration is almost complete when metal concentration is 10 µM (half equivalent that of Cu^{2+}). Further, addition of Cu^{2+} does not change the absorption profile. Such a titration curve is a indicative of a very high binding constant. The equilibrium is represented as:

$$M + 2L \overset{K}{\leftrightarrow} ML_2 \qquad \ldots\ldots\ldots \quad (5.1)$$

where K is the equilibrium constant. When, Cu^{2+} concentration is not too high, we may assume that, $[L_T] > [ML_2]$ and under this approximation the absorbance (A) value at 550 nm in the titration curve can be written as

$$A = \varepsilon_L L_t + \frac{KM_t L_t^2}{1 + KL_t^2}\left(\varepsilon_{ML_2} - \varepsilon_L\right) \qquad \ldots\ldots\ldots \quad (5.2)$$

In the above equation, ε_L is the molar extinction coefficient of RQMBD, L_t and M_t are the total concentration of RQMBD and Cu^{2+}, respectively. ε_{ML_2} is the molar extinction coefficient of the Cu-RQMBD complex. We plotted the absorbance at 550 nm against the Cu^{2+} concentration and got the binding isotherm as depicted in Figure 5.12(b). The isotherm was fitted with equation 5.2 that gives a binding constant of $10.8 \times 10^9\ M^{-2}$. To maintain the assumption

stated above, the curve is fitted till 6 μM of Cu^{2+} concentration.

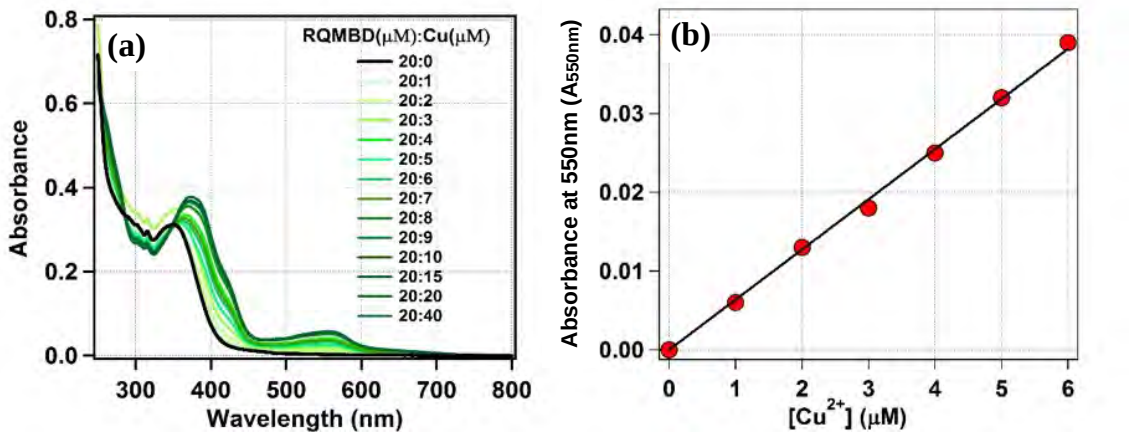

Figure 5.12 (a) UV-Visible titration profile of RQMBD (20 μM) upon gradual addition of Cu^{2+} (0–40 μM). (b) Determination of binding constant between RQMBD and Cu^{2+}.

5.3.5 Limit of detection

The limit of detection (LOD) is the lowest concentration of a substance that can be differentiated from the blank experiment.[41,42] To determine LOD, we need a linear calibration range. We have used UV-visible titration curve for this purpose where the absorption varies linearly with Cu^{2+} concentration.

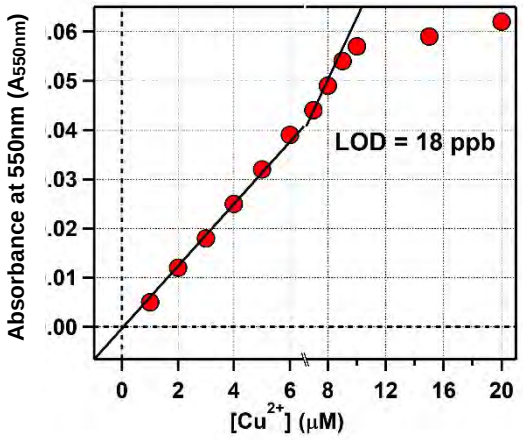

Figure 5.13 Determination of limit of detection of RQMBD towards Cu^{2+}.

From a linear fit in the range between 1 μM and 6 μM, we have calculated the LOD to be 18 ppb which is quite low than what is permissible in drinking water

(see Figure 5.13). Also, from the linear calibration curve it is clear that we can potentially use RQMBD for quantitative measurement of Cu^{2+}.

5.4 Conclusion

In conclusion, we have synthesized a novel quinolone derivative, *N^1, N^1*-diethyl-*N^4*-(quinolin-2-ylmethyl) benzene-1, 4-diamine, that turns out to be an excellent colorimetric chemosensor for Cu^{2+}. Easy methodology and fast response time of detection makes this a potential real time sensor for Cu^{2+}. It also shows high selectivity and sensitivity towards Cu^{2+} ions without any interference of other cations. In addition, the change in color from pale yellow to red shows its great ability for the visual sensing of Cu^{2+}. The binding constant is gigantic (in the order of 10^9). More importantly, the limit of detection of RQMBD (18 ppb) is below than the permissible limit of Cu^{2+} in water. We expect that this molecule can be used in a potential prototype device for preliminary detection of Cu^{2+} ions in environmental samples.

References

1 J. J. R. Fraústo da Silva and R. J. P. Williams, *The Biological Chemistry of the Elements: The Inorganic Chemistry of Life*, Oxford University Press, Oxford, UK, 2nd edn., 2001.

2 X. Chen, T. Pradhan, F. Wang, J. S. Kim and J. Yoon, *Chem. Rev.*, 2012, **112**, 1910–1956.

3 E. Crabb, E. A. Moore and L. E. Smart, Eds., *Concepts in Transition Metal Chemistry*, The Royal Society of Chemistry, Cambridge, UK, 2010.

4 M. Olivares and R. Uauy, *Am. J. Clin. Nutr.*, 1996, **63**, 791S–796S.

5 J. Su, J. Xu, Y. Chen, Y. Xiang, R. Yuan and Y. Chai, *Biosens. Bioelectron.*, 2013, **45**, 219–222.

6 M. C. Linder and M. Hazegh-Azam, *Am. J. Clin. Nutr.*, 1996, **63**, 797S–811S.

7 F. Yu, W. Zhang, P. Li, Y. Xing, L. Tong, J. Ma and B. Tang, *Analyst*, 2009, **134**, 1826–1833.

8 C. Shen and E. J. New, *Metallomics*, 2015, **7**, 56–65.

9 L. Yang, R. McRae, M. M. Henary, R. Patel, B. Lai, S. Vogt and C. J. Fahrni, *Proc. Natl. Acad. Sci.*, 2005, **102**, 11179–11184.

10 T. D. Rae, P. J. Schmidt, R. A. Pufahl, V. C. Culotta and T. O'Halloran, *Science*, 1999, **284**, 805–808.

11 P. G. Georgopoulos, A. Roy, M. J. Yonone-Lioy, R. E. Opiekun and P. J. Lioy, *J. Toxicol. Environ. Heal. Part B*, 2001, **4**, 341–394.

12 S. M. Wazir and I. Ghobrial, *J. Community Hosp. Intern. Med. Perspect.*, 2017, **7**, 265–268.

13 J. D. Huff, Y.-K. Keung, M. C. Thakuri, M. W. Beaty, J. Owen and I. Molnar, *Blood*, 2005, **106**, 1681.

14 M. R. Allen and D. B. Burr, in *Basic and Applied Bone Biology*, eds. D. B. Burr and M. R. Allen, Academic Press, San Diego, 2014, pp. 75–90.

15 G. J. Brewer, *Curr. Opin. Chem. Biol.*, 2003, **7**, 207–212.

16 G. Multhaup, A. Schlicksupp, L. Hesse, D. Beher, T. Ruppert, C. L. Masters and K. Beyreuther, *Science (80-.).*, 1996, **271**, 1406–1409.

17 H.-H. Wang, L. Xue, Z.-J. Fang, G.-P. Li and H. Jiang, *New J. Chem.*, 2010, **34**, 1239–1242.

18 E. Gaggelli, H. Kozlowski, D. Valensin and G. Valensin, *Chem. Rev.*, 2006, **106**, 1995–2044.

19 D. Strausak, J. F. B. Mercer, H. H. Dieter, W. Stremmel and G. Multhaup, *Brain Res. Bull.*, 2001, **55**, 175–185.

20 *Trace elements in human nutrition and health*, Geneva, Switzerland, 1996.

21 M. Ghaedi, F. Ahmadi and A. Shokrollahi, *J. Hazard. Mater.*, 2007, **142**, 272–278.

22 R. Rahil-Khazen, B. J. Bolann, A. Myking and R. J. Ulvik, *J. Trace Elem. Med. Biol.*, 2002, **16**, 15–25.

23 D. Grujicic and B. Pesic, *Electrochim. Acta*, 2002, **47**, 2901–2912.

24 Y. Hong, S. Jo, J. Park, J. Park and J. Yang, *Nanotechnology*, 2018, **29**, 215501.

25 E. S. Forzani, H. Zhang, W. Chen and N. Tao, *Environ. Sci. \& Technol.*, 2005, **39**, 1257–1262.

26 K. M. Gattás-Asfura and R. M. Leblanc, *Chem. Commun.*, 2003, 2684–2685.

27 J. Duay, J. E. Ortiz-Santiago and T. N. Lambert, *Electroanalysis*, 2017, **29**, 2685–2688.

28 S. Sun, B. Qiao, N. Jiang, J. Wang, S. Zhang and X. Peng, *Org. Lett.*, 2014, **16**, 1132–1135.

29 J. Yin, Y. Kwon, D. Kim, D. Lee, G. Kim, Y. Hu, J.-H. Ryu and J. Yoon, *J. Am. Chem. Soc.*, 2014, **136**, 5351–5358.

30 Y.-G. Zhang, Z.-H. Shi, L.-Z. Yang, X.-L. Tang, Y.-Q. An, Z.-H. Ju and W.-S. Liu, *Inorg. Chem. Commun.*, 2014, **39**, 86–89.

31 R. Martínez, A. Espinosa, A. Tárraga and P. Molina, *Tetrahedron*, 2008,

64, 2184–2191.

32 V. Chandrasekhar, S. Das, R. Yadav, S. Hossain, R. Parihar, G. Subramaniam and P. Sen, *Inorg. Chem.*, 2012, **51**, 8664–8666.

33 E. Hrishikesan, C. Saravanan, P. Kannan, *Ind. Eng. Chem. Res.*, 2011, **50**, 8225–8229.

34 P. Kaur, D. Sareen and K. Singh, *Talanta*, 2011, **83**, 1695–1700.

35 T. G. Jo, Y. J. Na, J. J. Lee, M. M. Lee, S. Y. Lee and C. Kim, *New J. Chem.*, 2015, **39**, 2580–2587.

36 M. Wang, K.-H. Leung, S. Lin, D. S.-H. Chan, D. W. J. Kwong, C.-H. Leung and D.-L. Ma, *Sci. Rep.*, 2014, **4**, 6794.

37 X. Xu, W. L. Daniel, W. Wei and C. A. Mirkin, *Small*, 2010, **6**, 623–626.

38 Y. J. Na, Y. W. Choi, J. Y. Yun, K.-M. Park, P.-S. Chang and C. Kim, *Spectrochim. Acta Part A Mol. Biomol. Spectrosc.*, 2015, **136**, 1649–1657.

39 J. Y. Noh, G. J. Park, Y. J. Na, H. Y. Jo, S. A. Lee and C. Kim, *Dalt. Trans.*, 2014, **43**, 5652–5656.

40 S. H. Faizi and A. Mashrai, *Acta Cryst.*, 2014, **769**, o905–o906.

41 Y. Ding, T. Li, W. Zhu and Y. Xie, *Org. Biommol. Chem.*, 2012, **10**, 4201–4207.

42 M. Shortreed, R. Kopelman, M. Kuhn and B. Hoyland, *Anal. Chem.*, 1996, **68**, 1414–1418.

Chapter 6

A Schiff base fluorescence turn-off Chemosensor for detection of Cu^{2+}

A new highly selective and sensitive Schiff-base chemosensor, BPIMP, was designed and synthesized for detection of copper ions (Cu^{2+}). This sensor exhibits high selectivity and efficient signaling behavior for Cu^{2+} by exhibited apparent fluorescence quenching for micromolar concentration of Cu^{2+} over other metal ions. In addition, the high affinity of chemosensor towards Cu^{2+} can be seen from the high overall binding constant value $K=1.515 \times 10^{11}\ M^{-2}$. The detection limit (0.032 μM) of BPIMP- Cu^{2+} is far lower than the World Health Organization (7.41 μM) limit for drinking water.

6.1 Introduction

The important roles of various metal ions in medicine, living systems and the environment has gained considerable attention of scientific community to develop highly selective and sensitive chemosensors for their recognition. Among these metals ions, copper ion is one of the most important metal ions which plays important roles in various physiological processes of biological ecosystem.[1–5] The redox-active nature of copper ions makes them an essential cofactor for a large variety of enzymes, including superoxide dismutase, cytochrome *c* oxidase, tyrosinase and maintenance of homeostasis in living organisms.[6–8] So, we have to include those food items in our daily meal which contains copper as it is necessary for our good health. However, excessive overloading of copper ions exhibits toxicity in that it causes various negative health effect such as gastrointestinal problems, liver and kidney failure and several neurodegenerative diseases, such as Menke's disease, Parkinson's disease, Alzheimer's disease and Wilson's disease.[9–13] The widespread use copper in various industrial and agriculture applications, makes copper a significant environmental pollutant because of its non-biodegradable, toxic and persistent nature.[14]

In order to detect Cu^{2+} ions at trace levels, a large number study has been reported which is comprises of traditional detection techniques such as atomic absorption spectroscopy (AAS),[15,16] inductively coupled-plasma mass spectroscopy atomic emission spectroscopy (ICP-MS/AES),[17–20] Stripping square-wave voltammetry (SWV), [21,22] ion selective electrode methods.[23,24] These techniques are time-consuming processes and cannot be used for real-time detection. A large number of fluorescent sensors that can detect Cu^{2+} cation have been developed and reported so far, such as monopyrenylalkylamine derivative,[25] 8-hydroxyquinoline derivative,[26] 2-aza-1,3-butadiene derivatives,[27] *N*-butyl-4,5-di[(pyridin- 2-ylmethyl)amino]-1,8-naphthalimide based on internal charge transfer (ICT),[28] azobenzene derivative etc.[29] Compounds containing hydroxybenzaldehyde upon condensation with

any amine functional group become an important class of NO- ligating chelators.[30,31] According to the Irving – Williams series, Cu^{2+} has the largest formation constant with ligands containing oxygen or nitrogen donor atoms among the first row of transition metal ions.[32] This factor provide a great advantage in the development of new Cu^{2+} chemosensors. Upon surveying the literature we found journals in which studies on a wide variety of interesting metal complexes with this type of ligand. Several closely related molecules have also been developed for sensing metal ions.[33] This attracts the attention of scientific community to focus on the development of such type of sensors.

In this paper, we report a Schiff-base chemosensor BPIMP based on *N*^{1}-phenylbenzene-1,4-diamine appended 3,5-di-*tert*-butyl-2 hydroxybenzaldehyde. This chemosensor successfully shows a prominent selective sensing behavior towards Cu^{2+} ion *via* a fluorescence turn-off route. For instant detection kit for Cu^{2+} ions, test strips were prepared by dipping the paper strips into the chemosensor solution followed by drying.

6.2 Experimental

6.2.1 Materials and methods

Both the starting materials, 3,5-di-*tert*-butyl-2 hydroxybenzaldehyde and *N*^{1}-phenylbenzene-1,4-diamine used in the synthesis of chemosensor are purchased from Sigma Aldrich and used without any further purification. Various Cu^{2+} salts (nitrate, chloride, bromide, chlorate and sulphate), nitrate salts of other metal ions (e.g., Na^{+}, K^{+}, Ca^{2+}, Mg^{2+}, Co^{2+},Cu^{2+}, Ni^{2+}, Zn^{2+}, Sr^{2+}, Cd^{2+}, Pb^{2+}) are bought from Sigma Aldrich. HPLC methanol (MeOH) was purchased from Finar Chemical Ltd., and is used for various solution preparation. The water used for this experiments is deionized water. Infrared spectra were recorded on Perkin-Elmer Lambda 2 spectrometer with KBr discs in the range 4000-400 cm^{-1}. UV-Vis absorption spectra of the samples were measured on a commercial spectrophotometer (UV2450, Schimadzu, Japan).

Fluorescence spectra were measured on fluorimeter (Fluoromax, Horiba Jobin-Yvon, USA).

6.2.2 General methods

Chemosensor BPIMP (0.1 mM) was dissolved in methanol to get the 0.1mM stoke solution. And then, 10 ml stoke solution were taken in to 100 ml volumetric flask and MeOH is added to the volumetric scale mark. Thus 10 µM methanolic solution of chemosensor BPIMP was obtained. Different metal ion solutions (1 mM) were prepared in MeOH. The stoke solutions of all metal ions are then diluted to 50 µM and then added to the 3ml of BPIMP solution. All spectral data were measured after 3 minute of sample preparation.

6.2.3 Synthesis and Characterization of BPIMP

Scheme 6.1 shows the synthetic procedure of formation of 2,4-di-*tert*-butyl-6-(((4(phenylamino)phenyl)imino)methyl)phenol (BPIMP) in a single step reaction. 184.24 mg,(1.0 mmol) of N^1-phenylbenzene-1,4-diamine was dissolved in 10 ml of absolute ethanol.[34] To this solution, 234.33 mg (1 mmol) of 3,5-di-*tert*-butyl-2 hydroxybenzaldehyde in 10 ml of absolute ethanol

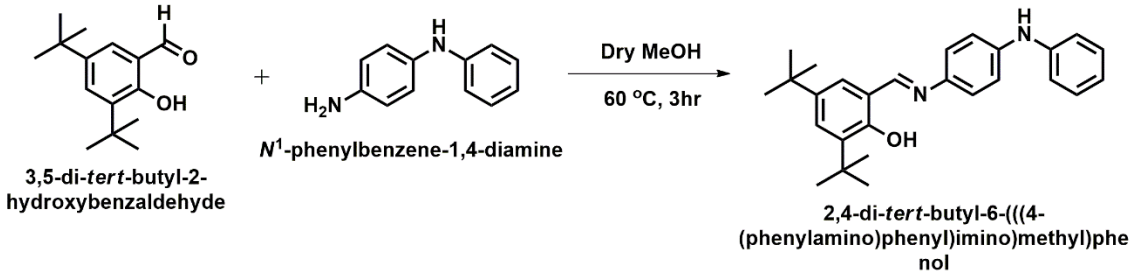

Scheme 6.1 The Synthetic route of sensor BPIMP

was added drop wise under stirring. Then, this mixture was stirred for 10 min, two drops of glacial acetic acid were added and the mixture was further refluxed for 3 hours. The resulting yellow precipitate was recovered by filtration, washed several times with a small portions of cold ethanol and then with cold diethyl ether to give 180 mg (83%) of 2,4-di-*tert*-butyl-6-(((4-(phenylamino)phenyl)imino) methyl)phenol (BPIMP). The crystal of the title

compound was obtained by slow evaporation from methanol. Characterization was done by ^{1}H NMR and ^{13}C NMR along with mass spectroscopy as shown in Figure 6.1, 6.2, and 6.3. ^{1}H NMR (500 MHz, DMSO-d_6) δ 1.30 ppm (singlet, 9H), δ 1.42 ppm (singlet, 9H), δ 6.87 ppm (triplet, J = 6.5 Hz, 1H), δ 7.08 ppm (multiplet, 4H), δ 7.23 ppm (triplet, J = 7.6 Hz, 2H), δ 7.31 ppm (singlet, 1H), **δ** 7.33 ppm (doublet, J = 8.6 Hz, 2H), δ 7.4 ppm (singlet, 1H), δ 8.33 ppm (singlet, 1H), δ 8.9 ppm (singlet 1H), δ 14. 20 ppm (singlet, 1H), δ2.47 ppm (deuterium of DMSO-d6), δ 3.5 ppm (residual water peak). ^{13}C NMR (125.7 MHz, DMSO-d_6) δ (ppm) 29.48, 31.48, 34.08, 34.78, 116.99, 117.51, 118.71, 120.46, 122.6, 126.73, 127.21, 129.47, 135.85, 139.25, 140.24, 143.07, 157.46, 161.13, 39.52 (peak of DMSO-d6). Figure 6.3 represent the mass spectra and is ESI-MS: m/z $[M+H]^+$ = 401.25.

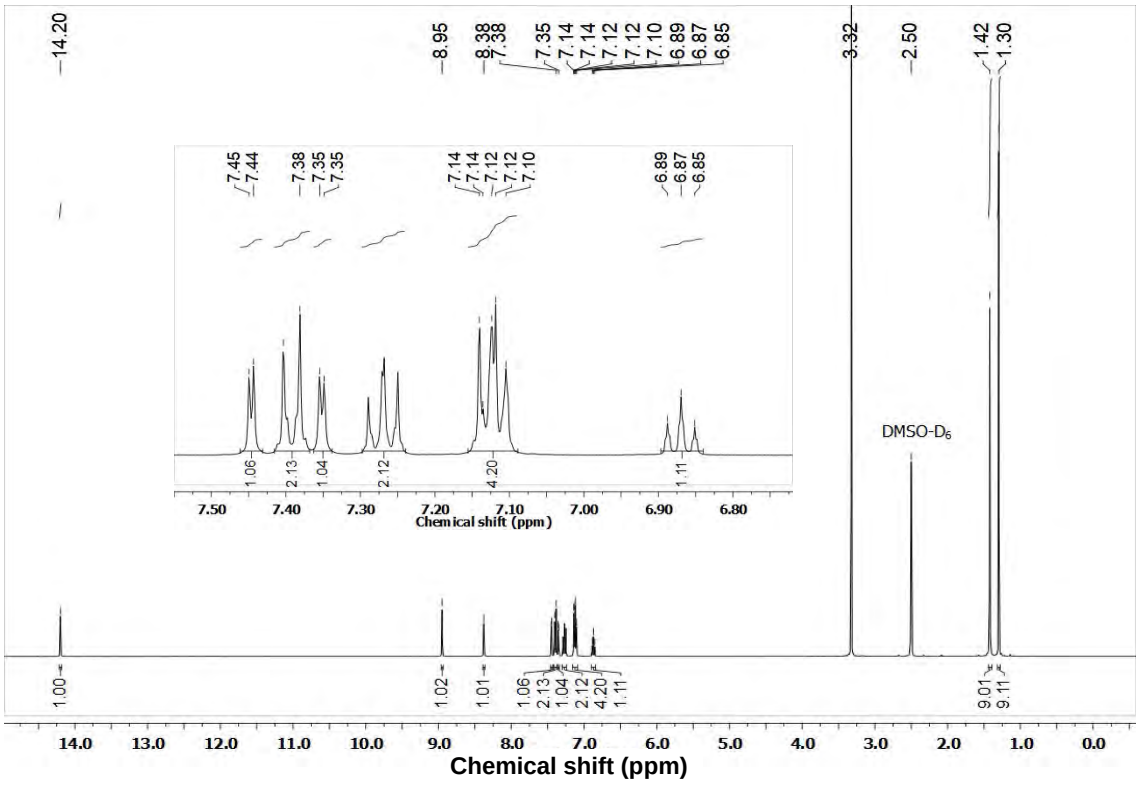

Figure 6.1 ^{1}H NMR spectrum of BPIMP in DMSO-d_6

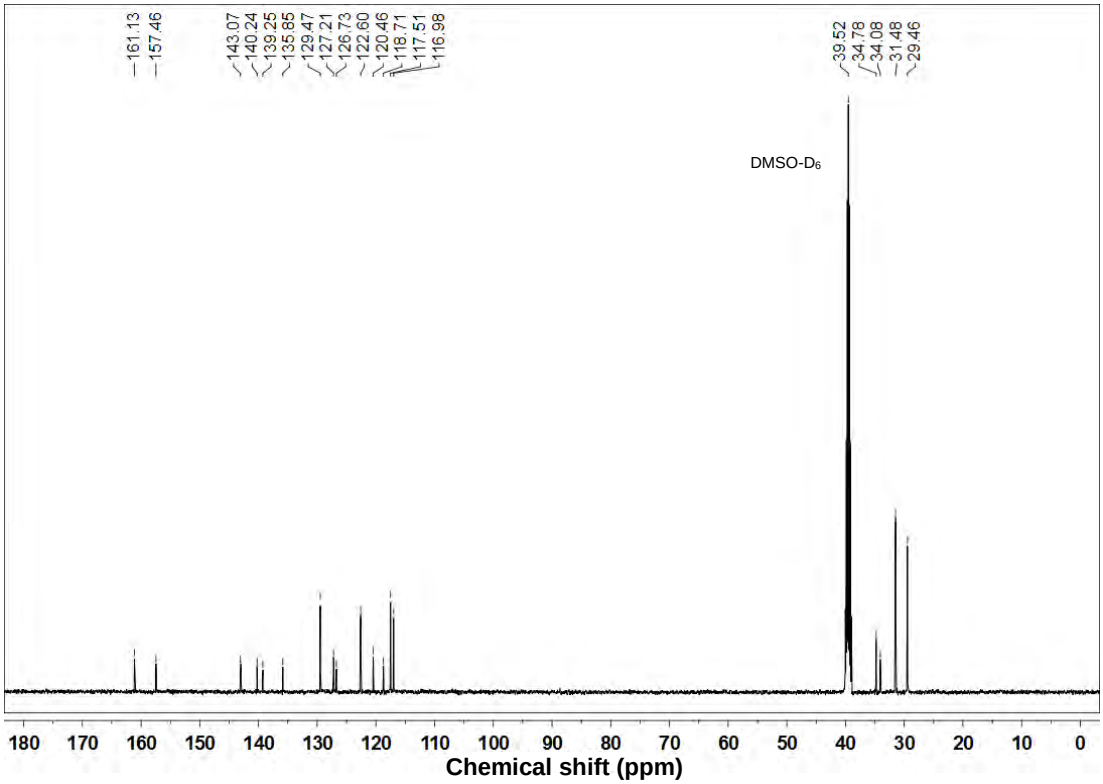

Figure 6.2 ^{13}C NMR spectrum of BPIMP in DMSO-d_6

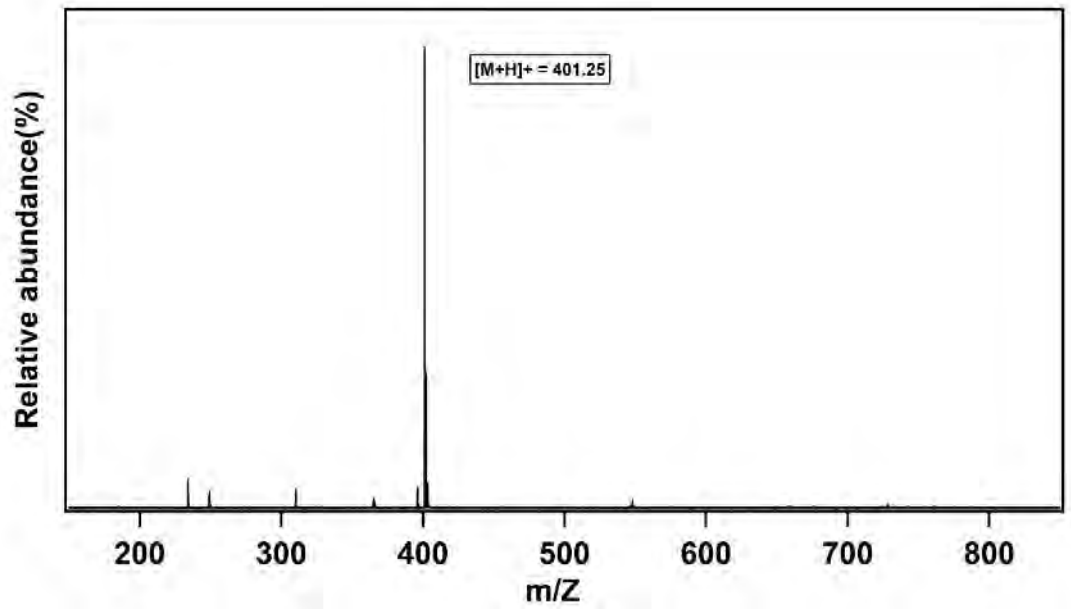

Figure 6.3 ESI-MS mass spectra of BPIMP.

6.3 Result and discussion

6.3.1 Synthesis and structural characterization.

The general synthetic route is given in Scheme 6.1. The target chemosensor BPIMP was easily synthesized by the reaction of *N*^{1}-

phenylbenzene-1,4-diamine and 3,5-di-*tert*-butyl-2 hydroxybenzaldehyde. The structure of the chemosensor was skillfully characterized by ^{1}H NMR, ^{13}C NMR, IR and ESI- Q-TOF mass spectrum analysis.

6.3.2 Spectral response of BPIMP to different metal ions

The selective response of the chemosensor BPIMP towards metals ions were used to investigate by the both absorption and fluorescence spectra. Figure 6.4 present the normalized absorbance and fluorescence spectra of our chemosensor in methanolic solution which shows a strong absorption band at 385 nm and a fluorescence band at 575 nm when excited at 385 nm. There are two nitrogen and one oxygen atom with lone pair electrons in BPIMP and it is anticipated that BPIMP can coordinated with metal ions and thus expedite changes its absorbance and fluorescence properties.

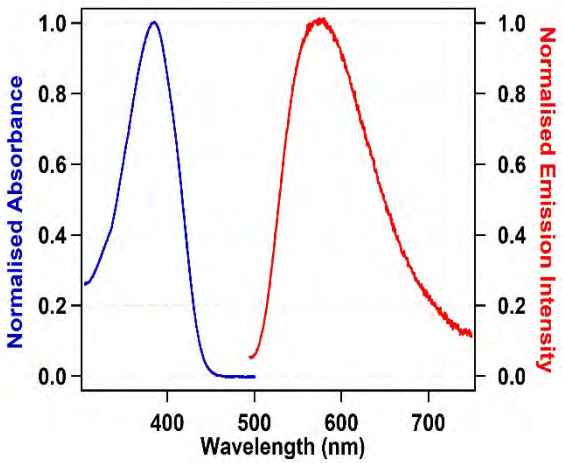

Figure 6.4 Normalized Absorbance and Fluorescence spectra of BPIMP in MeOH

The preliminary investigation of the absorption and fluorescence spectral studies showed that the treatment of BPIMP with 5 equivalent of various metal ions (Na^{+}, K^{+}, Mg^{+} ,Ca^{+}, Fe^{2+}, Co^{2+}, Ni^{2+}, Cu^{2+}, Zn^{2+}, Pb^{2+}, Sr^{2+},

Cd^{2+}, Br^{2+}, and Fe^{3+}) brought no appreciable change in its absorbance and fluorescence profile, except for Cu^{2+} (see Figure 6.5).

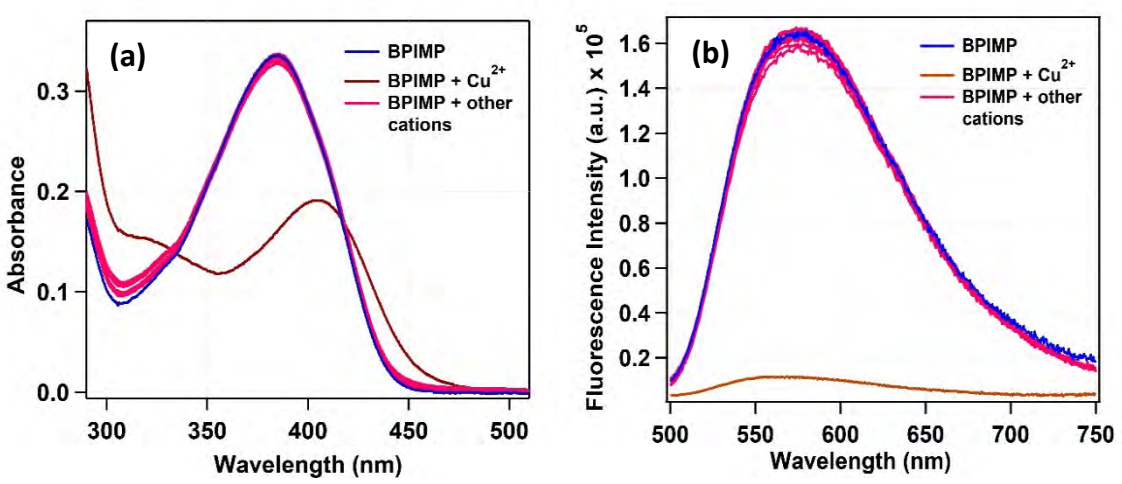

Figure 6.5 (a) UV-Vis absorption spectra of BPIMP (10 µM, in MeOH) solution upon addition of various metal ions (50 µM, in MeOH). (b) Emission spectra of BPIMP (10 µM, in MeOH) solution upon addition of various metal ions (50 µM, in MeOH).

A noticeable change in absorption spectrum of BPIMP was observed with addition of Cu^{2+} ions. The absorption maximum of BPIMP was red shifted to 405 nm ($\Delta\lambda$ = 20 nm) with a substantially diminished absorbance as shown in Figure 6.5(a). The emission response of BPIMP were also examined with various metal ions when excited at 385 nm. The results showed that only Cu^{2+} leads to a pronounced change in emission intensity as illustrated in Figure 6.5(b). The emission intensity of BPIMP reduced to 16 folds with addition of 5 equivalents of Cu^{2+}. These observation shows that sensor BPIMP has very good selectivity to Cu^{2+} ions in methanol solution.

6.3.3 Competitive experiment in presence of other metal ions

A critical parameter to measure the effectiveness of a chemosensor is its high selectivity towards target analyte over different competitive species. Therefore, a competitive experiment was conducted to measure any possible interference in the absorption and fluorescence response of chemosensor BPIMP towards 5 equiv. of Cu^{2+} in presence of excess amount of the competing metal ions like Na^{+}, K^{+}, Mg^{+}, Ca^{+}, Fe^{2+}, Co^{2+}, Ni^{2+}, Zn^{2+}, Pb^{2+}, Sr^{2+}, Cd^{2+}, Br^{2+},

and Fe^{3+}. This selectivity investigation carried out by monitoring the shift in absorption band as well as decrease in fluorescence intensity at 575 nm, the results are displayed in Figure 6.6.

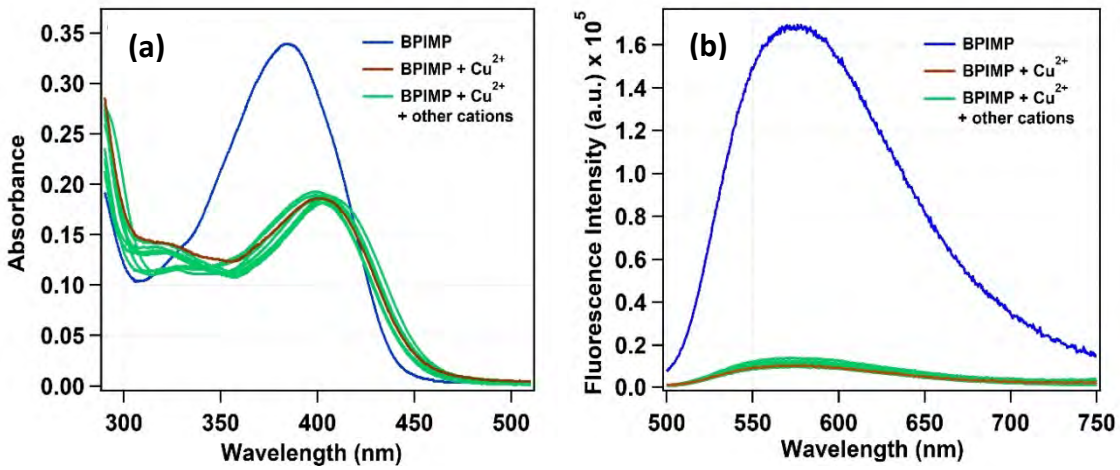

Figure 6.6 (a) Change in absorbance maxima position and its intensity of sensor BPIMP (10µM, in MeOH) on addition of Cu^{2+} and various other competitive metal ions. (b) Change in fluorescence intensity upon addition of Cu^{2+} and different competitive metal ions.

Even though a small amount of perturbation is prompted by competitive metal ions, the same amount of Cu^{2+} induces a red shifted the absorption maxima of the sensor, and near about 16 fold decrease in fluorescence intensity of BPIMP. This result pointed out that the recognition process of Cu^{2+} by BPIMP could not hinder by presence of above competitive ions. Therefore, our chemosensor is capable of detect of Cu^{2+} ions with high selectivity and sensitivity.

6.3.4 Effect of counter anions on the sensitivity of BPIMP

The effect of counter anion was also investigated for sensing ability of chemosensor BPIMP towards Cu^{2+} ion in methanolic solution. An experiment was performed in which the absorption and fluorescence response of BPIMP recorded in the presence of various copper salts with different counter ions including NO_3^{2-}, ClO_4^-, F^-, OAc^-, SO_4^{2-}, Br^-, and Cl^-. As we can see from Figure 6.7(a) and 6.7(b), our experimental finding clearly indicated that the existance of above counter anions could not interfere detection of Cu^{2+} ions.

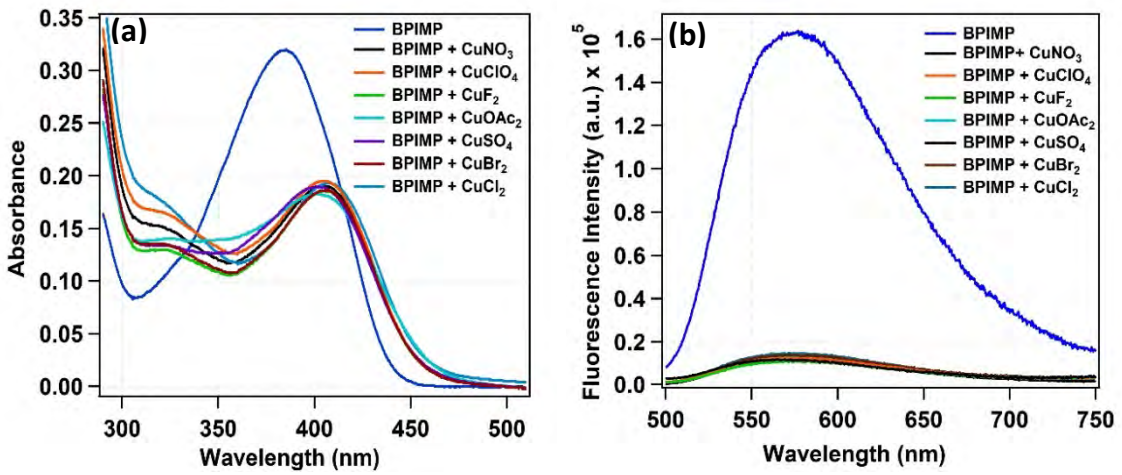

Figure 6.7 (a) Absorption spectra of BPIMP (10µM, in MeOH) in presence of various copper salts. (b) Fluorescence spectra of BPIMP (10µM, in MeOH) in presence of various copper salts.

6.3.5 Fluorescence titration experiment and determination of binding constant

The evaluation of sensing performance of chemosensor BPIMP towards Cu^{2+} ions was carried out by a fluorescence titration experiment of 10 µM solution of BPIMP with increasing concentration of 0-50 µM Cu^{2+} in methanol. As displayed in Figure 6.8(a), the fluorescence intensity of the solution started decreasing at 575 nm upon continuous increment of Cu^{2+}. The intensity of .Cu^{2+} was added, no further depletion in the fluorescence intensity observed when titrated with more than 20 µM Cu^{2+} concentration.

As we can see from Figure 6.8(b), it is clear that the plot cannot be represented as a single straight line. In our case, at higher copper concentrations a complexation is suspected to be in successive 2:1 stoichiometry.

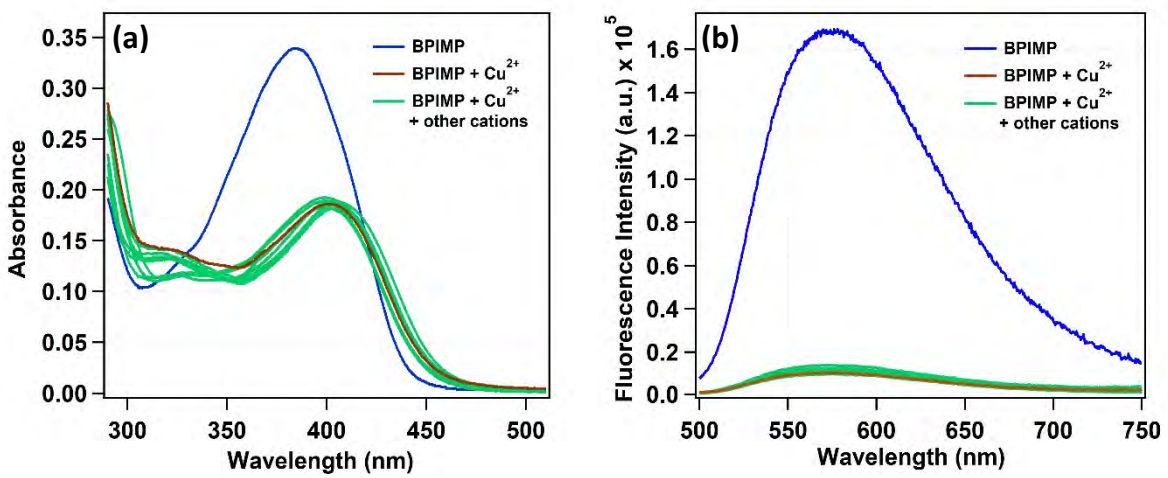

Figure 6.8 (a) Fluorescence response of BPIMP solution (10µM, in MeOH) upon addition of Cu^{2+} ions (0-50 µM, in MeOH). (b) plot of fluorescence intensity against the concentration of copper ions added to the sensor solution.

So, a nonlinear least-squares regression approach is applied for the fitting of the experimental plot. This method of analysis requires the estimation of preliminary parameter which are determined from the linear fitting the lower concentration data by using the Benesi-Hildebrand plots by equation 6.1.[35]

$$\frac{1}{I - I_0} = \frac{1}{K_1(I_1 - I_0)}\frac{1}{[Cu^{2+}]} + \frac{1}{I_1 - I_0} \qquad \ldots\ldots\ldots (6.1)$$

Here I_0 and I represent the fluorescence intensity of BPIMP solution in the presence and absence of Cu^{2+} ions. I_1 denotes the fluorescence intensity of the 1:1 complexation. Thus, from low concentrations we can estimate the values of K_1 and I_1. A 2:1 type host: guest model would be more appropriately explain the chances of involvement of more than one copper ion during the complexation with sensor BPIMP. The following equation has been derived for the stepwise formation of a 1:1 followed by addition of a second host to form a final 2:1 complex.[35]

$$\frac{I}{I_0} = \frac{1 + \frac{I_1}{I_0}K_1[Cu^{2+}] + \frac{I_2}{I_0}K_1K_2[Cu^{2+}]^2}{1 + K_1[Cu^{2+}] + K_1K_2[Cu^{2+}]^2} \qquad \ldots\ldots\ldots (6.2)$$

Here K_1 and K_2 are the association constant for the first and second BPIMP

molecule forming a complex with Cu^{2+} ion. I_1/I_0 and I_2/I_0 denotes the fluorescence reduction when every Cu^{2+} ion bound to one and two BPIMP molecules respectively. The use of nonlinear regression (NLR) programming helped in directly fitted the data using the equation 6.2. There are four parameters I_1, I_2, K_1, and K_2 estimated from equations 6.1 and 6.2 are employed as initial values. The correlation coefficients $r^2 \geq 0.979$ fit converged well towards all points as illustrated in Figure 6.8(b). From this nonlinear regression analysis, we obtained the two equilibrium constants of the inclusion complexes. K_1, and K_2 are 1.5 ×10^5 M^{-1} and 1.01× 10^6 M^{-1} respectively and overall binding constant $K = K_1.K_2$ calculated is 1.515 ×10^{11} M^{-2}.

6.3.6 Detection limit

The detection limit was calculated from a plot of the fluorescence changes as a function of concentration of Cu^{2+} ions following the procedure of literature as illustrated in Figure 6.9.[36] A graph of normalized fluorescent intensity is plotted against the Cu^{2+} ion concentration and data point was fitted with linear regression analysis. The point at which this line crossed the ordinate axis was taken as the detection limit.

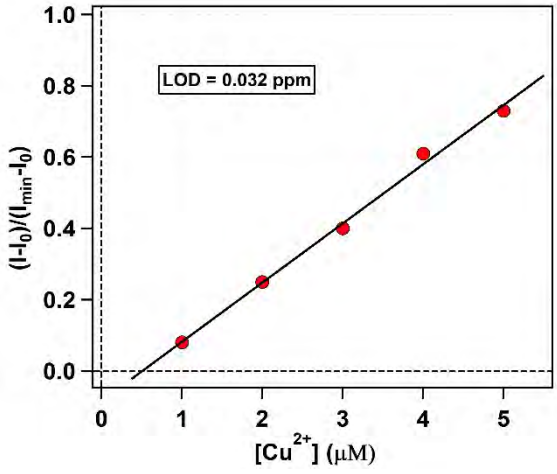

Figure 6.9 Limit of detection determination by a Plot of normalized fluorescence intensity against the Cu^{2+} ions concentration.

6.3.7 Practical application by colorimetric test kit

BPIMP (4 mg, 0.01 mmol) was dissolved in 5ml of methanol. Test kits of chemosensor were prepared by adding a few drops of BPIMP solution on filter papers to create spots, and then dried in vacuum. Nitrate salt of various metal ions like Na^{+}, K^{+}, Mg^{+} ,Ca^{+}, Fe^{2+}, Co^{2+}, Ni^{2+}, Cu^{2+}, Zn^{2+}, Pb^{2+}, Sr^{2+}, Cd^{2+}, Br^{2+}, and Fe^{3+} (0.002 mmol) was dissolved in 1mL MeOH, respectively. Then, by adding different metal ion solutions dropwise on to the test kits prepared above and dried at room temperature. We found a distinct color change from orangish yellow to greyish blue upon addition of copper(II) salt solution as shown in Figure 6.10.

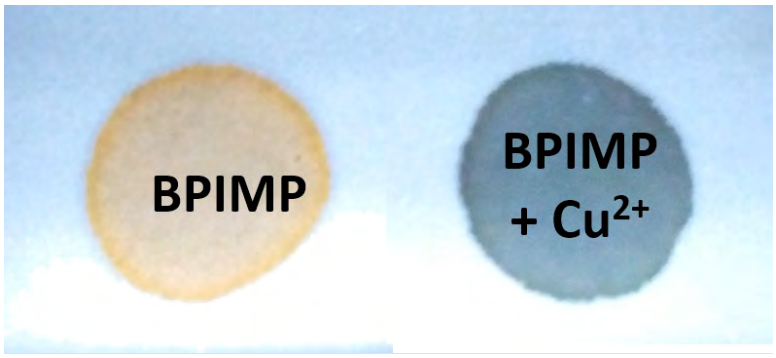

Figure 6.10 Use of paper strip for instant sensing of copper(II) ions.

6.4 Conclusion

In summary, we have synthesized a new 3,5-di-*tert*-butyl-2 hydroxybenzaldehyde derivative sensor BPIMP for Cu^{2+} with high sensitivity and selectivity. This compound displayed a fluorescence quenching when Cu^{2+} was added into its methanolic solution. This sensors' design strategy and remarkable photophysical characteristics would help to extend the development of fluorescent sensors for other ions.

References

1 X. Chen, X. Tian, I. Shin and J. Yoon, *Chem. Soc. Rev.*, 2011, **40**, 4783–4804.

2 X. Chen, T. Pradhan, F. Wang, J. S. Kim and J. Yoon, *Chem. Rev.*, 2012, **112**, 1910–1956.

3 Z. Liu, W. He and Z. Guo, *Chem. Soc. Rev.*, 2013, **42**, 1568–1600.

4 M. E. Moragues, R. Martínez-Máñez and F. Sancenón, *Chem. Soc. Rev.*, 2011, **40**, 2593–2643.

5 L. Gao, L.-L. Li, X. Wang, P. Wu, Y. Cao, B. Liang, X. Li, Y. Lin, Y. Lu and X. Guo, *Chem. Sci.*, 2015, **6**, 2469–2473.

6 P. Verwilst, K. Sunwoo and J. S. Kim, *Chem. Commun.*, 2015, **51**, 5556–5571.

7 P. Wang, A. Armutlulu, W. Jiang, B. Lai and R. Xie, *RSC Adv.*, 2019, **9**, 28312–28322.

8 J. Li, Y. Zeng, Q. Hu, X. Yu, J. Guo and Z. Pan, *Dalt. Trans.*, 2012, **41**, 3623–3626.

9 G. J. Brewer, *Curr. Opin. Chem. Biol.*, 2003, **7**, 207–212.

10 X. Zheng, K. H. Lee, H. Liu, S.-Y. Park, S. S. Yoon, J. Y. Lee and Y.-G. Kim, *Sensors Actuators B Chem.*, 2016, **222**, 28–34.

11 Y. Zhou, J. Zhang, H. Zhou, Q. Zhang, T. Ma and J. Niu, *J. Lumin.*, 2012, **132**, 1837–1841.

12 S. M. Wazir and I. Ghobrial, *J. Community Hosp. Intern. Med. Perspect.*, 2017, **7**, 265–268.

13 Y. H. Hung, A. I. Bush and R. A. Cherny, *JBIC J. Biol. Inorg. Chem.*, 2010, **15**, 61–76.

14 A. Macías-García, M. G. Corzo, M. A. Domínguez, M. A. Franco and J. M. Naharro, *J. Hazard. Mater.*, 2017, **328**, 46–55.

15 M. Ghaedi, F. Ahmadi and A. Shokrollahi, *J. Hazard. Mater.*, 2007, **142**, 272–278.

16 T. Stafilov and I. Karadjova, *Maced. J. Chem. Chem. Eng.*, 2009, **28**, 17–31.

17 J. Otero-Romaní, A. Moreda-Piñeiro, A. Bermejo-Barrera and P. Bermejo-Barrera, *Anal. Chim. Acta*, 2005, **536**, 213–218.

18 M. Wang, K.-H. Leung, S. Lin, D. S.-H. Chan, D. W. J. Kwong, C.-H. Leung and D.-L. Ma, *Sci. Rep.*, 2014, **4**, 6794.

19 J. S. Becker, A. Matusch, C. Depboylu, J. Dobrowolska and M. V Zoriy, *Anal. Chem.*, 2007, **79**, 6074–6080.

20 T. Kato, S. Nakamura and M. Morita, *Anal. Sci.*, 1990, **6**, 623–626.

21 T. Poursaberi, L. Hajiagha-Babaei, M. Yousefi, S. Rouhani, M. Shamsipur, M. Kargar-Razi, A. Moghimi, H. Aghabozorg and M. R. Ganjali, *Electroanalysis*, 2001, **13**, 1513–1517.

22 A. A. Ensafi, T. Khayamian, A. Benvidi and E. Mirmomtaz, *Anal. Chim. Acta*, 2006, **561**, 225–232.

23 W. Liu, J. Huang, Y. Zhu, H. Zhang, N. Ning and C. Song, *Anal. Lett.*, 2019, **52**, 353–362.

24 B. Hasani, A. Zamani, M. K. Moftakhar, M. Mostafavi, M. R. Yaftian and M. Ghorbanloo, *J. Anal. Chem.*, 2018, **73**, 82–90.

25 H. J. Kim, J. Hong, A. Hong, S. Ham, J. H. Lee and J. S. Kim, *Org. Lett.*, 2008, **10**, 1963–1966.

26 Y. Mei, P. A. Bentley and W. Wang, *Tetrahedron Lett.*, 2006, **47**, 2447–2449.

27 R. Martínez, F. Zapata, A. Caballero, A. Espinosa, A. Tárraga and P. Molina, *Org. Lett.*, 2006, **8**, 3235–3238.

28 Z. Xu, Y. Xiao, X. Qian, J. Cui and D. Cui, *Org. Lett.*, 2005, **7**, 889–892.

29 T. Gunnlaugsson, J. P. Leonard and N. S. Murray, *Org. Lett.*, 2004, **6**, 1557–1560.

30 M. Cazacu, S. Shova, A. Soroceanu, P. Machata, L. Bucinsky, M. Breza, P. Rapta, J. Telser, J. Krzystek and V. B. Arion, *Inorg. Chem.*, 2015, **54**, 5691–5706.

31 M. Ulusoy, H. Karabıyık, R. Kılınçarslan, M. Aygün, B. Çetinkaya and S. García-Granda, *Struct. Chem.*, 2008, **19**, 749–755.

32 H. Irving and R. J. P. Williams, *J. Chem. Soc.*, 1953, 3192–3210.

33 S. Y. Kim, S. Y. Lee, J. M. Jung, M. S. Kim and C. Kim, *Inorganica Chim. Acta*, 2018, **471**, 709–717.

34 P. Mukherjee, A. Das, M. S. H. Faizi and P. Sen, *ChemistrySelect*, 2018, **3**, 3787–3796.

35 N. Stojanovic, L. D. Murphy and B. D. Wagner, *Sensors*, 2010, **10**, 4053–4070.

36 M. Shortreed, R. Kopelman, M. Kuhn and B. Hoyland, *Anal. Chem.*, 1996, **68**, 1414–1418.

Chapter 7

A highly sensitive Schiff-base colorimetric chemosensor for visual detection of mercuric (Hg^{2+}) ions.

A Schiff-base colorimetric chemosensor (QMBA) was synthesized and investigated for its metal ion sensing properties. Chemosensor QMBA displayed excellent selectivity and sensitivity for Hg^{2+} *ion with a vivid color change to pink, which is visible to naked eyes via UV-Vis spectroscopy. The binding constant for complex formed QMBA-*Hg^{2+} *was found* $1.12 \times 10^5\ M^{-1}$. *The detection limit of probe QMBA for the analysis of* Hg^{2+} *was estimated nearly 10 PPB.*

7.1 Introduction

Mercury is considered as one of the most toxic and hazardous elements among the heavy and transition metal ions.[1–5] There appears continuing rising concern over mercuric ions, Hg^{2+} as a severe environmental pollutant and its deleterious effects on human health.[6] Hg^{2+} ion is released by a number of anthropogenic and natural sources into the environment. Combustion of fossil fuel, coal and gold mining, solid waste incineration, wood pulping, and chemical manufacturing are some industrial sources of mercury pollution resulting in its accumulation in topsoil, on plants, and in waters.[7–10] Bioaccumulation of mercury also occurs in plants, providing an entry route into the food.[11] Atmospheric deposition of Hg^{2+} on tree leaves reduces transpiration and photosynthesis in plants.[12] When Hg^{2+} enters in freshwater and marine ecosystems, the elemental or ionic mercury is converted by aquatic organisms to methylmercury, which subsequently accumulates in fishes and enters in our diet through the seafood.[13–16] This is the primary source of Hg^{2+} in human body. Apart from that, dental amalgams and vaccinations are potential causes of human exposure to mercury.[17–19] Hg^{2+} is easily absorbed into the human body, and even at low levels, Hg^{2+} affects the central nervous system and causes many neurological problems[20,21], including kidney failure[22,23], cognitive and motion disorders, dysfunction of the immune system, and Minamata disease.[24,25] United States Environmental Protection Agency (U.S. EPA) standard for the maximum safe level of mercury in edible fish and in drinking water is is 0.55 ppm and 0.02 ppm respectively.[8] Therefore, much efforts have been devoted toward the design of efficient method for the sensitive determination of trace amount of mercury. The traditional analytical techniques for sensitive and selective measurement of Hg^{2+} including inductively coupled plasma-mass spectroscopy (ICPMS)[26], cold-vapor atomic absorption spectrometry (CV-AAS)[27], cold vapor atomic fluorescence spectrometry (CV-AFS)[28], X-ray absorption spectroscopy[29], and voltammetry[30] require higher concentration of the metal ion, expensive instrumentation and trained operators or is time-

consuming. So, there is an essential need for the development of accurate, rapid, and low-cost ways to detect trace amounts of Hg^{2+}.

In the past few years, various sensors based on fluorescenence[31–33], quantum dots[34,35], biomolecules[36], and nanoparticles[37,38] have been developed for the detection of Hg^{2+}. Colorimetric detection has some obvious advantages compared to other methods, such as simple instrumentation, easy evaluation, the ability to monitor quickly and in real-time.[39–43] Therefore, much effort has been devoted to exploring new and more reliable colorimetric chemosensors for Hg^{2+} with high sensitivity and selectivity.

Schiff-base type colorimetric sensors and their transition metal complexes have attracted widespread attention in analytical fields. Especially, Schiff bases containing two nitrogen chelating groups in their structures have received considerable attention and for further studies due to their specific properties. In most areas of coordination chemistry, multidentate ligands have been commonly used as a metal-binding reagent.[5] Complexes of the bidentate ligand (*N*-(quinolin-2ylmethylene)-[1,1'-biphenyl]-4-amine) (QMBA) have been prepared[44,45] as a new class of metal complexes. However, we believe that this is the first study to the best of our knowledge, which reveals the ability of ligand (QMBA) as a potential colorimetric chemosensor for metal ion detection. In this chapter, we report a simple and effective Schiff-base colorimetric chemosensor (QMBA), which could selectively detect Hg^{2+} among a series of ions with hypersensitivity. Selective complexation of Hg^{2+} with imine N and quinoline N atoms leads to a specific colorimetric response that is apparent to naked eyes.

7.2 Experimental

7.2.1 Materials and Methods

Methanol was purchased from Alfa Aesar Chemical Co. Quinoline-2-carbaldehyde, 4-Aminobiphenyl and all nitrate salts of a series of metal ion used were purchased from Sigma-Aldrich Chemical Co. and used as received.

A commercial spectrophotometer (UV2450, Schimadzu, Japan) was used to measure the UV–vis absorption spectra of the samples. ^{1}H NMR spectra were obtained on a JEOL JNM LA (400 MHz) spectrometer.

7.2.2 General procedures:

A stock solution of chemosensor QMBA (0.2 mM) was prepared in methanol. Metal ion solutions (2 mM) of the nitrate salts were prepared in CH_3OH. The stock solution of QMBA was diluted to 10 µM and stock solutions of all metal ions was also diluted according to the experimental requirements.

7.2.3 Synthesis and characterization of QBMA

Chemosensor, QMBA *N*-(quinolin-2ylmethylene)-[1,1'-biphenyl]-4-amine) was synthesized by the condensation of Quinoline-2-carbaldehyde and [1 1'-biphenyl]-4-amine through a nucleophilic substitution reaction in an adequate yield as shown in Scheme 7.1 with same procedure as reported earlier.[45]

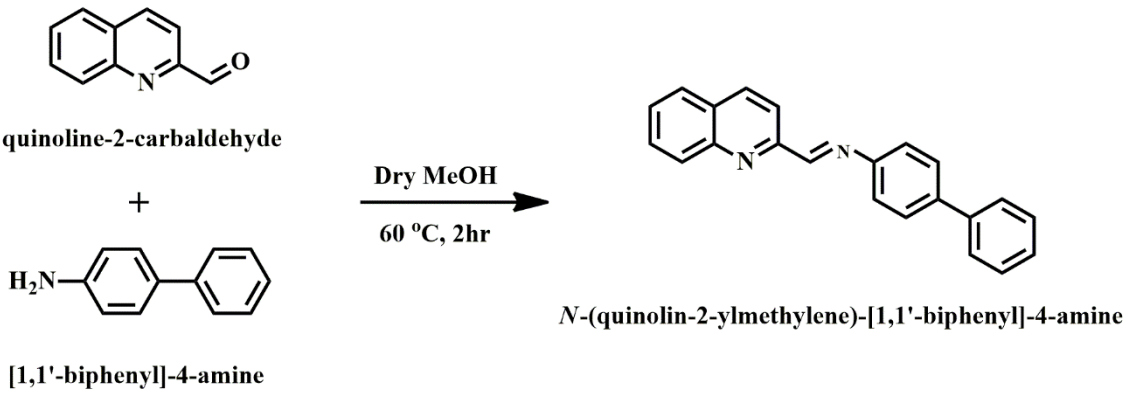

Scheme 7.1 Schematic representation of synthetic route of QMBA.

516.12mg (3.05mmol) of [1 1'-biphenyl]-4-amine was dissolved in 15ml of anhydrous methanol. 471.51 mg (3mmol) of quinoline 2-carbaldehyde dissolved in 10 ml of methanol was then added to the above solution dropwise during stirring. After keeping this solution for stirring at room temperature for another 10 minutes, two drops of glacial acetic acid were added to it. Then, the resulting mixture was refluxed for 2 hours. A yellowish crude was obtained,

which then filtered and washed with ethanol (3 x 3 ml). A yellow powder was obtained with a good yield of 77% (760.47 mg) after the recrystallization with methanol by slow evaporation of solvent after dried in a vacuum desiccator. M.P. = 125.1–126.8 °C. ^{1}H NMR is illustrated in Figure 7.1. ^{1}H NMR (400 MHz, methanol-d_4): δ 8.81 (s, 1H, CH=N), 8.40 (d, J = 8 Hz, 1H), 8.33 (d, J = 8 Hz, 1H), 8.11 (d, J = 12 Hz, 1H), 7.97 (d, J = 8.0 Hz, 1H), 7.81 (t, J = 8 Hz, 1H), 7.65 (t, J = 8 Hz,1H), 7.40 (d, J = 8 Hz, 2H)7.26 (t, J = 8 Hz, 2H), 7.16 (m, 4H), 6.90 (t, J = 8 Hz, 1H) ppm.

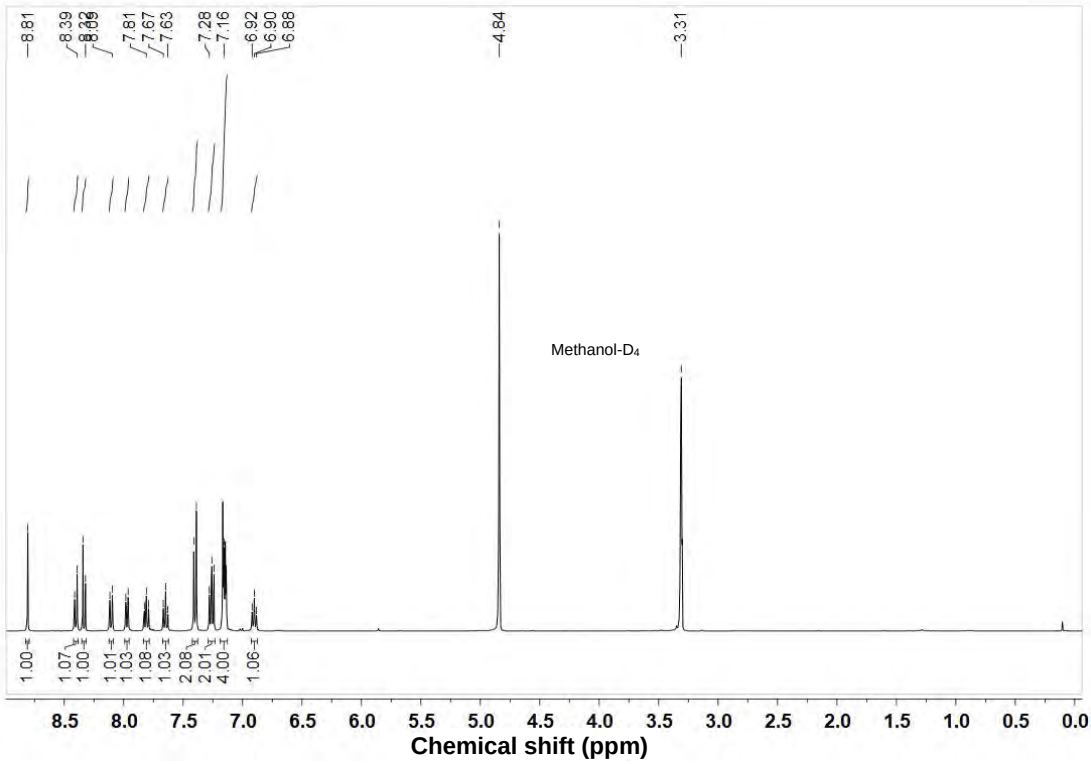

Figure 7.1 ^{1}H NMR spectrum of QMBA in CD_3OD.

7.3 Result and Discussion

7.3.1 Selectivity and sensitivity experiment for QMBA towards Hg^{2+}

The study of steady-state absorption was performed for QMBA in methanol at 10 µM concentration. It shows an absorption band with maxima at ~413 nm. The extinction coefficient of QMBA is determined to be 17700±300 $M^{-1}Cm^{-1}$. No apparent change in QMBA absorbance was observed after 20

minutes, which means no chemosensor degradation occurred. The primary investigation of sensing ability of QMBA was carried out with a series of metal ions such as Na^{+}, K^{+}, Mg^{2+}, Ca^{2+}, Al^{3+}, Cr^{2+}, Mn^{2+}, Fe^{2+}, Co^{2+}, Ni^{2+}, Zn^{2+}, Pb^{2+}, Cd^{2+}, Ba^{2+}, and Hg^{2+} in a 10 µM CH_3OH solution of QMBA. It was observed that the addition of 2 equivalent of Hg^{2+} ions to the chemosensor QMBA resulted in a dramatic change in absorption maxima from 410 nm to 530 nm as well as color changes from colorless to pink. The color does not fades away even after 24 hours. The addition of 2 equialent. of other metal salts as Na^{+}, K^{+}, Mg^{2+}, Ca^{2+}, Al^{3+}, Cr^{2+}, Mn^{2+}, Fe^{2+}, Co^{2+}, Ni^{2+}, Zn^{2+}, Pb^{2+}, Cd^{2+}, and Ba^{2+} did not produce any significant changes in spectrum or color of the QMBA solution as depicted in Figure 7.2. and 7.3 respectively. The change in color induced after the addition of Hg^{2+} ions and the redshift in absorbance maximum by 120 nm occurred instantaneously.

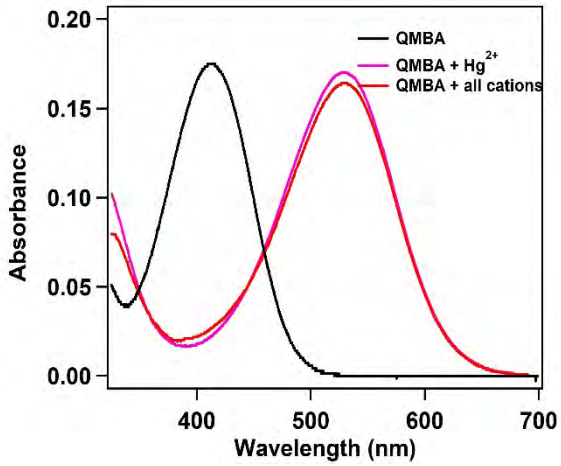

Figure 7.2 UV-Vis Absorption spectra of QMBA (10 µM, in methanol) and QMBA in the presence of 2 equivalent of metal ions.

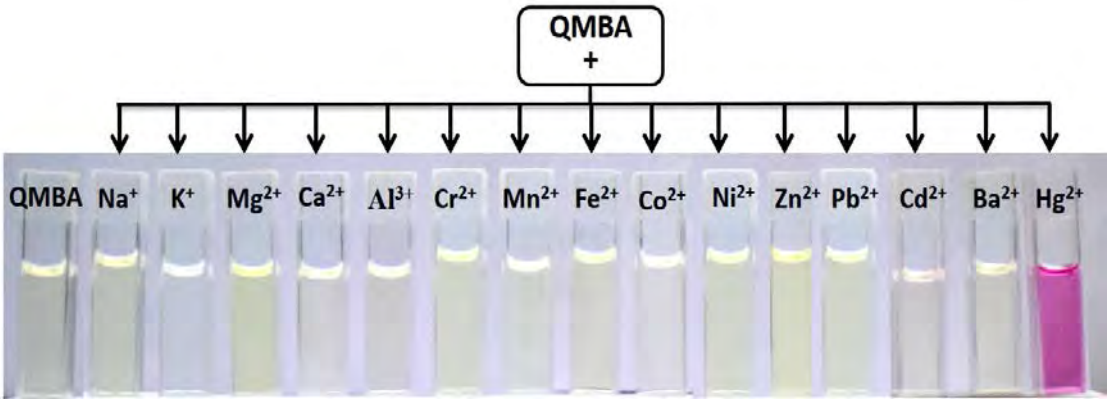

Figure 7.3 Photographic image showing the change in color of QMBA solution (10 μM in methanol) after adding 2 equivalent of different metal ions.

7.3.2 Competitive experiment with other metal ions

An important parameter to evaluate the chemosensor performance is its high selectivity toward the target analyte over other interfering species. Thus, we have conducted competition experiments in the presence of 2 equivalent of Hg^{2+} mixed with 10 equivalent of different metal ions to unearth the tolerance power of QMBA towards other metal ions. As illustrated in Figure 7.4, we did not observe any alteration in the absorption changes caused by the addition of 2 equivalent of Hg^{2+} ions by addition of an excess of other cations.

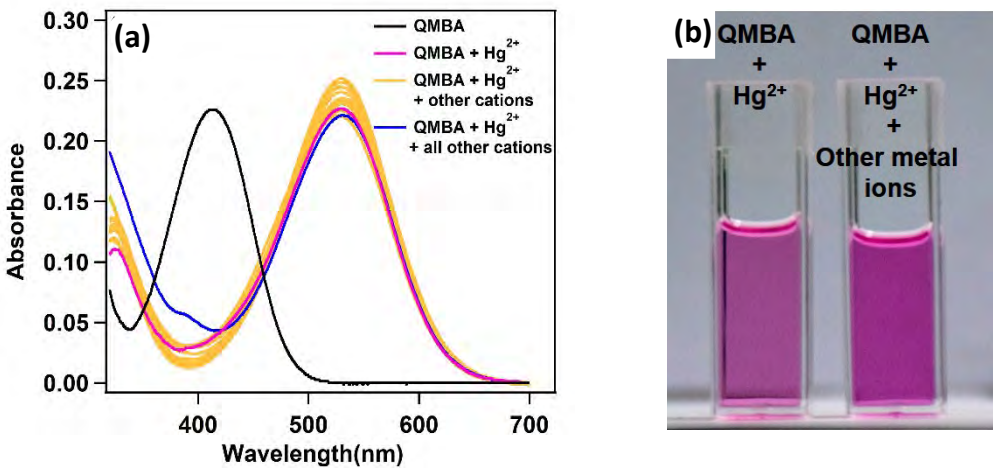

Figure 7.4 (a) spectra of QMBA (10μM), QMBA (10μM) and Hg^{2+} (20 μM), and QMBA (10 μM) and Hg^{2+} (20 μM) in the presence of other metal ions(e.g., Na^{+}, K^{+}, Mg^{2+}, Ca^{2+}, Al^{3+}, Cr^{2+}, Mn^{2+}, Fe^{2+}, Co^{2+}, Ni^{2+}, Zn^{2+}, Pb^{2+}, Cd^{2+} and Ba^{2+} in excess (100 μM). (b) Photographic image of competitive experimentations.

Here, to mention that if we add Hg^{2+} in the solution of QMBA and excess other metal ions, then also a similar result is obtained.

7.3.3 Measurement of binding stoichiometry and binding constant

The binding stoichiometry of complex formed between QMBA and Hg^{2+} was determined by using Job's plot method[46] in which we monitored the change in the absorption intensity of the solution at 530 nm. Here we have varied the concentration of QMBA and Hg^{2+}, keeping their total concentration fixed at 50 μM. From Figure 7.4, it is clear that complexation occurs at 1:1 ratiometric binding between QMBA and Hg^{2+}.

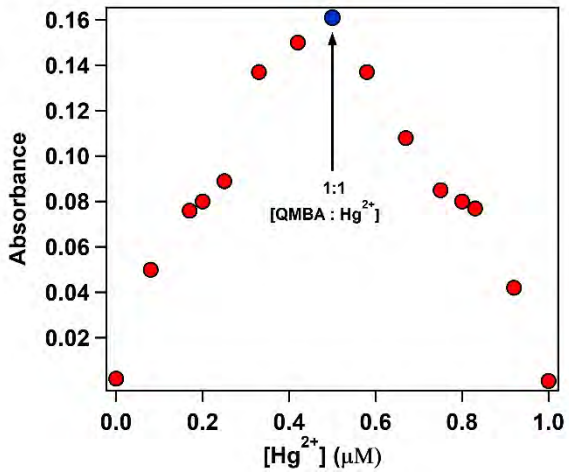

Figure 7.5 Job's plot of QMBA with Hg^{2+} showing binding stoichiometry of Cu^{2+}: QMBA is 1:1.

A UV–Vis titration experiment was performed to quantitatively study the cation-sensing ability of QMBA in CH_3OH by using 10 μM solution of QMBA. With the incremental addition of Hg^{2+} ions 0 -25 μM to chemosensor solution, we saw a gradual decrease in intensity of the absorption peak at 410 nm along with the gradual formation of a new band peak at 530 nm. An isosbestic point at 458 nm, as depicted in Figure 7.6(a) indicating a continuous formation of a new complex between QMBA and Hg^{2+} ions, which was accountable for the visible color change from light yellow to pink. The intensity of absorbance at 530 nm increased nearly fifteen fold, which was also responsible for the generation of intense pink color after the addition of mercury

(II) nitrate into the solution of chemosensor QMBA. The titration is complete at 25 µM concentration of Hg^{2+}, and further addition of Hg^{2+} to QMBA doesn't make any change. The association constant K was determined to be 1.12×10^5 M^{-1} using equation 7.1.[47]

$$A = \varepsilon_L \times L_T + \frac{1}{2} \times (\varepsilon_{LH} - \varepsilon_L) \times \left(L_T + H_T + \frac{1}{K}\right) + \sqrt{\left(L_T + H_T + \frac{1}{K}\right)^2 - 4 \times L_T \times H_T} \quad \ldots\ldots\ldots (7.1)$$

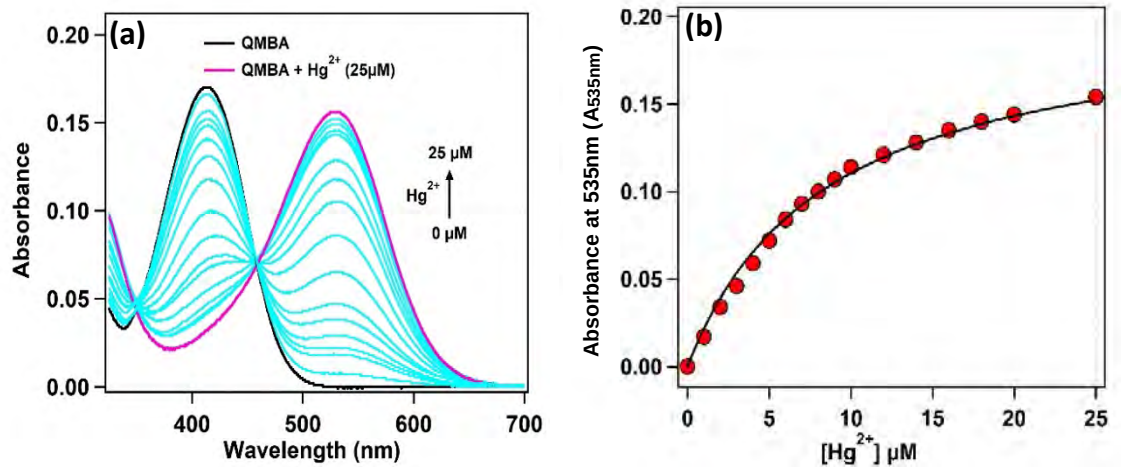

Figure 7.6 (a) UV- Visible titration profile of QMBA (10 µM) upon gradual addition of Hg^{2+} (0 to 25 µM). (b) Binding isotherm for the determination of binding constant between QMBA and Hg^{2+}.

Where A is absorbance, ε_L is the molar absorptivity of the Ligand, QMBA, H_t is the total concentration of Hg^{2+}, L_T is the total concentration of QMBA, K is binding constant and ε_{LH} is molar absorptivity of the complex between QMBA and Hg^{2+} The value of ε_T and $[L]_t$ are known and the value of K and ε_{HG} are unknown. We determined the value of K and ε_{HG} by fitting the titration data with nonlinear regression analysis from the best curve fit. The association constant K was determined to be 1.12×10^5 M^{-1}.

7.3.4 Limit of detection

Limit of detection (LOD) is the lowest concentration of a substance that can be differentiated from the blank of the solution. We have used the UV-

Visible titration curve in the range up to 6 µM of Hg^{2+} concentration, where the change of absorption with concentration is liner.[48] A linear fit (see Figure 7.7) in this range gives the LOD value of 10 ppb which is quite low than the maximum permissible limit in edible fish.

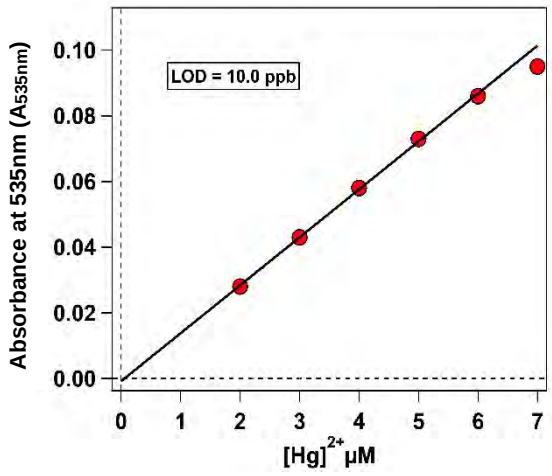

Figure 7.7 Linear fit of the absorbance of QMBA (10 µM) on gradual addition of Hg^{2+}

7.4 Conclusion

In conclusion, we have successfully designed and synthesized a simple colorimetric probe QMBA based on quinoline containing imine functionality having the capability of recognizing Hg^{2+} ion. Chemosensor QMBA showed a clear colorimetric response toward Hg^{2+} with color changes in CH_3OH. Meanwhile, the colorimetric detection of Hg^{2+} ion showed excellent tolerance towards the interference of other metal ions. UV-Visible spectroscopy confirmed the binding process and a good detection limit for Hg^{2+} ion which is under the allowable limit set by the U.S. Environmental Protection Agency (EPA) for edible fish.

References

1 A. W. Czarnik, *Acc. Chem. Res.*, 1994, **27**, 302–308.

2 A. P. de Silva, D. B. Fox, A. J. M. Huxley and T. S. Moody, *Coord. Chem. Rev.*, 2000, **205**, 41–57.

3 J. F. Callan, A. P. de Silva and D. C. Magri, *Tetrahedron*, 2005, **61**, 8551–8588.

4 L. Prodi, *New J. Chem.*, 2005, **29**, 20–31.

5 B. Kaur, N. Kaur and S. Kumar, *Coord. Chem. Rev.*, 2018, **358**, 13–69.

6 E. M. Nolan and S. J. Lippard, *Chem. Rev.*, 2008, **108**, 3443–3480.

7 O. Malm, *Environ. Res.*, 1998, **77**, 73–78.

8 U. States, *Fact Sheet Mercury Update : Impact on Fish Advisories*, Washington, DC, 2001.

9 S. M. Gustin, M. Coolbaugh, M. Engle, B. Fitzgerald, R. Keislar, S. Lindberg, D. Nacht, J. Quashnick, J. Rytuba, C. Sladek, H. Zhang and R. Zehner, *Environ. Geol.*, 2003, **43**, 339–351.

10 P. Chu and D. B. Porcella, *Water. Air. Soil Pollut.*, 1995, **80**, 135–144.

11 D. W. Boening, *Chemosphere*, 2000, **40**, 1335–1351.

12 J. A. Fleck, D. F. Grigal and E. A. Nater, *Water. Air. Soil Pollut.*, 1999, **115**, 513–523.

13 M. Nendza, T. Herbst, C. Kussatz and A. Gies, *Chemosphere*, 1997, **35**, 1875–1885.

14 A. Renzoni, F. Zino and E. Franchi, *Environ. Res.*, 1998, **77**, 68–72.

15 J. Burger and M. Gochfeld, *Environ. Res.*, 2004, **96**, 239–249.

16 J. S. Kuwabara, Y. Arai, B. R. Topping, I. J. Pickering and G. N. George, *Environ. Sci. \& Technol.*, 2007, **41**, 2745–2749.

17 J. Forman, J. Moline, E. Cernichiari, S. Sayegh, J. C. Torres, M. M. Landrigan, J. Hudson, H. N. Adel and P. J. Landrigan, *Environ. Health Perspect.*, 2000, **108**, 575–577.

18 B. A. Dye, S. E. Schober, C. F. Dillon, R. L. Jones, C. Fryar, M.

McDowell and T. H. Sinks, *Occup. Environ. Med.*, 2005, **62**, 368–375.

19 M. E. Pichichero, E. Cernichiari, J. Lopreiato and J. Treanor, *Lancet*, 2002, **360**, 1737–1741.

20 P. Kaur, M. Aschner and T. Syversen, *Neurotoxicology*, 2006, **27**, 492–500.

21 G. Shanker, L. A. Mutkus, S. J. Walker and M. Aschner, *Mol. Brain Res.*, 2002, **106**, 1–11.

22 K. Eto, H. Tokunaga, K. Nagashima and T. Takeuchi, *Toxicol. Pathol.*, 2002, **30**, 714–722.

23 L. Magos and T. W. Clarkson, *Ann. Clin. Biochem.*, 2006, **43**, 257–268.

24 R. K. Zalups and S. Ahmad, *J. Am. Soc. Nephrol.*, 2004, **15**, 2023–2031.

25 R. K. Zalups and L. H. Lash, *Toxicol. Appl. Pharmacol.*, 2006, **214**, 88–97.

26 N. H. Bings, A. Bogaerts and J. A. C. Broekaert, *Anal. Chem.*, 2006, **78**, 3917–3946.

27 R. Kunkel and S. E. Manahan, *Anal. Chem.*, 1973, **45**, 1465–1468.

28 H. Vogg, H. Braun, M. Metzger and J. Schneider, *Waste Manag. \& Res.*, 1986, **4**, 65–73.

29 A. Bernaus, X. Gaona, J. M. Esbrí, P. Higueras, G. Falkenberg and M. Valiente, *Environ. Sci. \& Technol.*, 2006, **40**, 4090–4095.

30 P. Ugo, L. M. Moretto, P. Bertoncello and J. Wang, *Electroanalysis*, 1998, **10**, 1017–1021.

31 B. Gu, L. Huang, W. Su, X. Duan, H. Li and S. Yao, *Anal. Chim. Acta*, 2017, **954**, 97–104.

32 F. Ye, X. Liang, K. Xu, X. Pang, Q. Chai and Y. Fu, *Talanta*, 2019, **200**, 494–502.

33 Q. Su, Q. Niu, T. Sun and T. Li, *Tetrahedron Lett.*, 2016, **57**, 4297–4301.

34 P. Kaewanan, P. Sricharoen, N. Limchoowong, T. Sripakdee, P. Nuengmatcha and S. Chanthai, *RSC Adv.*, 2017, **7**, 48058–48067.

35 Y. Wang, L. Yang, B. Liu, S. Yu and C. Jiang, *New J. Chem.*, 2018, **42**, 15671.

36 J. Liu and Y. Lu, *Angew. Chemie Int. Ed.*, 2007, **46**, 7587–7590.

37 A. K. Manna, K. Rout, S. Chowdhury and G. K. Patra, *Photochem. Photobiol. Sci.*, 2019, **18**, 1512–1525.

38 Q. Li, F. Wu, M. Mao, X. Ji, L. Wei, J. Li and L. Ma, *Anal. methods*, 2019, **11**, 4014–4021.

39 A. Krishna, V. Tekuri, M. Mohan and D. R. Trivedi, *Sensors Actuators B. Chem.*, 2019, **284**, 271–280.

40 J. J. La Clair and K. D. Janda, *Org. Lett.*, 1999, 1996–1999.

41 Y. Sie, C. Li, C. Wan, J. Chen, C. Hu, H. Yan and A. Wu, *Inorganica Chim. Acta*, 2017, **467**, 325–329.

42 S. Tatay, P. Gaviña, E. Coronado and E. Palomares, *Org. Lett.*, 2006, **8**, 3857–3860.

43 Y. Fu, H. Li and W. Hu, *European J. Org. Chem.*, 2007, **2007**, 2459–2463.

44 Y. Dong, P. Wang, R. Fan, W. Chen, A. Wang and Y. Yang, *J. Coord. Chem.*, 2017, **8972**, 0–1.

45 Y.-W. Dong, R.-Q. Fan, W. Chen, H.-J. Zhang, Y. Song, X. Du, P. Wang, L. Wei and Y. Yang, *Dalt. Trans.*, 2017, **46**, 1266–1276.

46 F. Ulatowski, D. Kajetan, T. Ba and J. Jurczak, *J. Org. Chem.*, 2016, **81**, 1746–1756.

47 A. E. Hargrove, Z. Zhong, J. L. Sessler and E. V Anslyn, *New J. Chem.*, 2010, **34**, 348–354.

48 M. Shortreed, R. Kopelman, M. Kuhn and B. Hoyland, *Anal. Chem.*, 1996, **68**, 1414–1418.

Chapter 8

Concluding Remarks and Future Outlook

This section summarizes the study and observation of this thesis, points out the limitations and describes the future perspectives of the present work. The main focus was the design, synthesis and properties of new chemosensors for transition metals ions as they play important roles in the areas of chemical, biological, and environmental systems. A total of five chemosensors were developed successfully for a low level (PPB to PPM) detection of Cu^{2+}, Fe^{3+} and Hg^{2+}. The mechanism and the way of detection for these chemosensors are different ranging from a vivid color change of the solution in presence of the metal ion to the quenching of fluorescence and fluorescence turn-on, as well. The most significant point to mention that all the chemosensors developed here are easy to synthesize and are very cheap and can be used to investigate a given sample without any pre-treatment. The developed colorimetric sensors are more significant in my opinion because np instrumentation required to identify the metal ion. However, still many extensions of this present research deserves further consideration.

The present chapter is splitted into three parts. First part brings the thesis to a conclusion. The second presents a discussion of the contribution and limitations of the current work and the last part discusses the future outlook.

8.1 Conclusion of Thesis chapters

In this thesis, I mainly focus on development and evaluation of chemosensors for transition metal ions like Fe^{3+}, Cu^{2+}, and Hg^{2+}, which are considered to possess potential toxicity for human health and environmental pollution. Below, I conclude the final essence of all the chapters.

8.1.1 Chapter 1

This chapter describes the significance of transition metal ion *viz.* Fe^{3+}, Cu^{2+}, and Hg^{2+} on biota and environment (both the benefits and ill-effects). I also explained the fundamental aspect of designing of chemosensors and their characteristic. A major emphasis was given in this chapter to understand the

different mechanistic pathways of analyte sensing by the chemosensor on the basis of electronic configurational change upon interaction.

8.1.2 Chapter 2

This chapter basically throws light on the different experimental and computational methods, which was used to identify and understand the interaction between the metal ion and the chemosensor.

8.1.3 Chapter 3

Iron is one of the most biologically and environmentally important metal ion and an easy and selective detection of the same with a high sensitivity is desired. This chapter comprises of designing and synthesis of a new chemosensor, which we named as PYAP. PYAP was successfully used for selective detection of Fe^{3+} ion with high sensitivity. Moreover, the response time for the detection was found in minutes time scale. Other metal ions e.g., Na^{+}, K^{+}, Ba^{2+}, Mg^{2+}, Al^{3+}, Cr^{3+}, Co^{2+}, Ni^{2+}, Cu^{2+}, Zn^{2+}, Cd^{2+}, Pb^{2+} and Ag^{+} barely influenced the detection of Fe^{3+} by PYAP. The stoichiometric of the complex formed between PYAP and Fe^{3+} in the methanol is found to be 2:1 and the estimated value of binding constant is found to be $5.12 \pm 0.6\ mM^{-2}$.

8.1.4 Chapter 4

The chemosensor QMAP reported in this chapter was synthesized using a one step process. UV-Visible absorption spectroscopy was used to identify its potential as a selective Cu^{2+} sensor, which reveals a red-shift of 23 nm in absorption band and change in color was observed. The detection of Cu^{2+} is found to be effective even in presence of other metal ions and was found to sense copper ion in the form of most of its salts like nitrate, sulphate, chloride and acetate. Spectroscopic titration and the Job's plots suggest a 1:2 binding between the Cu^{2+} ion and QMAP and the binding constant is found to be$1.3 \times 10^{10}\ M^{-2}$. ^{1}H NMR and ^{13}C NMR, FT-IR, and HR-MS (ESI) spectrum reveals that the metal is binding to QMAP with the help of the lone pairs on nitrogen.

DFT calculation provided a further details about the binding action and better insight of the system.

8.1.5 Chapter 5

This chapter describe design and synthetization of a novel chemosensor RQMBD was by the reduction of a Schiff base for the detection of trace amount of Cu^{2+} ions. RQMBD showed a high selectivity recognition for Cu^{2+} ions by the color change from pale yellow to red in methanol. We have observed this vivid colorimetric change with fast response time with our naked eyes. The sensor also exhibit great sensitivity towards Cu^{2+} ions as there was no interference observed with other metal ions. The prospective binding mechanism of the compound form between L and Cu^{2+} ions was studied using the job's plot method. A good limit of detection of RQMBD (25 μM) below than the minimum standard criteria for water and higher binding constant $K=1.8 \times 10^{8}\ M^{-2}$ makes this sensor a potential tool for onsite detection of Cu^{2+} ions.

8.1.6 Chapter 6

This chapter summarized design and synthesis of a new highly selective and sensitive Schiff-base chemosensor, BPIMP, used for detection of copper ions (Cu^{2+}). This chemosensor demonstrates exhibits high selectivity and efficient signaling behavior for Cu^{2+} by exhibited apparent fluorescence quenching for micromolar concentration of Cu^{2+} over other metal ion in methanol. In addition, the high affinity of chemosensor towards Cu^{2+} can be seen from the high overall binding constant value $K=1.515 \times 10^{11}\ L\ Mol^{-1}$. The detection limit (0.032 μM) of BPIMP- Cu^{2+} is far lower than the World Health Organization (7.41 μM) limit for drinking water.

8.1.7 Chapter 7

A Schiff-base colorimetric chemosensor (QMBA) was successfully synthesized and investigated for its metal ion sensing properties. All the study was done by using methanol as solvent. Chemosensor QMBA displayed

excellent selectivity and sensitivity for Hg^{2+} ion with a vivid color change to pink, which is visible to naked eyes via UV-Visible spectroscopy. Meanwhile, the colorimetric detection of Hg^{2+} ion showed excellent tolerance towards the interference of other metal ions. The limit of detection of sensor QMBA for the analysis of Hg^{2+} was estimated nearly 100 nM which is under allowable limit set by the U.S. Environmental Protection Agency (EPA). The binding constant for complex formed QMBA-Hg^{2+} was found 1.12×10^4 M^{-1}.

8.2 Contributions of Thesis

This thesis contributes to the elementary idea of design and development of new chemosensors for transition metal ions through steady state absorption and fluorescence spectroscopic methods. Here, I have successfully synthesized and used five Schiff-bases for the selective and sensitive detection of Fe^{3+}, Cu^{2+}, and Hg^{2+} in the PPB to PPM level. In some cases, the detection is found to be possible without the help of any instrument that gives an additional importance to the developed chemosensors. In all the cases the detection was found to be very specific to a particular metal ion without any interference from the other ions (cations of counter anions) present in the system. The detection time is found to be fast and the binding constant turns out to be very large for all the cases.

8.3 Future outlook

While this thesis has demonstrated the fundamental idea of development of imine based molecules as potential sensor of the transition metal ion, many opportunities for extending the scope of this thesis still remains. This section presents some of these outlooks. It is desired that all the chemosensor should have a direct practical application towards environmental samples. This implies that the chemosensors should work in aqueous medium, which is lacking largely in the present thesis. The applicability of the synthesized molecule for detection of selective metal ions in living cell is also an important part to establish the applicability of the chemosensors. In future, one can introduce an

ionic part in my chemosensors to make them water soluble so that one can use them in green chemistry application.

List of Publication

*1. Faizi, M. S. H.; Gupta, S.; Mohan K., V.; **Jain, V. K.**; Sen, P. Highly Selective Visual Detection of Fe^{3+} at ppm Level. *Sensors Actuators, B Chem.* **2016**, *222*, 15–20.

2. Mohan, K., V.; Das, N.; **Jain, V. K.**; Khan, T.; Pandey, S. K.; Faizi, M. S. H.; Daniel, J.; Sen, P. Highly Selective and Sensitive (PPB Level) Quinolin-Based Colorimetric Chemosensor for Cu(II). *ChemistrySelect* **2020**, 5(30), 9435-9442.

3. Mukherjee, P.; Gupta, S.; Ra, S.; Yadav, R.; **Jain, V. K.**; Raval, J.; Sen, P. Ramping of PH Across the Water-Pool of a Reverse Micelle. *Langmuir* **2016**, No. 32, 1693–1699.

* included in thesis